Investigating resting-state functional connectivity in health and epilepsy using Magnetoencephalography

Bethany Charlotte Routley

Supervisors: Krish D. Singh and Khalid Hamandi

A thesis submitted to Cardiff University for the degree of Doctor of Philosophy

June 2017

Summary

It is now widely accepted that different areas of the brain are functionally connected even in the absence of explicit task demands, the so-called 'resting-state'. Differences in resting-state connectivity between groups are increasingly used as a marker of pathology in a number of neurological diseases and neuropsychiatric disorders. However, in order for a specific pattern of functional connectivity to represent a valid biomarker, it must be proven to be stable and reliably measurable in the absence of disease or disorder. Further, much is still unknown about the biological basis and purpose of resting-state activity, that may help to elucidate the functional relevance in patient groups.

Magnetoencephalography (MEG) is a technique that is well suited to the study of resting-state connectivity because it provides a direct inference of synchronised neuronal activity. In chapter two of this thesis, the test-retest repeatability of two different approaches to assessing functional coupling of brain areas using MEG is examined. Having established a preferential analysis pipeline, chapter three compares frequency band-limited MEG connectivity with functional connectivity derived from BOLD-fMRI data. The connectivity pipeline is then used for two different applications. First, the approach is combined with pharmacological intervention in healthy subjects in order to investigate the role of AMPA receptors in the glutamate system on the MEG signal and functional connectivity (chapter four). The final experimental chapter focuses on comparing functional connectivity in a group of generalised epilepsy patients with age- and gender-matched healthy control subjects. Taken together, the results of this thesis have implications for the study of functional connectivity in the resting-state using MEG, particularly the sensitivity of the technique to microscale as well as macroscale changes.

Declaration and Statements

DECLARATION

This work has not been submitted in substance for any other degree or award at this or any other university or place of learning, nor is being submitted concurrently in candidature for any degree or other award.

Signed …… (candidate) Date ……

STATEMENT 1

This thesis is being submitted in partial fulfillment of the requirements for the degree of PhD

Signed …… (candidate) Date ……

STATEMENT 2

This thesis is the result of my own independent work/investigation, except where otherwise stated, and the thesis has not been edited by a third party beyond what is permitted by Cardiff University's Policy on the Use of Third Party Editors by Research Degree Students. Other sources are acknowledged by explicit references. The views expressed are my own.

Signed …… (candidate) Date ……

STATEMENT 3

I hereby give consent for my thesis, if accepted, to be available online in the University's Open Access repository and for inter-library loan, and for the title and summary to be made available to outside organisations.

Signed …… (candidate) Date ……

STATEMENT 4: PREVIOUSLY APPROVED BAR ON ACCESS

I hereby give consent for my thesis, if accepted, to be available online in the University's Open Access repository and for inter-library loans **after expiry of a bar on access previously approved by the Academic Standards & Quality Committee.**

Signed …… (candidate) Date ……

Acknowledgements

A number of people have been instrumental in the completion of this thesis. I would like to offer heartfelt thanks to my supervisors, Krish Singh and Khalid Hamandi. Not only have your support, guidance and expertise been crucial throughout my PhD, but it was also your combined input and encouragement during my MSc that afforded me the opportunity to take up a PhD at CUBRIC in the first place.

I am grateful to the MRC MEG Partnership Doctoral Training Grant (MR/K501086/1) and the School of Psychology for provision of financial support over the past 3½ years.

Undertaking my PhD within a collaborative cohort in the UK MEG Partnership was a stroke of luck that I could not have predicted. Sharing in conferences, training and social events with counterparts around the UK has made my PhD experience all the more rewarding. A particular thanks goes to my fellow student at Cardiff, Lorenzo Magazzini, for sharing the load on data collection and fielding many technical questions from me and the rest of the sites in the process.

I would like to extend thanks to other people at CUBRIC who have helped me along the way. Among these are Dr Cyril Charron for the many, *many* instances of IT assistance, Dr Suresh Muthukumaraswamy for fostering my interest in pharmacological MEG, and all of the CUBRIC MEG lab for helpful feedback and scientific discussion. A special mention must go to Laura Whitlow and Gemma Williams, for the endless supply of tea breaks and pep talks.

Lastly, a personal thank-you has to go to my family. The support from both my parents and sisters has been unwavering, and the down days were greatly improved with a generous quota of countryside air, family dinners and dog walks. I owe a debt of gratitude to my husband, Joe, who has dealt tirelessly with the highs and lows of my PhD experience. Thank you for your unfaltering confidence in my ability to actually finish and submit a PhD thesis!

Data Collection

All analyses presented in this thesis were performed by me.

The MEG data presented for the repeatability study in chapter 2 was collected by me.

The MEG Partnership data presented in chapter 3 was collected by me, together with Dr Lorenzo Magazzini. The 100 Brains fMRI data presented in the same chapter was collected by Sonya Foley-Bozorgzad.

The pharmacological MEG data presented in chapter 4 was collected by me, together with Dr Suresh Muthukumaraswamy.

The epilepsy patient MEG data presented in chapter 5 was collected by Dr Khalid Hamandi, Dr Lisa Brindley , Dr Suresh Muthukumaraswamy and Dr Gavin Perry.

Impact of this Thesis

The work contained in chapter 4 is currently in submission for publication:

Routley, B. C., Hamandi, K., Singh, K. D., & Muthukumaraswamy, S. D. (in submission). The effects of AMPA receptor blockade on resting magnetoencephalography (MEG) recordings.

Glossary

The following abbreviations are used throughout the work:

AAL - automated anatomical labelling

AMPA - alpha-amino-3-hydroxy-5-methyl-4-isoxazolepropionic acid

BOLD - blood oxygen level dependent

fMRI - functional magnetic resonance imaging

GABA - gamma-aminobutyric acid

IGE - idiopathic generalised epilepsy

JME - juvenile myoclonic epilepsy

LCMV - linearly constrained minimum variance

MEG - magnetoencephalography

MNI - Montreal Neurological Institute

MRI - magnetic resonance imaging

NMDA - N-methyl-D-aspartate

PMP - Perampanel

ROI - region of interest

RSN - resting state network

SAM - synthetic aperture magnetometry

Contents

1 General introduction

1.1 Rationale

It is widely accepted that the brain is active even when not explicitly executing a task. Furthermore, non-invasive imaging experiments show that resting brain activity exhibits a stereotypical set of functionally connected networks (Raichle, 2009). Resting-state is attractive because it is simple to set-up and simple to perform. However, in order for a 'biomarker' of disease to be valid, it is important to establish reliability and variability of the measurement technique in the absence of disorder (Mayeux, 2004). Gaining a better understanding of the complex neural dynamics that give rise to neuroimaging signals is also critical to interpretation of the underlying causes of group differences in functional connectivity at rest.

One of the many disorders where the resting-state offers a viable investigative technique is epilepsy. Though convention dictates a distinction between focal and generalised epilepsies, the condition as a whole is increasingly thought of as a disorder of neural networks (see reviews by Hamandi, Routley, Koelewijn, & Singh, 2016; Kramer & Cash, 2012), associated with dysfunction in the excitation-inhibition balance (Engel, 1996). So, achieving a robust marker of dysfunction outside ictal periods, and being able to understand the processes giving rise to these changes, are important to further advancing our understanding of the disorder.

Therefore the work contained in this thesis is an attempt to disentangle some of the issues relating to functional connectivity in the resting-state using MEG. In particular, I first attempt to establish the reliability and validity of a common approach to estimating functional connectivity. Then, apply this approach in a number of scenarios relating to understanding the underlying signal generation and epilepsy-related changes in functional connectivity.

1.2 A brief background on magnetoencephalography (MEG)

1.2.1 The biophysical and technical basis of the MEG signal

The MEG signal is thought to arise from summation of inhibitory and excitatory post-synaptic potentials in neural populations (Lopes de Silva, 2010). Only neurons in an open-field orientation produce a measurable net signal and the most common of these, the pyramidal neuron, is believed to form the greatest contribution to the signal measurable by MEG. However, MEG is not sensitive to activity in a single neuron, but rather requires 10,000-50,000 neurons to become synchronously active (Murakami & Okada, 2006). The current dipoles associated with mass coherent activity of neurons produce primary volume currents that are able to pass unencumbered through the head and are measurable at the scalp using MEG (Hämäläinen, Hari, Ilmoniemi, Knuutila, & Lounasmaa, 1993). This theory is supported by studies showing that the MEG signal bears the closest correspondence to invasive recording of local field potentials (LFPs) that also measure post-synaptic potentials (Adjamian et al., 2004).

There are a number of pertinent theoretical and technical considerations. MEG is not sensitive to all dipole orientations, such that radial sources are likely to be silent (Figure 1-1). However, given the size of cortical patch required to generate MEG signal, it is likely in practice that little of the cortex is truly silent (Hillebrand & Barnes, 2002). Rather, MEG sensitivity falls away with depth from the sensors (Hillebrand & Barnes, 2002). There is some evidence that it is possible to detect signal from deep structures (Cornwell, Johnson, Holroyd, Carver, & Grillon, 2008), but it is likely that localisation accuracy for these regions will be poorer compared to more superficial sources.

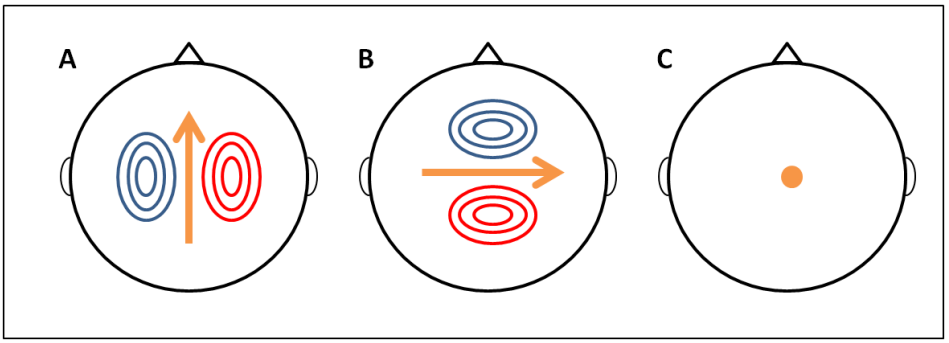

Figure 1-1. Diagrammatic representation of potential cortical dipole orientations and relative 'visibility' with MEG. Orange arrows represent a single dipole and blue and red circles represent magnetic field lines entering and exiting the head. **(A)** Anterior-posterior tangential source and **(B)** left-right tangential source both produce field patterns that are detectable with MEG. **(C)** Radial source (superior-inferior alignment on grey matter sheet) will be MEG-silent. The gyral crests of the grey matter sheet carry greatest likelihood of radial orientations (Hillebrand & Barnes, 2002). Figure adapted without permission from Singh (2006).

The first MEG recordings were made using single sensors (Cohen, 1968, 1972). Following this pioneering work the technique has developed through multi-channel arrays to present day whole-head helmet coverage systems (Hari & Salmelin, 2012). The magnetic fields in the brain are extraordinarily small (10^{-12} tesla), and the potential noise sources are many orders of magnitude larger by comparison. Specialist hardware helps to overcome this issue. Superconducting quantum interference devices (SQUIDs) sensors are highly sensitive to magnetic fields, and are coupled to the brain's magnetic fields via flux transformers consisting of a pickup coil and a coupling coil (Vrba & Robinson, 2001). Both the SQUIDs and flux transformers are stored inside a dewar and cooled to -269˚C to be kept operational. There are a number of available configurations for the flux transformer pickup coil, and the system used to conduct the research contained in this thesis is a CTF MEG 275 containing first order axial gradiometers (Figure 1-2). The additional winding of the first-order gradiometers compared to magnetometers acts as a noise cancellation

system. Magnetic field noise which appears that same to both coils of the gradiometer will create a current that is equal and opposite, thus reducing noise by a factor of 100 compared to magentometers (Vrba & Robinson, 2001). It is possible to convert data recorded using axial gradiometers to planar gradient formation (Oostenveld, Fries, Maris, & Schoffelen, 2011). Additionally, the entire system is housed within a shielded room to screen out environmental noise. Noise from mains electronics can be filtered out post-collection. Further, data can be analysed in synthetic third-order gradiometer mode to reduce the noise further by up to a factor of 100 (Vrba & Robinson, 2001). In the CTF 275 system used throughout this thesis, this is achieved by use of 29 reference magnetometers located in the centre of the dewar that can be used to regress out additional noise.

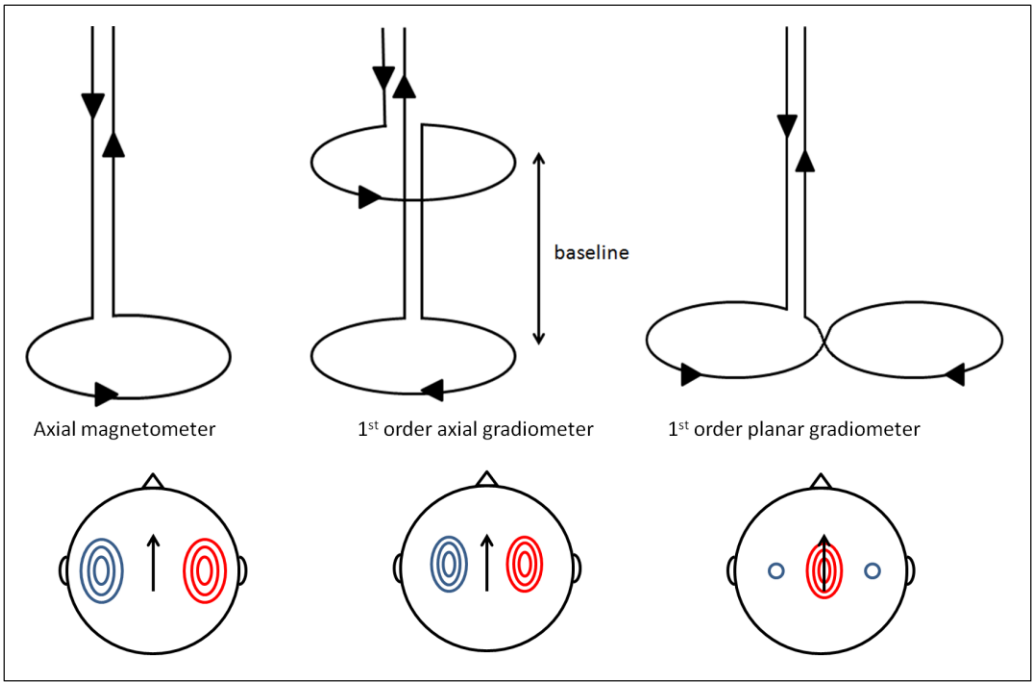

Figure 1-2. Schematic showing three pickup coil configurations (top) and representative field maps for each type (bottom). The axial magnetometer consists of one wire winding whereas the 1st order axial gradiometer has an additional wire winding for noise cancellation purposes (note the more focal field map). The planar gradiometer formation produces a field pattern where the signal maxima is produced directly over the dipole. Adapted without permission from Singh (2006).

1.2.2 Analysing MEG data

With whole-head MEG systems comes the potential to accurately estimate both timecourses and spatial locations of discrete neural sources (Mosher, Leahy, & Lewis, 1999). In order to do so, one must first solve the 'forward problem' by determining the magnetic field pattern that could be generated by a known current distribution (also known as the lead fields). MEG is less sensitive to uncertainties in the conductivity profile of the head compared to other non-invasive neurophysiological techniques (i.e. EEG), so solving the forward problem is relatively straightforward (Singh, 2006).

However, having solved the forward problem, one must still estimate the location of the current sources given a particular magnetic field distribution across sensors, known as the 'inverse problem' (Mosher et al., 1999). The inverse problem suffers from non-uniqueness, meaning that there is not enough information in the data received to provide an unambiguous solution. However, adding a priori constraints relating to the temporal or spatial distribution of current can help to reduce the estimate to a single solution and the success of any given inverse solution is dependent on these a priori constraints (Singh, 2006). There are a number of approaches to solving the inverse problem. These include equivalent dipole fitting, which models a single active source at any given moment (Wood, 1982) and distributed current models that attempt to estimate a continuous current distribution that is generating the observed response (e.g. minimum norm - Hämäläinen & Ilmoniemi, 1994; Lin et al., 2006).

Another common source estimation approach, and the one that is used throughout this thesis, is beamforming. This class of source model, also known as a virtual sensor approach, constructs a spatial filter that scans across all locations in the given grid to

estimate the signal at every grid location (Vrba & Robinson, 2001). The virtual sensor at each location in the grid is the sum of the weighted signal from all sensors that gives maximal sensitivity to activity in that location (Hillebrand, Singh, Holliday, Furlong, & Barnes, 2005), whilst supressing contributions from other, non-target, locations. The main assumptions in beamforming are that the data are generated by a discrete set of current dipoles, and that no two distinct cortical areas exhibit perfect temporal coherence with one another (Hillebrand & Barnes, 2005). Although this means that distant sources that are highly correlated with one another will be 'invisible' using a beamformer, this is not a likely scenario in the study of spontaneous oscillatory activity. The key advantage for the purposes of working with resting-state data is that beamforming is suited to studying activity that is not necessarily tightly phase-locked to a stimulus (Singh, 2006), and provides additional noise rejection that is beneficial when analysing non-averaged data (Vrba, 2002).

1.3 The functional role of neural oscillations

1.3.1 Contextual overview

One of the first demonstrations of oscillatory activity in the human brain was made by the founder of EEG, Hans Berger, when he observed large rhythmic fluctuations in recordings at 10Hz when subjects opened and closed their eyes (Berger, 1929). In the years since, oscillations in a number of other frequency bands have also been observed. The putative functional role, mechanisms and interpretation of band-limited oscillations have been extensively studied and it is not feasible to cover each of these here (for reviews on the gamma and theta bands respectively, see: Buzsaki & Wang, 2012; Colgin, 2013). Broadly and simply speaking, oscillatory activity between 1 and 100Hz can be classified into a number of frequency bands. Although there are

no clearly defined boundaries set upon the various frequency bands, the bandings used throughout this thesis consistent with previous work (Brookes et al., 2011b; Koelewijn et al., 2015; Muthukumaraswamy et al., 2013b; Nutt et al., 2015) are as follows: delta (1-4Hz), theta (4-8Hz), alpha (8-13Hz), beta (13-30Hz), low gamma (30-50Hz) and high gamma (50-90Hz). The putative functional role of band-limited oscillations with respect to spontaneous functional connectivity is discussed further below (sub-section 1.3.2).

Traditionally, the oscillatory signals measured with MEG could be divided into two categories. First, activity that is tightly time- and phase-locked to a stimulus (i.e. the evoked response), and secondly activity that is sustained throughout stimulus presentation and is time- but not phase-locked to stimulus onset (i.e. the induced response; Pfurtscheller & Lopes da Silva, 1999). However, recent thinking suggests that spontaneous oscillatory activity occurring at rest in multiple frequency bands and, more specifically, the way in which these oscillations are coupled may be functionally relevant (Engel, Fries, & Singer, 2001).

1.3.2 Neural oscillations as an intrinsic coupling mechanism

Oscillations may become coupled in a number of ways, and some suggest that oscillatory connectivity by phase or amplitude represent 'intrinsic coupling modes' of the human brain (Engel, Gerloff, Hilgetag, & Nolte, 2013a). There is no accepted account of the purpose of spontaneous oscillations in the brain, but many candidate processes link to cognitive operations related to predictive coding (Schölvinck, Leopold, Brookes, & Khader, 2013). For example, animal work shows that spontaneous activity exhibits progressive adaptation to intensive visual stimulation, with responses over time becoming more similar to stimulus-evoked responses (Berkes, Orbán, Lengyel, & Fiser, 2011; Fiser, Chiu, & Weliky, 2004). This is taken to

suggest that spontaneous oscillations are involved in making dynamic predictions about sensory stimuli (Berkes et al., 2011). It has also been shown that spontaneous activity prior to presentation of a stimulus can affect perception of said stimulus (Romei et al., 2008). This is taken as further evidence for the involvement of background activity in modulating excitability in a predictive manner (Romei et al., 2008).

One general framework of oscillatory function that is pertinent to the study of RSNs comes from Donner and Siegel (2011). In this model, oscillations broadly serve two dimensions of function associated with distinct patterns of oscillatory behaviour (Figure 1-3). Encoding processes, such as discrimination of visual features is said to be served by local gamma oscillations, whereas low frequency oscillations facilitate integrative functions such as perceptual inference via long-range interactions (Donner & Siegel, 2011). This framework is well supported by a large body of evidence suggesting that local gamma oscillations are involved in encoding processes (Adjamian et al., 2004; Gray & Singer, 1989; Kopell, Ermentrout, Whittington, & Traub, 2000). Studies also associate activity in low-frequency bands with integrative processes such as sensory perception and perceptual decision making (Hipp, Engel, & Siegel, 2011; Lou, Li, Philiastides, & Sajda, 2014). Further, this framework is also consistent with the notion that alpha oscillations represent a process of active inhibition (Jensen & Mazaheri, 2010) rather than cortical idling, as was once presumed (Pfurtscheller, Stancák Jr, & Neuper, 1996). An example of the dissociative low-high frequency processes co-existing can be seen in a study by Frien and Eckhorn (2000). Using invasive recordings in awake monkey cortex, they found that the range of coupling distance was significantly higher for low frequency compared to high frequency oscillations, and high frequency oscillations were significantly modulated by stimulus properties where low frequencies were not. Subsequent work confirmed

these observations (Leopold, Murayama, & Logothetis, 2003), and taken together these findings support the framework suggested by Donner and Siegel (2011). Moreover, a recent study of visual cortical areas suggests that low and high frequency oscillations may differentially mediate feedback and feedforward processes respectively (Michalareas et al., 2016). In this study, Michalareas et al inferred a number of feedforward and feedback projections in human visual cortex from reterograde tracing of homologous areas in macaque visual cortex. They then used frequency resolved Granger causality of human MEG data to show that causal influences in feedforward pathways were predominant in the gamma band whereas alpha and beta interactions were most dominant in the feedback projections. Moreover, a cortical hierarchy of human visual cortex constructed from these results showed good concordance with the known hierarchy of macaque visual cortex (Michalareas et al., 2016). This study provides an additional functional account of oscillations in different frequencies that builds on the framework of Donner and Siegel (2011).

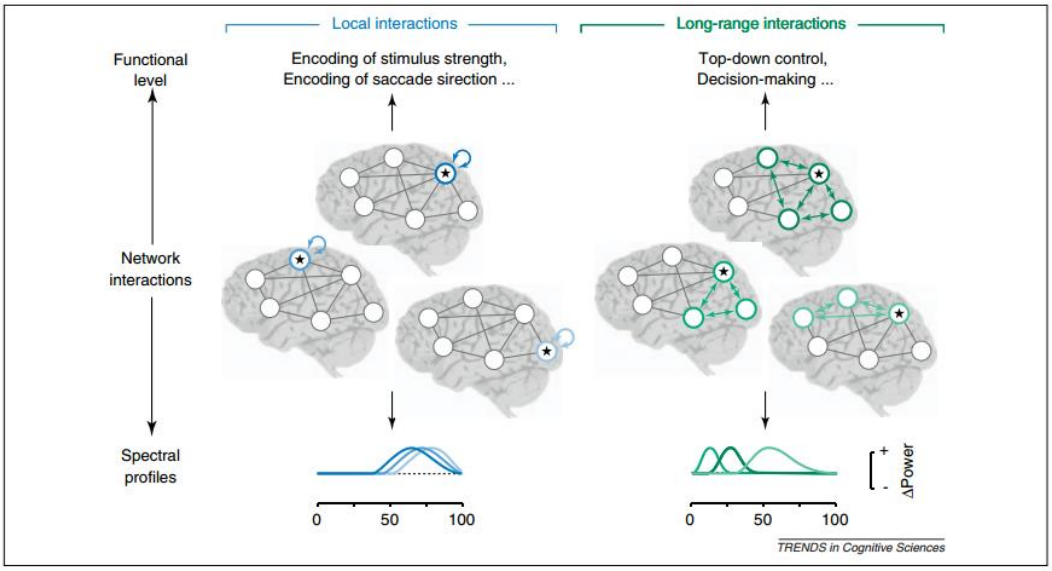

Figure 1-3. Network interactions shaping spectral profiles of cognitive functions, taken from Donner and Siegel (2011). Local encoding functions correspond most closely to modulations in the gamma band. Integrative functions represent longer-range network

integration and correspond to spectral profiles in lower frequencies, particularly the beta band. Copyright 2011 by Elsevier, reprinted with permission.

1.3.3 Neuromodulation and the role of neurotransmitters

Animal and modelling studies suggest that oscillatory activity is intrinsically linked to the balance of excitation and inhibition in the brain (Brunel & Wang, 2003; Scheffzuk et al., 2013). Using MEG in conjunction with pharmacological manipulation (pharmacoMEG) offers a way to study this balance selectively and non-invasively in humans (Muthukumaraswamy, 2014). The main excitatory and inhibitory neurotransmitters in the brain are glutamate and GABA, respectively. Several studies have highlighted that manipulation of the GABAergic system impacts oscillatory behaviour. For example, benzodiazepines have been shown to increase beta power over somatosensory cortex (Jensen et al., 2005) as well as causing widepsread increases in band-limited power across a diffuse set of brain regions (Hall, Barnes, Furlong, Seri, & Hillebrand, 2010). To date, no human studies have focused specifically on the glutamate system. This gap in current knowledge is addressed further in chapter 4.

There is also evidence that the chemoarchitecture of the brain may specifically underwrite certain aspects of functional connectivity. For example, a recent study using human and macaque data found that cortical areas with higher density of excitatory receptors showed increased functional connectivity in fMRI than those with higher proportional density of inhibitory receptors (van den Heuvel et al., 2016). Alterations to RSN activity have been shown using pharmacoMEG and pharmacoEEG with drugs acting on a wide range of neurotransmitter systems, including serotonin (Muthukumaraswamy et al., 2013b), GABA (Fingelkurts et al., 2004) and dopamine (Heinrichs-Graham et al., 2014). Further work could elucidate the contribution of a

number of different neurotransmitters to functional connectivity and help to bridge the gap between generative models of oscillatory activity in animals and humans.

1.4 The resting-state in functional neuroimaging

1.4.1 Rest as an experimental paradigm

The use of the resting-state in neuroimaging research has grown exponentially in recent years, along with the interest in macroscale functional connectivity and connectomics. Using the online citation index 'Web of Science' (http://wok.mimas.ac.uk/), the search terms 'resting-state' and 'connectivity' or 'networks' yield 471 MEG papers on the topic between 2000 and 2016, with publications increasingly on a yearly basis (Figure 1-4). Replacing MEG with fMRI in search term lengthens the list by a factor of approximately seven, and yields 3514 records.

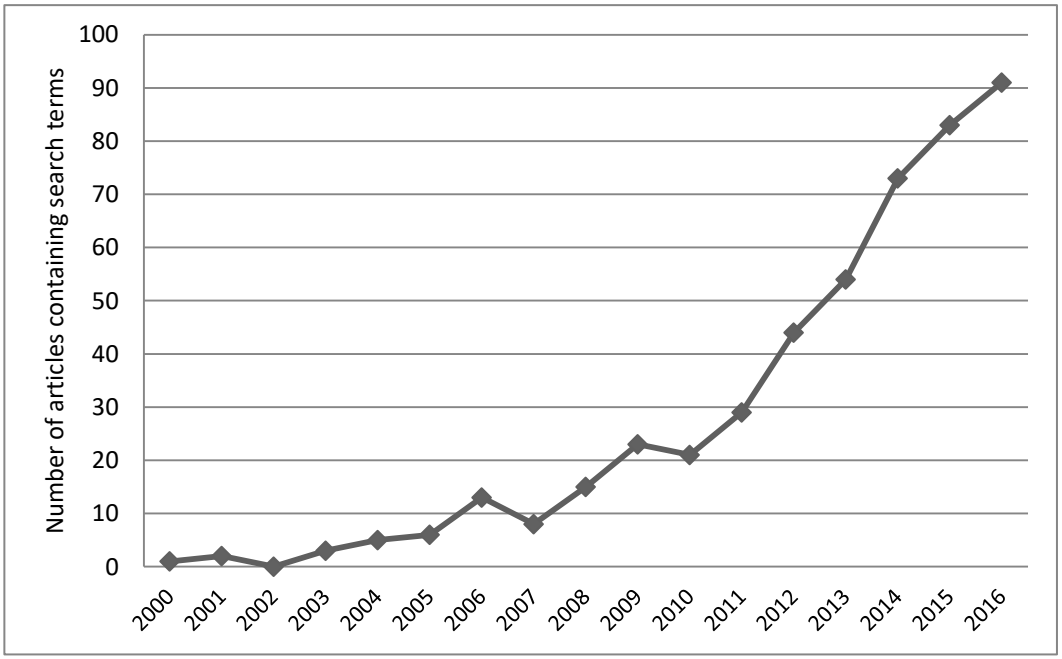

Figure 1-4. Web of Science citation search for the number of papers published between 2000 and 2016 containing the following search terms: ((Magnetoencephalography OR

MEG) AND (resting-state OR rest) AND (networks OR connectivity)). Last retrieved 05/06/2017.

The seminal paper suggesting that distinct regions of the brain could be functionally coupled at rest was published in the mid-1990s using fMRI (Biswal, Zerrin Yetkin, Haughton, & Hyde, 1995). Further fMRI and PET studies showed that this so-called 'default-mode' network of regions were intrinsically coupled during the resting-state and became less active during tasks (Greicius, Krasnow, Reiss, & Menon, 2003; Raichle et al., 2001). This pioneering work paved the way for fMRI studies showing intrinsic connectivity in a number of different resting-state networks (RSNs; Fox et al., 2005; Wang et al., 2008). There is also evidence that RSNs persist as 'background' coupling patterns even during the performance of tasks (Smith et al., 2009).

1.4.2 Studying functional connectivity at rest using MEG

As indicated above, the study of functional connectivity at rest continues apace in the fMRI community. An exploration of RSN literature in fMRI is beyond the scope and remit of this thesis (see reviews by Greicius, 2008; Raichle, 2009; van den Heuvel & Hulshoff Pol, 2010) but it is crucially worth noting that using fMRI, researchers have found differences in RSNs in a variety of neurological diseases and disorders including Alzheimer's disease (Sorg et al., 2007), schizophrenia (Liang et al., 2006) and depression (Greicius et al., 2007). Instead, we focus here on the relatively small but growing body of work concerning resting-state connectivity in MEG. Some postulate that oscillatory activity represents an important coupling process in the brain, so MEG is ideally suited to studying functional connectivity of this type (Engel et al., 2013a; Engel et al., 2013b; Schnitzler & Gross, 2005). Additionally, as an electrophysiological method MEG does not rely on hemodynamic coupling to neuronal activity that may itself be affected by disease or disorder, as is the case of

fMRI (Brookes et al., 2011a). Please see the introductory section of chapter 3 for expansion on this point.

It stands to reason that the information dense MEG signal provides a number of ways to characterise functional connectivity. In the broadest terms, the two categories that have overtaken many others in popular use during recent years are phase-phase coupling and amplitude-amplitude coupling (O'Neill, Barratt, Hunt, Tewarie, & Brookes, 2015). Phase coupling assesses fixed phase relationships between two sources (Hillebrand, Barnes, Bosboom, Berendse, & Stam, 2012; Lachaux, Rodriguez, Martinerie, & Varela, 1999), and amplitude coupling looks for synchronisation among the power envelopes of two sources (Brookes et al., 2011b; Hipp, Hawellek, Corbetta, Siegel, & Engel, 2012). The precise nature of the relationship and differences between phase and amplitude coupling is still unclear. This has led to the suggestion that phase and amplitude coupling represent mechanistically different but linked processes (Canolty & Knight, 2010; Engel et al., 2013a). However, some studies suggest that it is possible to assess connectivity equivalently using a variety of estimates and approaches (Colclough et al., 2016; Tewarie et al., 2014). The estimate to be used throughout this thesis is amplitude envelope correlation, so from here we focus on approaches using this coupling type.

A number of methods use a seed-based approach to estimate band limited power envelope correlations. One of the first examples used fMRI-guided seed regions to measure activity in the dorsal attention and default mode networks in MEG (de Pasquale et al., 2010). The authors found good correspondence with RSNs in fMRI, but correlation in MEG was limited to the same hemisphere as the seed (de Pasquale et al., 2010). However, other studies using seed-based approaches have been able to demonstrate connectivity between primary sensory cortices across both hemispheres

(Brookes et al., 2011a; Hipp et al., 2012). These investigations also show that amplitude-amplitude coupling is mediated at quite slow timescales, with amplitude envelopes co-varying over seconds or tens of seconds (Hipp et al., 2012).

Another important new approach proposed the used of independent component analysis (ICA; Brookes et al., 2011b; Hall, Woolrich, Thomaz, Morris, & Brookes, 2013). Here, ICA was applied in the temporal domain in order to generate, in a data-driven way with no *a priori* input, RSNs that represent areas with a fixed amplitude relationship across the recording time. This technique was also extended to include a GLM of task-based data (Luckhoo et al., 2012). Yet another method estimated a whole-brain connectivity matrix based on a single virtual sensor representative for each region of the Automated Anatomical Labelling (AAL) atlas (Hillebrand et al., 2012; Tzourio-Mazoyer et al., 2002). This approach initially used the Phase Lag Index, but has also been successfully applied with power envelope correlations (Tewarie et al., 2014).

Regardless of approach, one of the key factors in the use of amplitude coupling methods is the removal of spurious correlation (O'Neill et al., 2015). Hipp et al. (2012) showed that using simple envelope correlation results in a trivial spatial pattern of coupling with strongest connectivity in neighbouring sources and rapid decay with distance from the reference point. This is presumed to arise due to the ill-posed inverse problem resulting in signal leakage whereby activity at a single source is measured at multiple sensors (Engel et al., 2013a; Hipp et al., 2012; O'Neill et al., 2015). Several leakage correction methods have been suggested, but most involve removal of zero phase-lag activity. There is some evidence that zero-lag synchronisation does occur across discrete cortical areas (Frien, Eckhorn, Bauer, Woelbern, & Kehr, 1994). Thus there is a possibility that the process of

orthogonalisation may remove true functional connectivity but on balance, the benefit of removing spurious connectivity outweighs this small potential loss. In one example, sources across the grid are orthogonalised in a pairwise fashion prior to calculation of power envelope correlations (Hipp et al., 2012). Another method extends this approach to orthogonalise all sources with respect to each other in a multivariate fashion (Colclough, Brookes, Smith, & Woolrich, 2015). The orthogonalisation methods detailed in Hipp et al (2012), and Colclough et al (2015) are used in chapter 2.

Using these and other similar methods, researchers have been able to establish alterations to connectivity in many scenarios including childhood epilepsy (Koelewijn et al., 2015), depression (Nugent, Robinson, Coppola, Furey, & Zarate Jr, 2015) and schizophrenia (Liddle et al., 2016). The clearest connectivity structure in MEG, and often those where group differences manifest, can be seen in the alpha and beta bands (8-30Hz). This is consistent with the framework that positions low-frequency oscillations as carriers of long range integration across the cortex (Donner & Siegel, 2011).

1.4.3 Resting-state connectivity as a 'biomarker'

Resting-state connectivity and RSNs seem to be sensitive to specific changes in a number of different patient groups (Arbabshirani, Kiehl, Pearlson, & Calhoun, 2013; Bartolomei et al., 2006; Franzen et al., 2013). This leads some to suggest that resting-state functional connectivity represents a biomarker of disease or disordered state. For example in a recent study, authors were able to divide depression patients on the basis of connectivity patterns into four distinct subtypes associated with differing symptom profiles and reactivity to neurostimulation treatment (Drysdale et al., 2017). The concept of a 'biomarker' in basic and clinical research is being continually

re-evaluated but there is a general consensus that a biomarker should be a reliable index of health or disease that can be objectively measured (Strimbu & Tavel, 2010). For the context of neuroimaging connectivity, measures should be consistent within subjects over time and repeatable at the group level (Colclough et al., 2016; Garces, Martin-Buro, & Maestu, 2016). There is evidence from fMRI studies that RSNs are repeatable between subjects and over multiple recordings sessions (Damoiseaux et al., 2006), but the criterion of robustness is likely contingent on each measuring technique and analysis pipeline.

With regards to MEG, few studies have specifically investigated the stability and repeatability of functional connectivity estimates in the absence of disease or disorder. It has been suggested that connectivity estimates are consistent for an individual over repeated recordings and show little inter-individual variation (Colclough et al., 2016). However, another study showed that whilst group estimates are stable, there is some variability in RSNs at the single-subject level (Wens et al., 2014), so this issue is not yet resolved. It is also possible that small changes at any analysis stage may affect the reproducibility of estimates, so it is important to validate any new pipeline in its entirety prior to application in patient groups. These points are expanded further in the introductory section of chapter two.

1.5 Epilepsy as a network disorder

1.5.1 Epidemiology and diagnosis of epilepsy

Epilepsy is a neurological disorder characterised by the presence of seizures, and is associated with abnormally increased synchronisation (hypersynchrony) of oscillatory activity in neural populations (Gloor, 1979). Epilepsy is one of the most common

serious neurological disorders affecting approximately 50 million people worldwide, with proportionately higher incidence in low and middle income countries (WHO, 2017). In the UK, the prevalence of epilepsy is estimated at between 0.61% and 0.76%, depending on region (Thomas et al., 2012). The epidemiology and aetiology of the disorder is hugely complex (Savage, 2014), but for diagnostic purposes, seizures are broadly classified as focal or generalised. Symptoms of focal seizures will vary considerably depending on location but could include abnormal sensations, psychic aberrations and involuntary movements (Braeutigam, 2013). The most commonly recognised generalised seizures include temporary loss of consciousness (absences) and tonic-clonic seizures associated with jerky convulsions (Savage, 2014). Given the heterogeneity of this family of disorders, it is unsurprising that successful treatment of epilepsy is also complex (Yeager et al., 2005), and up to 20-30% of patients are refractory to anti-epileptic medication (Sander, 1993).

The International League Against Epilepsy (ILAE) published a new classification framework this year, following an extensive period of consultation (Fisher et al., 2017; Scheffer et al., 2017). Prior to this year, the last ratified classification was in 1989 (ILAE, 1989). The current classification as of March 2017 can be seen in Figure 1-5. The first step of is based on diagnosing seizure type followed by further diagnosis of epilepsy type and, if applicable, specific syndrome (Scheffer et al., 2017). Attempts should be made at every stage of diagnosis to delineate aetiology, but up to 60% of epilepsy cases are recorded as arising from unknown causes (WHO, 2017). Critically, the new framework introduces a new epilepsy type named 'combined generalised & focal', taking into consideration a mounting body of evidence suggesting that in many cases there is no clear distinction between focal and generalised epilepsies (Beghi, 2017). Please see section 1.5.2 for further expansion on this point.

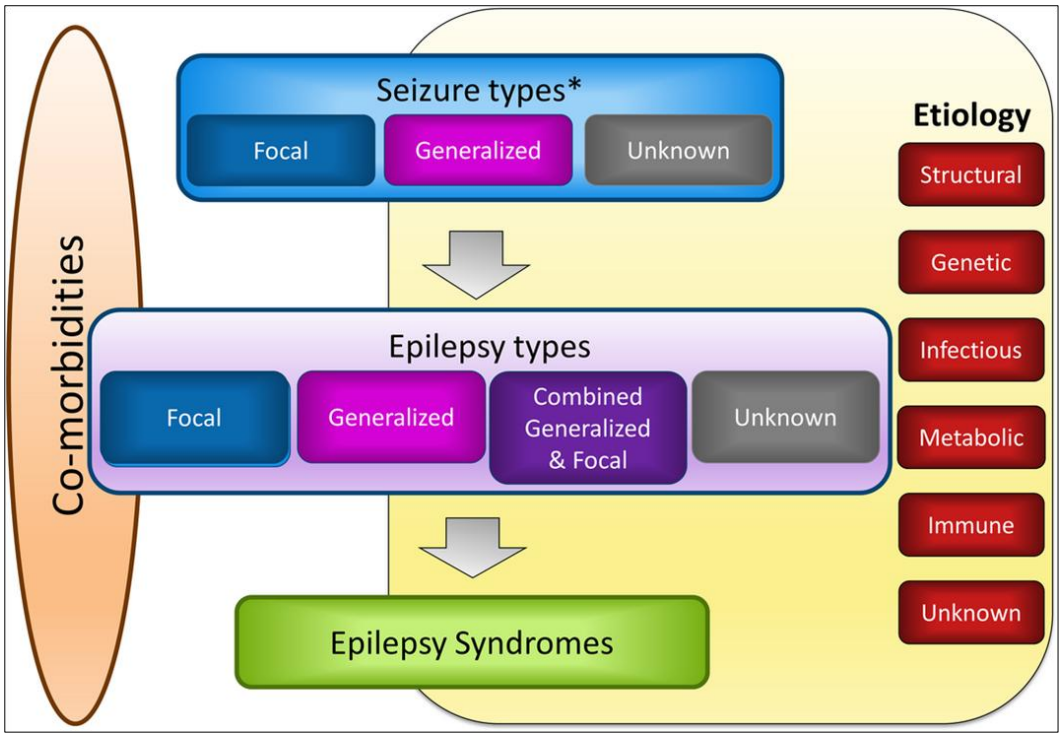

Figure 1-5. Latest framework for classification of the epilepsies, taken from Scheffer et al (2017). Copyright 2017 by John Wiley and Sons. Reprinted with permission.

1.5.2 Focal vs. generalised features and network dynamics

There is by now a strong suggestion that the distinction between focal and generalised epilepsies may not be as clear-cut as it was once believed, and that epilepsy should be considered a network disorder (Spencer, 2002). Widespread activation throughout the brain has been found in focal epilepsies (Alarcon et al., 1994; Lieb, Engel, & Babb, 1986) and there is also evidence to suggest that even generalised epilepsies may have focal features (Meeren, Pijn, Van Luijtelaar, Coenen, & Lopes da Silva, 2002). Furthermore, many studies actively demonstrate network involvement in epilepsy. For example, a recent MEG study found that longer seizure duration was associated with greater connectivity in the beta band between the epileptogenic zone and other brain regions (Madhavan, Heinrichs-Graham, & Wilson, 2013). Moreover, even when surgery for focal epilepsy is considered successful (i.e. freedom from seizures with loss of awareness), a small number of patients continue

to have simple partial seizures (de Tisi et al., 2011). Some proponents of the network view in epilepsy therefore suggest that removal of the epileptogenic zone identified during pre-surgical mapping will be successful only if the area acts as a critical hub within the so-called epileptogenic network (Richardson, 2012).

The functional interactions across the brain in epilepsy are also likely to be dynamic, and show some degree of temporal sequencing. In a study of generalised absence seizures, the authors found a cascade of events including long-range desynchronisation prior to absence seizure onset, followed by increases in both local and long-range phase synchronisation lasting for the duration of the ictal event (Amor et al., 2009). Findings of desynchronisation such as these lend weight to the idea that hyposynchrony in the wider network pre-ictally may help to contribute to both focal and generalised ictogenesis (Uhlhaas & Singer, 2006), and that the regions susceptible to this effect are person-specific and stable over time (Aarabi, Wallois, & Grebe, 2008). This finding also indicates that it may be possible to detect epilepsy-related changes in the brain during non-ictal periods. However, relatively fewer studies have examined differences in connectivity during paroxysm-free background recordings. Those that have are somewhat mixed, with some studies suggesting altered connectivity at rest (Luo et al., 2012b; Niso et al., 2015) and others finding no evidence of disruption to background activity (Moeller et al., 2011). Please see the introduction to chapter five for further discussion on this point. A better understanding of this facet of the disorder may help contribute to knowledge around transition to seizure.

1.5.3 The use of MEG in the study of epilepsy

Due to the fact that signals in both EEG and MEG arise from the synchronous firing of large numbers of neurons, these techniques by their nature emphasise synchronous

activity whilst highly unsynchronised activity is cancelled out. These non-invasive neurophysiological techniques, particularly EEG, are widely used in diagnosis and planning for epilepsy. In the USA, MEG is an FDA-approved clinical evaluation tool for epileptic foci localisation and pre-surgical planning, and is used in clinical context to varying degrees elsewhere (Braeutigam, 2013). Studies have shown good concordance between MEG localisation of ictal activity and localisation from invasive recordings (Eliashiv, Elsas, Squires, Fried, & Engel, 2002; Fujiwara et al., 2012).

Though EEG and MEG are considered complementary techniques, there is one key difference that arguably make MEG the advantageous technique for the study of functional connectivity in epilepsy. Electrical fields can be smeared as they travel through different tissue compartments to the scalp, so EEG is particularly affected by the conductivity profile of the head (van den Broek, Reinders, Donderwinkel, & Peters, 1998). Magnetic fields, and therefore MEG, are less susceptible to signal diffusion by different tissue compartments (Hämäläinen et al., 1993; van den Broek et al., 1998). This volume conduction problem in EEG means that there is increased overlap between the signals recorded at two separate sensors. This can be particularly problematic when trying to measure connectivity because the signal overlap can create spurious synchrony between electrodes where none actually exists in the brain (Lachaux et al., 1999).

1.6 **Thesis objectives**

Studying functional connectivity in the resting-state, using MEG, offers a useful tool to understand more about neural oscillations and the role of neurotransmission underlying the signal, as well as the effects of neurological disease. Therefore, the key aims to be addressed by the experimental chapters of this thesis are as follows:

1. I first seek to investigate the test-retest reliability of two amplitude coupling approaches to functional connectivity in MEG. To this end, I will analyse data from repeated scans of healthy individuals taken a week apart using both connectivity approaches and assess group and single subject level stability, in order to establish a preferential pipeline for subsequent analysis.

2. Having established an analysis pipeline, I will compare band-limited MEG connectivity with connectivity in fMRI. This analysis will be completed using a healthy cohort of 88 participants scanned as part of the UK MEG Partnership database collection.

3. I will investigate the role of glutamate in generation of the resting-state MEG signal using pharmacoMEG with an anti-epileptic compound in healthy subjects. Perampanel is a newly licensed drug acting as a selective AMPA antagonist that allows, for the first time, the study of specific AMPA-mediated glutamatergic processes non-invasively in human subjects.

4. Finally, I will apply the connectivity method in an epilepsy group in order to investigate changes to background activity that could indicate the mechanisms of the enduring seizure-prone state in this population. Specifically, the patients included in this analysis all have a diagnosis of Juvenile Myoclonic Epilepsy, one of the most common forms of Idiopathic Generalised Epilepsy that has previously been associated with aberrant network activity in the resting-state.

2 Assessing the repeatability of oscillatory resting-state networks in healthy individuals

2.1 Abstract

The study of functional neural networks and how they map on to cognitive and sensory performance is a well-established topic of neuroimaging research. Increasingly, there is a focus on understanding how these networks may be used to measure differences in functionality between groups, and whether these provide novel biomarkers of neurological or neuropsychiatric conditions. Recently developed techniques have enabled network analysis to be conducted using magnetoencephalography (MEG) data. However, these approaches are still relatively novel, so it is important to validate the methods prior to application in patient groups. For a biomarker to be meaningful it should be characteristically stable for an individual in the absence of disease or disorder. Here, we investigated the test-retest reproducibility of resting-state connectivity derived, using two different approaches to assessing amplitude coupling between MEG timeseries. We additionally investigated the effects of methodological choices on these connectivity estimates. On the basis of the results, we establish a suitable pipeline for application in subsequent experiments.

2.2 Introduction

2.2.1 Measuring functional connectivity from MEG data

The study of how individual cortical areas connect both structurally and functionally to one another has greatly influenced our current understanding of the brain as a networked system. In recent years there has been a considerable surge in interest in the networks of cortical regions that are functionally connected at rest (resting state networks; RSNs), and the differences in these networks between individuals or groups. Typically, RSNs have been investigated using fMRI (see reviews by Smith et al., 2013; van den Heuvel & Hulshoff Pol, 2010). Nevertheless, there is now an emergence of approaches designed for use with other data modalities, particularly those which provide more direct measures of neuronal activity, such as MEG.

In one of the seminal approaches to deriving RSNs using MEG data, an independent component analysis (ICA) is used to reconstruct cortical networks that co-vary in their activity over time, by means of temporal correlations between band limited power envelopes (Brookes et al., 2011a). This technique has been applied successfully to healthy controls, both at rest (Brookes et al., 2011b; Hall et al., 2013) and during cognitive tasks (Brookes et al., 2012; Hall et al., 2013). Networks re-constructed in this way show good concordance with networks derived using fMRI (Brookes et al., 2011a), but without reliance upon indirect changes to blood oxygenation to measure cortical activity. Studies have also found this technique to be sensitive to group differences, for example following pharmacological manipulation (Muthukumaraswamy et al., 2013a; Muthukumaraswamy et al., 2015) and in neurological and neuropsychiatric conditions such as epilepsy (Koelewijn et al., 2015) and major depressive disorder (Nugent et al., 2015).

Another key approach uses an atlas-guided beamformer to generate source space signals before calculating functional connectivity (Hillebrand et al., 2012). Here, rather than computing some connectivity measure across every voxel, the brain is parcellated based on a standardised atlas (e.g. Automatic Anatomical Labelling, AAL; Tzourio-Mazoyer et al., 2002) and a single virtual sensor is chosen as a representative timecourse for each ROI. This approach was initially suggested to aid interpretation of functional connectivity in MEG and also to enable greater ease of multi-modal comparison. The authors used a phase coupling measure (phase lag index) as this method is thought to be less affected by volume conduction effects than other measures of functional connectivity (Hillebrand et al., 2012). However, this atlas-based approach to source localisation has also been successfully used with an envelope correlation method for amplitude coupling (Tewarie et al., 2014), a measure which has shown to be more robust in resting-state MEG (Colclough et al., 2016).

In the intervening years, the idea of an atlas-based beamformer has been taken up in a number of studies. This approach has been shown to be sensitive to group changes in source power and frequency in diseases including multiple sclerosis (Van der Meer et al., 2013) and Alzheimer's disease (Engels et al., 2016). Furthermore, it has been used as a method for source estimation during the recent development of new and extended methods for characterising pan-spectral hierarchy and graph theoretical organisation in brain networks (Brookes et al., 2016; Tewarie, van Dellen, Hillebrand, & Stam, 2015).

2.2.2 Repeatability of resting-state functional connectivity

Central to the appeal of the resting-state paradigm in clinical research, and no doubt a key factor in its popularity, is the value it affords in patient populations where the

ability to perform more demanding cognitive tasks may be compromised (e.g. Alzheimer's disease, schizophrenia; Greicius, 2008). Indeed, differences between groups in resting-state functional connectivity are increasingly identified as potential biomarkers of disease or disorder, for example in epilepsy (Quraan, McCormick, Cohn, Valiante, & McAndrews, 2013) or schizophrenia (Arbabshirani et al., 2013). However, if functional connectivity and neural network measures are to be used as biomarkers in this way, it is important to determine whether these metrics are stable for each person over time in the absence of disease or disorder. In fMRI, the spatial pattern of RSNs has been demonstrated to show consistency and overlap across healthy individuals (Damoiseaux et al., 2006). Other fMRI work has also shown that RSNs exhibit spatial reproducibility over repeated scans (Braun et al., 2012; Meindl et al., 2010). There has also been some work investigating network and connectivity repeatability using MEG. One MEG study demonstrated, using a seed-based network analysis, that primary sensory RSNs exhibit topographical variability both within and between subjects, and this variability relates to within-network connectivity levels (Wens et al., 2014). Overall, however, individual variability in spatial pattern was found to be minimised by sufficient group averaging. Some studies have investigated repeatability of graph theory metrics in studying RSNs with MEG (Deuker et al., 2009; Jin, Seol, Kim, & Chung, 2011), but neither specifically consider repeatability of the underlying estimates of connectivity.

When considering the reproducibility of resting state network activity it is worth noting that there are many choices to made between a number of common approaches, even within a single pipeline. So, it is important to consider that small changes to the analysis pipeline may impact results. Trying to capture how different techniques can vary outcomes is key in order to enable comparison between studies in the literature. A recent comparison of twelve different connectivity estimation

methods for MEG found that power envelope correlations performed most consistently at group- and subject-level, ahead of other techniques including phase coupling measures (Colclough et al., 2016). Moreover, Tewarie et al (2014) suggest that similar estimates can be obtained from both phase lag index and amplitude envelope correlations.

2.2.3 Aims

This study had two key aims. Firstly, we examined the test-test repeatability of two different methods of characterising resting state network connectivity using MEG, namely the ICA analysis first described by Brookes et al (2011a) and an approach using the atlas-based beamformer described by Hillebrand et al (2012). Both methods use power envelope correlations but each approach expresses this estimate within a different context.

The second aim was to additionally compare small variations in parameters of the analysis pipeline and the impact, if any, these may have on results. This aim was examined using variations in only the second analysis approach with the atlas-guided beamformer, since there is typically more variation within this approach in the existing literature.

Ultimately we hoped to be able to establish, on the basis of these results, a preferential pipeline for connectivity analysis in subsequent experiments.

2.3 Methods

2.3.1 Subjects

Twenty-one healthy volunteers (6 males, 15 females; mean age 22 years, range 19-34 years) with normal or corrected-to-normal vision participated in the study after giving informed consent. All procedures were approved by the Cardiff University School of Psychology research ethics committee. All participants had a previously acquired structural MR scan (1mm isotropic FSPGR) that was used for source localisation.

2.3.2 Stimuli and Procedure

Subjects were seated upright in the MEG scanner inside a magnetically shielded room. For the resting state recording, subjects were instructed to maintain fixation on a red fixation spot whilst 600 seconds of data was recorded. The visual fixation point was displayed on a Mitsubishi Diamond Pro 2070 monitor (1024 pixels x 768 pixels resolution, 100Hz refresh rate). All stimulus delivery was controlled by Matlab software. The data were collected as part of a 45-minute scan, in which the resting-state recording was always completed first. The scan was repeated a second time for all participants, between 6 and 8 days later.

2.3.3 MEG Recordings

Whole-head MEG recordings were made using a CTF-Omega 275 channel system sampled at 1200Hz, and analysed in synthetic third-order gradiometer mode. An additional 29 reference channels were recorded for noise cancellation purposes. Four of the 275 channels were turned off due to excessive sensor noise. Eye movements and blinks were monitored using vertical and horizontal electrooculogram (EOG) recordings. To achieve MEG/MRI co-registration, electromagnetic coils were placed at fixed distances from anatomical landmarks (left and right periauricular, nasion) prior to the MEG recording, and localised inside the scanner before and after each

task. The fiduciary locations were verified using digital photographs and later marked on the anatomical MRI. Data recordings were acquired continuously.

2.3.4 Connectivity method 1: Independent Component Analysis

The data were divided offline into 2 second intervals. Trials containing artefacts including eye movements or excessive blinks were excluded from further analysis. For the first analysis, an independent component analysis (ICA) approach developed for use with MEG resting state data was applied (Brookes et al., 2011b; Hall et al., 2013). An outline of this pipeline is shown in Figure 2-1.

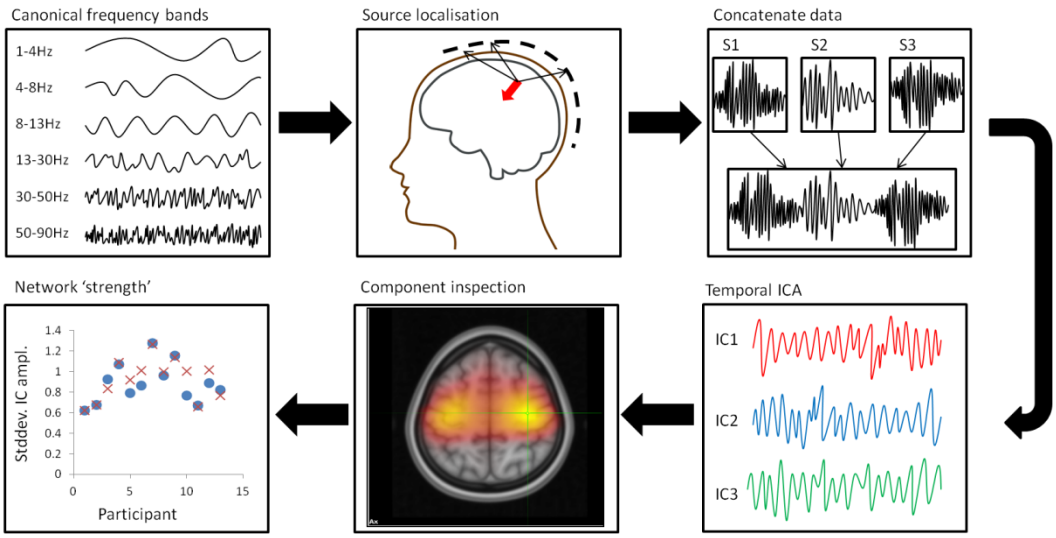

Figure 2-1. Brief outline of the ICA analysis pipeline. Band-filtered data are source estimated using a beamformer. Data from all subjects and sessions is concatenated prior to temporal ICA. Resulting components are inspected for plausibility, and the standard deviation of component amplitude for each subject and recording session is used as a measure of network strength.

Data were filtered into 6 frequency bands: 1-4, 4-8, 8-13, 13-30, 30-50, and 50-90Hz. These band limits are consistent with previous work investigating resting state MEG (Brookes et al., 2011a; Hall et al., 2013; Muthukumaraswamy et al., 2013b). A synthetic aperture magnetometry (SAM) beamformer algorithm (Vrba & Robinson, 2001) was used to generate source space signals for each subject and session in each

of the frequency bands given above. For the first analysis, assessing the stability of network activity over time, the virtual-sensor timeseries at each voxel was first calculated for each subject, session and frequency range separately. The individual 2s trials are concatenated together to give a single virtual-sensor timeseries that lasts for the whole experimental session. A Hilbert transform is applied to each timeseries, in order to generate the analytic signal and then extract the amplitude envelopes for each virtual sensor (Brookes et al., 2011b; Swettenham, Muthukumaraswamy, & Singh, 2009). These amplitude envelopes are temporally down-sampled to 1s, both for computational efficiency and because most of the correlated network structure arises from slower timescales than this (Brookes et al., 2011b; Hipp et al., 2012). For all subjects and sessions, these amplitude timeseries were then concatenated together at each voxel, for each frequency band separately. A temporal ICA analysis was then applied to the concatenated data to derive 15 independent components for each frequency band. The spatial pattern of these components indicate a series of areas that show strong amplitude-amplitude coupling over the recording time and are thus assumed to be functionally connected.

We produced high resolution images of each component for each frequency band in standard space. These images were examined in order to identify existing resting state networks (RSNs). Both the sensorimotor network and visual network seen in previous work were robustly evident in the 13-30Hz band, and were chosen as an exemplar to assess stability and repeatability for each subject. The standard deviation of each component's amplitude was subsequently used as a proxy for network strength.

To assess overall repeatability of the network collapsed across subjects, the standard deviation was computed for session 1 and session 2 separately. To assess

repeatability for each subject, a one-step forward moving window (20 samples in size) was used to generate standard deviations from the component amplitude data for each subject and session, up to 600 values per session (less bad trials). A bootstrapping approach (10,000 bootstrapped means) was then used to derive confidence intervals for the standard deviations for each subject and session. This approach allows assessment of stability of the network for each subject and session whilst minimising the effect of outliers in the data.

2.3.5 Connectivity method 2: Atlas-based analysis

For the second method, we used an atlas based beamformer approach (Hillebrand et al., 2012) to estimate power envelope correlations across the whole brain, and varied two parameters in order to test the effects of methodological manipulations on the experimental outcomes. A brief outline of the analysis steps along with the parameter manipulations used in this comparison can be found in Figure 2-2.

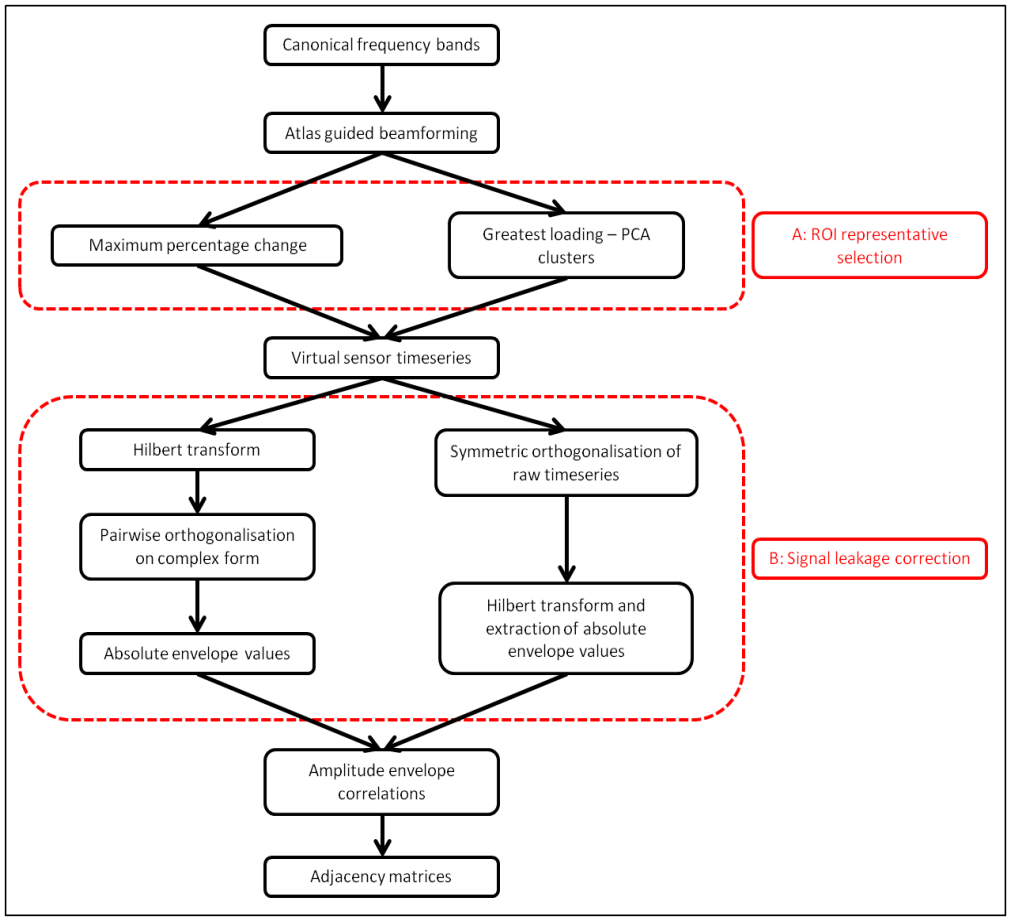

Figure 2-2. Brief outline of the atlas-based connectivity pipeline. Data is filtered into frequency bands and an atlas guided beamformer approach (90 regions) is applied for source localisation. Source space connectivity is estimated using amplitude-amplitude correlation in each of the atlas regions, to create a connectivity matrix for each individual. We additionally conducted a 4-way comparison to test the effects of 2 parameter variations at point A (ROI representative selection) and B (leakage correction) on the resulting adjacency matrices.

For this analysis, we used the pre-processed data as outlined in the previous analysis, and first applied a series of LCMV beamformers implemented in Fieldtrip (Oostenveld et al., 2011) to reconstruct sources on a 6mm grid, in the same six frequency bands as used previously: 1-4Hz, 4-8Hz, 8-13Hz, 13-30Hz, 30-50Hz and 50-90Hz. As with the ICA pipeline, the individual 2s trials are concatenated together to give a continuous virtual-sensor timeseries for the whole experimental session. These source-estimated timeseries, in each frequency band, were then parcellated into 90 ROIs

based on the automatic anatomical labelling (AAL) atlas (Hillebrand et al., 2012). At this stage, we incorporated out first parameter manipulation in the choice of the representative timeseries for each ROI. The first alternative was to use the timecourse of the single voxel, within each ROI, that had the highest average percentage power change across the recording, similarly to choosing a peak voxel. In the second alternative, we performed Principal Components Analysis (PCA), of all ROI timecourses to generate the number of components which explain 95% of the power variance in the ROI. Typically this yields around 250-300 virtual sensors, compared to 90 for the peak-voxel approach.

We then make our second methodological decision. Due to the ill-posed inverse problem, the timecourses for multiple sources may co-vary as a result of signal leakage, giving rise to spurious connectivity (O'Neill et al., 2015). Here, we choose between two approaches to correct for this. The first, pairwise orthogonalisation, is done during the connectivity estimation stage and removes zero lag correlations between each pair of sensors (Hipp et al., 2012). A Hilbert transform is performed on the virtual sensor timeseries, and the complex form of the analytic signal is used to calculate the relative phase of each pair of sources in order to remove zero-lagged signal (Hipp et al., 2012). For the second alternative, we applied a multivariate extension to the former, termed symmetric orthogonalisation (Colclough et al., 2015). This two step approach first finds the set of orthonormal vectors that are closest to the original ROI timecourses. Then, the magnitude and orientation of these vectors is iteratively adjusted to reach a corrected solution that varies minimally from the original uncorrected timecourses. Ultimately, this produces a mutually orthogonal set of timecourses for the included ROIs where zero-lag correlations have been removed and remaining correlations are assumed to reflect true biological coupling (Colclough et al., 2015). The Hilbert transform is then computed on these

orthogonalised timecourses and the amplitude envelope extracted (Colclough et al., 2015).

The amplitude envelopes were then cross-correlated to derive a connectivity matrix based on amplitude coupling across ROIs. At this stage, if PCA timecourse selection was used, we need to reduce the size of the correlation matrices to 90x90 so that they can be combined across participants and sessions. This is done, for each pair of 90 ROIs, by picking the peak correlation measure between any pair of voxels within the two ROIs. Correlation coefficients within this final matrix, for each dataset, were then transformed to a normalised z-scores using Fisher's transform and an estimate of the effective degrees of freedom from the raw timeseries. These normalised z-scores are then suitable for taking forward for statistical analyses.

For the comparison of parameter manipulations, we used all possible combinations so that for each participant and scan session, we produced 4 adjacency matrices (Table 2-1).

		Condition			
		MC-PO	PCA-PO	MC-SO	PCA-SO
ROI Representative	Max. change	✓		✓	
	PCA		✓		✓
Leakage correction	Pairwise	✓	✓		
	Symmetric			✓	✓

Table 2-1. Comparison of parameter variations in the atlas-based connectivity approach. For each participant, we generated four connectivity matrices based on all possible combinations of the two alternatives at each stage of manipulation.

2.4 Results

2.4.1 Repeatability of ICA network activity

From the 8 RSNs extracted in the seminal paper using this ICA method (Brookes et al., 2011b), the sensorimotor and visual networks in the beta band (13-30Hz) were the most unambiguously identified from the present data. As mentioned above, these networks were consequently chosen as exemplars to assess stability and repeatability across sessions and for each individual.

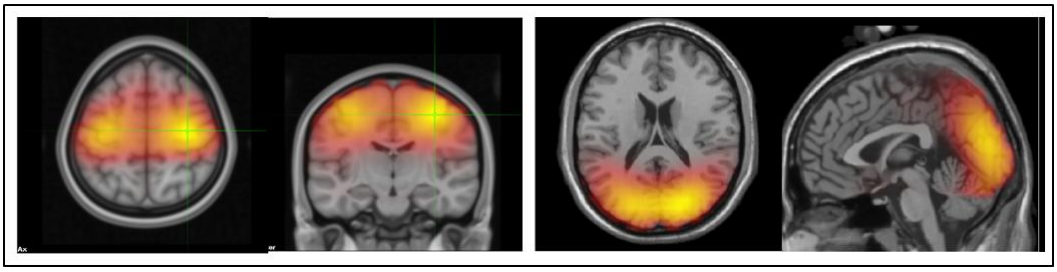

Figure 2-3. Spatial maps of the sensorimotor (left) and visual (right) network components re-constructed in the beta band (13-30Hz) using ICA.

The mean network strength and standard deviation for each component and session is shown in Table 2-2. A paired t-test on the component means confirmed that the differences between the two sessions were non-significant (Sensorimotor network: t(20)=0.1251, p>0.05, Visual network: t(20)=0,p>0.05).

	Sensorimotor Network		Visual Network	
	Session 1	**Session 2**	**Session 1**	**Session 2**
Mean	**0.95**	**1.01**	0.97	0.95
Std Dev	**0.22**	**0.20**	0.31	0.29

Table 2-2. Component means and standard deviations (std dev) for each component and recording session, collapsed across subjects. Units are nAm.

In order to assess inter- and intra-individual variability in network strength and stability of the network over each 10-minute recording session, a moving window was applied to each individual timeseries (subject and session). This calculated the standard deviation of 20 chunks of the timeseries at a time, then moved on one sample and repeated the calculation until the number of standard deviation values was equal to the original number of samples in the timeseries (range 460-600). This approach allowed calculation of a mean standard deviation of power (hereto referred to as the 'network strength') for each timeseries, and was necessary in order to use bootstrapping to derive confidence intervals. The outcomes of this process for both networks and sessions for each individual are plot in Figure 2-4. Both the sensorimotor and visual networks show considerable inter-individual variability in the index of strength, with the lowest and highest individuals differing by a factor of approximately 3 in each component. Conversely, there is very little intra-individual variation from session to session. Intraclass correlation coefficients (ICCs) were used to assess repeatability. The ICC for the sensorimotor network was 0.959, and for the visual network was 0.938. ICCs above 0.75 are considered excellent agreement (Cicchetti, 1994). Thus, the ICCs for both networks indicate a high level of consistency in the network activity over time. The confidence intervals are generally small and clustered about the mean for each session, indicating that the network strength was stable for each person over each 10-minute recording.

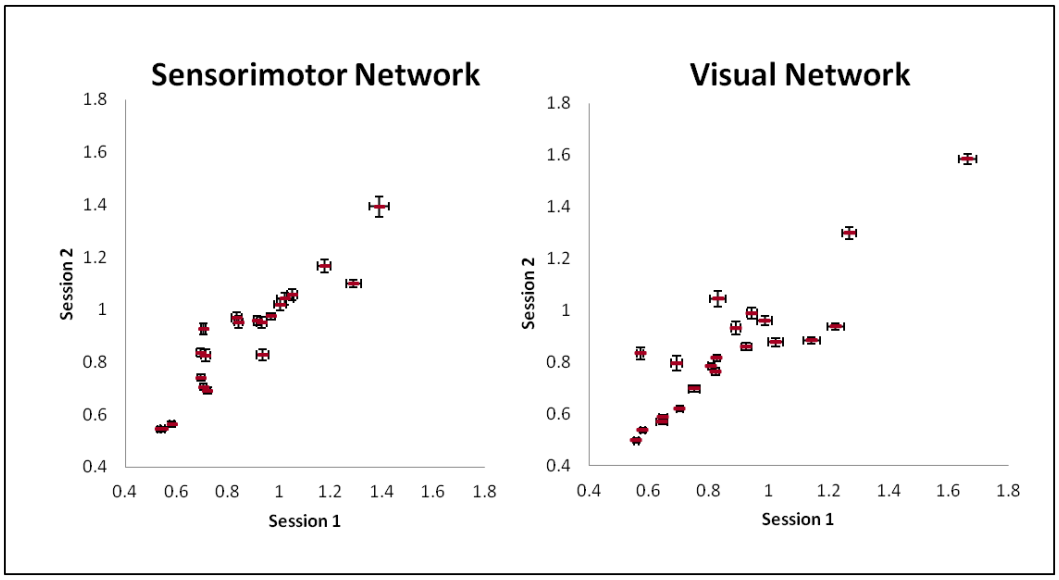

Figure 2-4. Temporal standard deviation of the amplitude envelope (network activity) in the sensorimotor (left) and visual (right) network components, for each individual. In both cases, session one is plot against session two to show the strength of repeatability for each individual over time.

To examine any potential influence of head geometry on network strength, the standard deviation of power in each component was subsequently correlated with two indices for brain size - 1) the intracranial volume extracted using FreeSurfer from the anatomical MRI, and 2) the Euclidean distance from left to right periauricular fiducial points. Neither index correlated with activity in the RSNs (see Table 2-3**).**

	Sensorimotor Network		Visual Network	
	Session 1	**Session 2**	**Session 1**	**Session 2**
ICV	**0.0468**	**0.2100**	**0.1712**	**0.3634**
Head Size	**0.0851**	**0.0253**	**0.0703**	**0.1731**

Table 2-3. Correlations (Pearson's r) of activity in the sensorimotor and visual networks (for session 1 and 2) with two structural indices - intracranial volume (ICV) and left-right fiducial distance (head size). All correlations were non-significant at α =0.05.

In order to further rule out any artefacts in the analysis method as an explanation for the repeatability results, we also correlated activity levels between the two networks and sessions (Figure 2-5**) and found no significant correlations.**

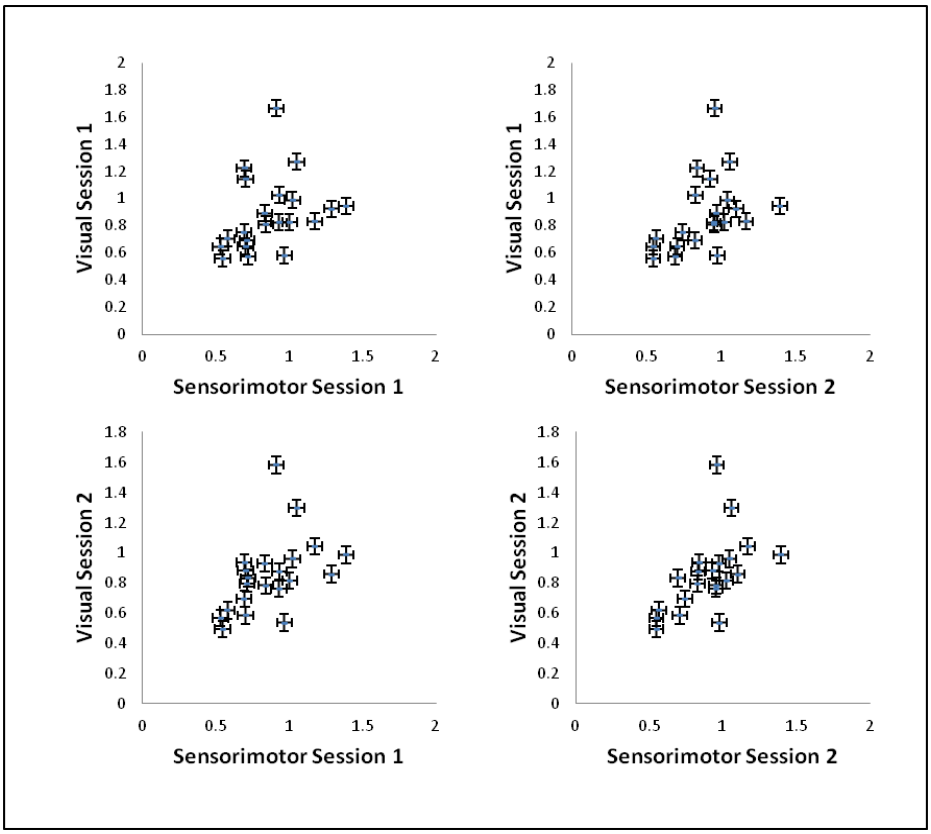

Figure 2-5. Cross-plots of network activity correlations between the two networks for all combinations of sessions. None of these correlations were significant at α=0.05.

Lastly, we correlated network activity with a measure of the magnitude of the beamformer weights multiplied by noise in order to ensure that no bias was introduced during weights normalisation prior to the ICA (Table 2-4**), and again the results of these correlations were not significant.**

	Sensorimotor Network		**Visual Network**	
	Session 1	**Session 2**	**Session 1**	**Session 2**
Weights*Noise	0.13	0.04	0.29	0.28

Table 2-4. Correlations (Pearson's r) between activity in each network and session and the respective session beamformer weight*noise measure. None were significant at α=0.05.

2.4.2 Effect of parameter variations on atlas based network activity

For the atlas-based connectivity method, we first considered the effect of small parameter manipulations on connectivity estimates. This yielded four conditions: maximum change with pairwise orthogonalisation (MC-PO), PCA with pairwise orthogonalisation (PCA-PO), maximum change with symmetric orthogonalisation (MC-SO) and PCA with symmetric orthogonalisation (PCA-SO). In contrast to the ICA method, the atlas-based connectivity technique estimates connectivity across the whole brain using a single representative timeseries for each of the 90 AAL ROIs. These connectivity values can be plot in a 90x90 matrix where each point represents the correlation value between a pair of regions (Figure 2-6). Stronger orange colouration in the matrix is indicative of increased connectivity between a pair of regions.

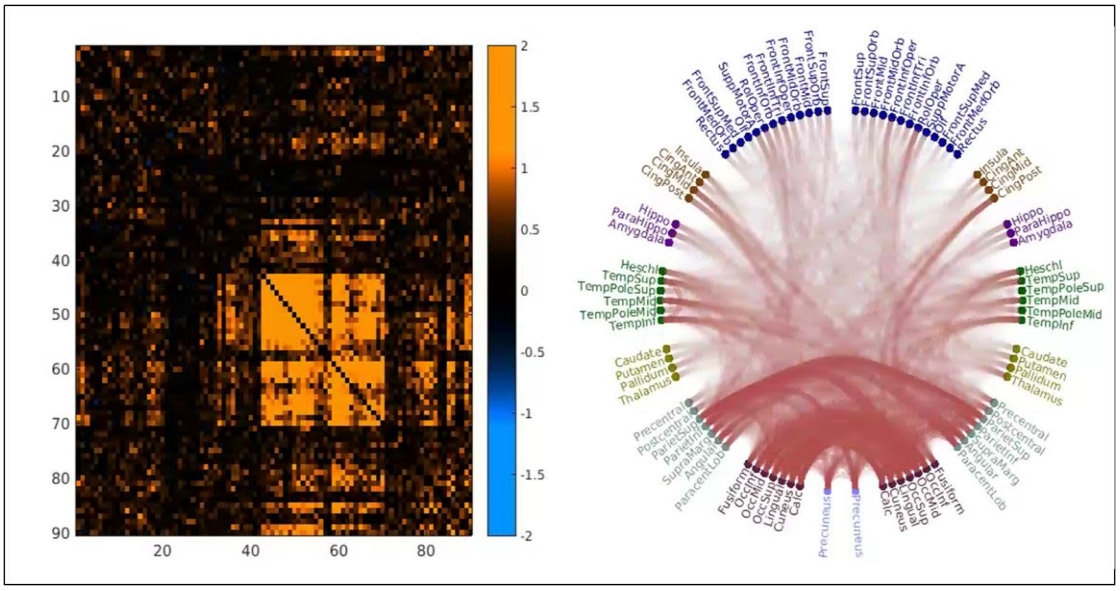

Figure 2-6. Examples of the plots used throughout this thesis to display connectivity matrices. The map shown is the first session of the MC-SO condition in the alpha band (8-13Hz). In the adjacency matrix (left), the 90 AAL regions are plotted along both the X

and Y axes, and each element in the matrix represents the amplitude coupling between the two given regions. Stronger orange colouration indicates a stronger positive correlation between two regions. The same connectivity data is shown in a different way, using a circular network plot that uses neuroanatomical information to give a more structurally organised representation (right). Positive connections between regions are plotted as a red line and increased line opacity indicates a stronger connection between two regions. In this case, the strongest correlation structure can be seen in parietal and occipital areas. Please note that the ROI order here is consistent with other figures in this chapter and throughout the remaining chapters of this thesis.

The adjacency matrices for each parameter variation condition can be seen in Figure 2-7. A densely connected 'hub' corresponding to parietal and occipital areas is evident in the alpha and beta bands. There is little clear structure in the gamma matrices in any condition. In general, symmetric orthogonalisation yields more spatially structured matrices, but the combination of PCA for virtual sensors and symmetric orthogonalisation leads to poorly resolved connectivity structures.

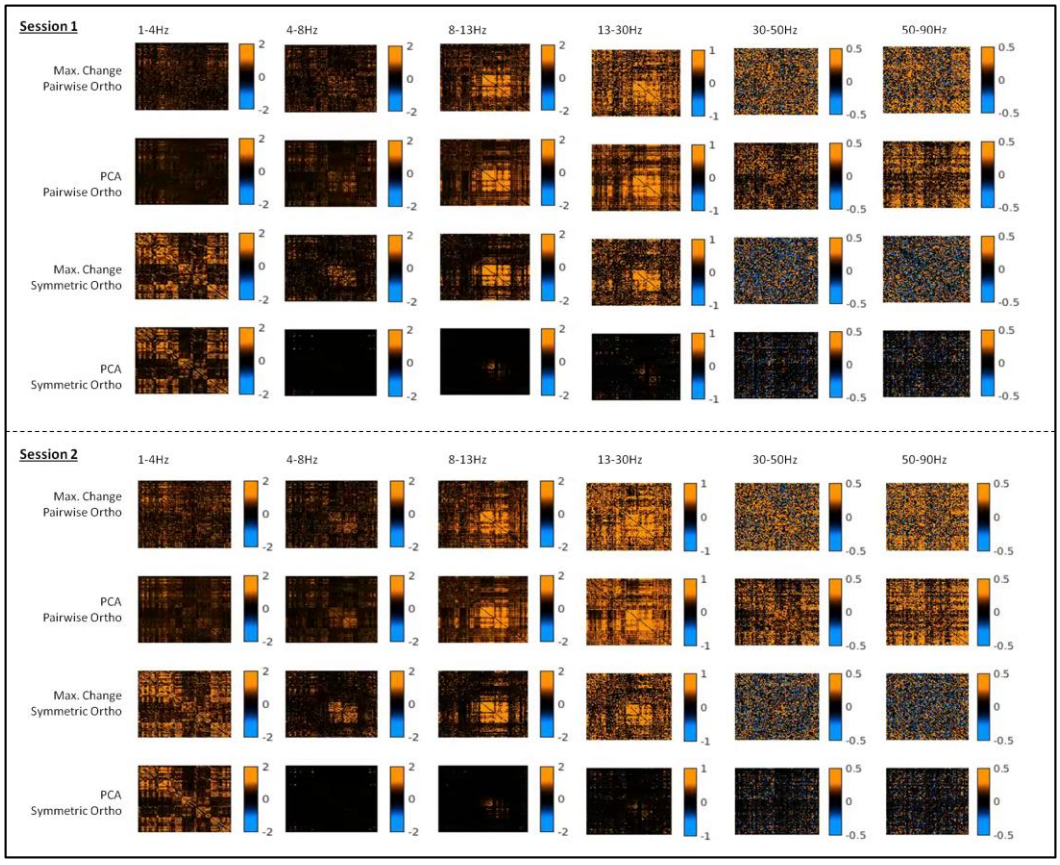

Figure 2-7. Average connectivity matrices for each of the parameter variation conditions and frequency bands, for scan session 1 (top) and scan session 2 (bottom). The 90 AAL regions are plotted along both the X and Y axes, and each element in the matrix represents the amplitude coupling between the two given regions. The matrices for all conditions within a given frequency band are plotted at the same scale for ease of comparison.

In order to reduce noise and aid interpretation, we chose to threshold the adjacency matrices using a bootstrapping procedure across participants. We combined the band limited matrices for session one and two together, and ran 10,000 permutations in order to create a binary mask, including only those connections that were present within the top 5% of connections for 95% of the bootstrap iterations. The thresholded matrices further highlight a strong occipito-parietal connectivity profile in the alpha and beta bands across all conditions, except PCA-SO (Figure 2-8). No connections in the high gamma band and only one frontal connection in the low gamma band survive the thresholding procedure following symmetric orthogonalisation. A relatively higher number of suprathreshold connections can be seen in both the low and high gamma bands following pairwise orthogonalisation.

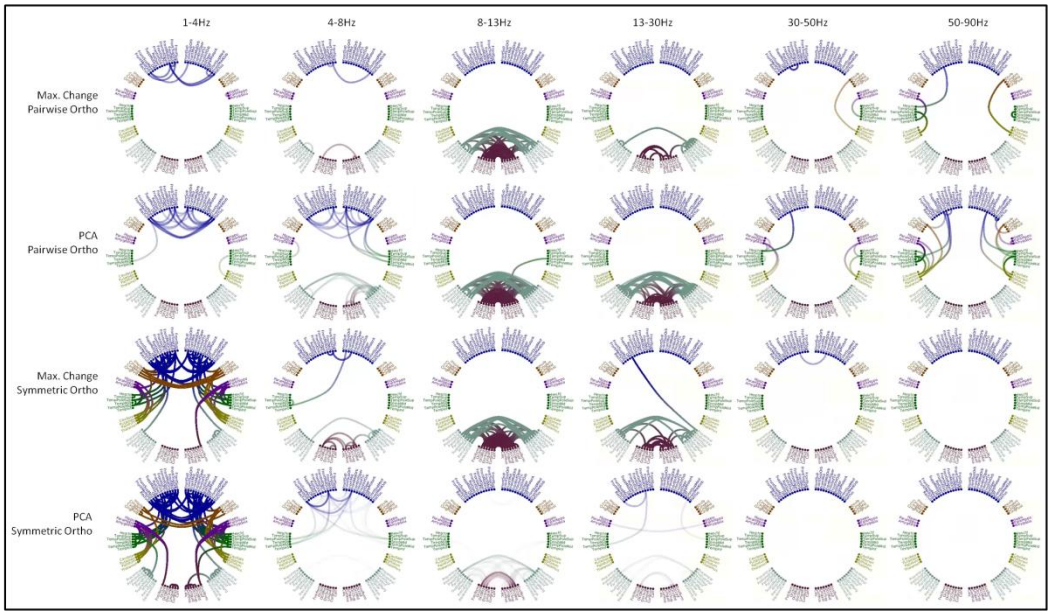

Figure 2-8. Thresholded connectivity maps for each of the four conditions and six frequency bands. AAL areas are split left/right, and grouped around the plot from frontal regions (top), through cingulate cortex, temporal lobe, basal ganglia, sensorimotor regions, occipital cortex and precuneus (bottom). Each line represents a connection that falls within the top 5% of strongest connections for 90% of bootstrap iterations, and increased opacity indicates a stronger connection. For display and ease of comparison, the scaling for all conditions within a frequency band is the same but varies across bands.

2.4.3 Repeatability of atlas based network activity

As well as comparing differences between pipeline conditions, we assessed the repeatability of these AAL-based connectivity methods between sessions. To this end, we summed across the rows of the thresholded z-matrix to extract a single representation of connectedness for every AAL region (herein called connection strength). Global connection strength is plot in Figure 2-9, and shows that the distribution of connection strength is somewhat variable between participants, but measures of central tendency show good agreement between sessions. In order to test formally for group-level differences in connectivity between sessions, we conducted a randomisation test (10,000 permutations) on the connection strength and found no statistical differences between sessions, for any frequency band or condition (at α=0.05).

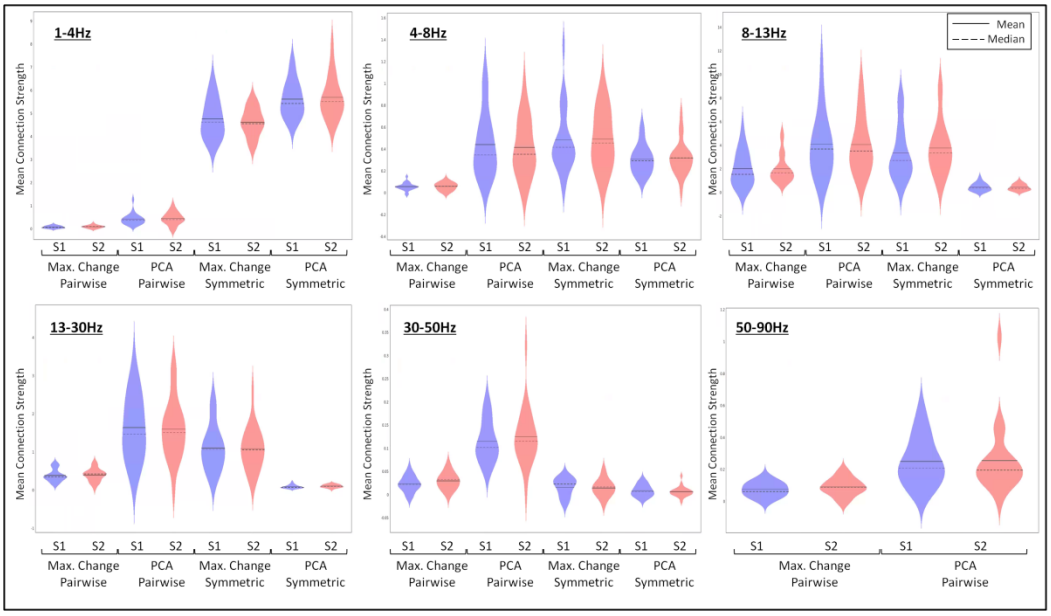

Figure 2-9. Violin plots showing global connection strength across sessions and conditions, for each of the frequency bands studied. Two plots are absent from the 50-90Hz range due to the fact that no connections survived thresholding in the high gamma band following symmetric orthogonalisation. The connection strength indicates how connected any given AAL region is to all other regions in the adjacency matrix - here we plot the mean of this measure for each participant, in all of the frequency bands and conditions studied. There were no significant statistical differences between sessions, for any frequency band or condition.

Having established stability between sessions at the group level for the AAL connectivity methods, we also wanted to examine test-retest consistency of individual subject estimates. To this end, we calculated ICCs (3,1) using the mean connection strength for each participant in session one and session two. We found the highest absolute agreement in connectivity estimates in the alpha, beta and theta bands for each condition, along with poor agreement across delta and gamma bands (Table 2-5).

	MC-PO	**PCA-PO**	**MC-SO**	**PCA-SO**
Delta	0	0.4	0.18	0.57

Theta	0.65	0.7	0.71	0.35
Alpha	0.75	0.8	0.81	0.71
Beta	0.74	0.77	0.71	0.57
Low Gamma	0	0.07	0.21	0.004
High Gamma	0.47	0.6	n/a	n/a

Table 2-5. ICC values for each condition and frequency band. A field containing 'n/a' denotes that either no connections survived thresholding, and a field containing 0 indicates that the scale was unreliable. Values less than 0.40 are considered poor agreement, 0.41-0.59 indicate fair agreement, between 0.6 and 0.74 are considered good agreement, and values above 0.75 are considered excellent agreement (Cicchetti, 1994).

As in the ICA analysis, we also examined the potential effects of head geometry on network activity. Here, we correlated the mean connection strength with both the intracranial volume and the Euclidean distance between left and right preauricular fiducial points (head size), for each condition and frequency band. There were no significant correlations (at α=0.05) between mean connection strength and head geometry, for any condition or frequency band. A full table of Pearson's r values can be found in Appendix A.

2.5 Discussion

2.5.1 Repeatability of ICA-derived RSNs

The current study examined the test-retest repeatability of two different approaches to assessing amplitude coupling using MEG data. The results of the first method, using temporal ICA to derive spatial network patterns, suggest that there is some

degree of variability between individuals but also that the strength of network activity for each individual is stable over a ten minute recording period. Furthermore, these results show good repeatability on two sessions taken one week apart. Activity within the networks does not correlate with metrics of head geometry, and cannot be accounted for by potential bias in beamformer weighting over sessions.

Determining the stability of RSNs in the absence of illness is of key importance in using networks as a marker of presence, progression or treatment of disease or disorder. However it is similarly important due to the novelty of analyses in this area, to validate and replicate the findings of new network techniques. Here, we found that the mean strength of both networks studied was reproducible over two recording sessions. This is in line with the results from another study showing that MEG-ICA derived networks are stable over different recording sessions and tasks (Brookes et al., 2012), and provides indication that the recording technique is robust.

However, the ICA analysis results also illustrate variation between individuals in the strength of activity, for both the sensorimotor and visual network. One existing MEG study also demonstrated inter-individual variability in within-network connectivity levels (using seed-based networks), that was related to individual variation in topography of the RSNs (Wens et al., 2014). In our ICA analysis we were concerned with spectral properties of the networks, and so did not examine the spatial similarities between individual network topologies and the RSN generated from the group data. So, it is possible that the RSNs explored here may show individual variation in topography as reported by Wens et al, and more investigation would be required to extrapolate the link between spatial topography and activity within the RSNs further. It is also worth noting that in the previous work the effects of individual variation on network topography were substantially reduced by averaging

over ≥12 subjects (Wens et al., 2014), and the present study used almost double this subject threshold to generate RSN maps.

2.5.2 Atlas-based approach to whole-brain connectivity

Similarly to the ICA analysis, the results of the second method using an atlas-guided approach to estimate whole brain connectivity matrices show, in general, good test-retest reproducibility that is minimally affected by choice of representative virtual sensor for the ROIs and the signal leakage correction method. We additionally found that regardless of small variations in the analysis pipeline, the alpha and beta bands show the strongest connectivity structure over occipital and parietal areas. This is consistent with a number of studies finding evidence of a so-called 'rich club' in both structural and functional networks (Grayson et al., 2014; van den Heuvel & Sporns, 2011).

The current study adds to a small number of MEG studies that have previously examined the repeatability of resting-state networks. One study compared four connectivity estimates in MEG and concluded that reliability was dependent on the metric being used and frequency band being studied, with amplitude envelope correlation showing greatest reliability in the beta band (Garces et al., 2016). The strong ICC values observed in the alpha and beta bands in the present study are in accordance with these findings. Another comprehensive study suggested that amplitude envelope correlations performed best among 12 functional connectivity estimates in terms of group-level repeatability, single-subject reliability and between-subject consistency (Colclough et al., 2016). In the present study, we did not compare envelope correlations with other connectivity methods. Nevertheless, our findings of no significant group-level differences between sessions along with moderate

distribution of connectivity between subjects and good intra-subject consistency are in agreement with Colclough et al.

2.5.3 Settling on the most appropriate pipeline for the present work

When comparing between the methods used here, there are several considerations to be made. Firstly, the ICA pipeline described here includes no signal leakage correction. Although we show using the AAL approach that there is little variation between orthogonalisation techniques, previous work has shown that non-corrected power envelope correlations exhibit a higher level of repeatability than those with correction applied (Colclough et al., 2016). This suggests that highly repeatable signal leakage may be contributing somewhat to the repeatability observed in the ICA network activity. On a related note, the ICA analysis reconstructs source activity at a large number of cortical locations over the chosen grid. There is some evidence that this makes subsequent connectivity analysis more prone to field spread, even if leakage correction is done by removing zero lag correlations (Schoffelen & Gross, 2009). Finally, using the ICA approach, one must visually inspect the resulting components in order to decide which is biologically plausible and/or interesting given a particular research question. In contrast, the AAL approach requires no subjective interpretation of components and the thresholding procedure offers a data-driven approach to reducing noise or spurious connectivity in the whole-brain connectivity matrices. Taken together, these observations indicate that atlas-based methods, such as the AAL, offers a more suitable approach to estimation of whole brain resting-state connectivity, for the purposes of this thesis.

We did not investigate every possible parameter variation in the AAL pipeline. However, those we did use had minimal effect on resulting connectivity matrices, with one key exception. In the PCA-SO condition, connectivity matrices were poorly

resolved, even for connections that were strongly visible in all other conditions. There may be a number of potential reasons for this. The initial matrix derived from the PCA selection is much larger than the end 90x90 output (approximately 270-300 sensors). Further, each of the 90 'tiles' (clusters of virtual sensors explaining variance in that region) in the initial matrix derived from the PCA is self-orthogonalised. We suggest that the combination of these factors result in reduced signal-noise ratio and limit the degrees of freedom such that the symmetric orthogonalisation algorithm cannot simultaneously orthogonalise the required number of timeseries.

This anomaly notwithstanding, symmetric orthogonalisation resulted in more spatially resolved, or less 'noisy', matrices. This difference seems reasonable given that the pairwise orthogonalisation corrects timecourses in a pairwise fashion and so does not take into account secondary correlations between areas. Further, more connections in the gamma bands survived thresholding following pairwise orthogonalisation compared to symmetric orthogonalisation. Connectivity in the gamma band is known to have the highest potential for contamination by muscle artefacts (Muthukumaraswamy, 2013). Moreover, in simulations the symmetric orthogonalisation performs more efficiently in terms of minimising spurious correlations (Colclough et al., 2015). Therefore it is prudent to use symmetric orthogonalisation in subsequent analyses. The combination of PCA virtual sensor selection and symmetric orthogonalisation did not perform well, as discussed above. If this alone were not reason enough to elect to use the voxel of maximum change in subsequent analysis, we also note that for pairwise orthogonalisation, using the voxel of maximum percentage change performed equivalently with constructing virtual sensors based on PCA for maximal variance. Further, the former is more computationally efficient so it is reasonable to select the voxel of maximum percentage change as the ROI representative for subsequent analyses.

2.6 **Conclusion**

The study of inter- and intra-individual differences in cortical oscillations is gaining pace and links to fundamental questions in psychology and medicine about how and why humans differ from one another. Here we have presented results to suggest that the strength of activity in RSNs exhibits stability over repeated sessions, using both ICA and atlas-based approaches to assess amplitude coupling across the brain. These results add to a growing body of literature suggesting that RSNs represent a trait marker of function and may be used in a valid way as biomarkers of neurological disease and neuropsychiatric disorder. Based on the results of the current study and discussion above we elect to use the atlas-based connectivity approach, with maximum percentage change virtual sensors for each ROI and symmetric orthogonalisation leakage correction, in the subsequent experiments of this thesis.

3 Comparing MEG and fMRI resting-state connectivity in a normative database

3.1 Abstract

There are multiple neuroimaging modalities that can be used to investigate the functional interactions between brain regions in RSNs. Recent methodological advances mean that neurophysiological techniques such as magnetoencephalography (MEG) are increasingly used to investigate neural networks, but functional magnetic resonance imaging (fMRI) remains the method most typically used to study functional connectivity. Each modality has strengths and weaknesses but both are used, often independently, in attempts to understand altered connectivity patterns in neurological diseases and neuropsychiatric disorders. A good understanding of the relationship between connectivity measures derived using different modalities is crucial to help build a comprehensive picture of any particular pathology. Using a combined MEG and fMRI approach can further allow insight into the process and variations of neurovascular coupling. In the previous experiment, we established the test-retest reliability of a connectivity analysis pipeline that uses an atlas-based source reconstruction and leakage corrected amplitude coupling estimates. Here, we apply this pipeline to a larger normative dataset in attempts to replicate the previous findings, and compare MEG resting-state amplitude-amplitude connectivity with connectivity estimates derived using fMRI.

3.2 Introduction

3.2.1 The relationship between the MEG and BOLD-fMRI signals

The phrase 'neural activity' is a nonspecific term encompassing a complex series of events that give rise to measurable signals for multiple neuroimaging techniques. Methodological advances in recent years mean that researchers have unprecedented access to study, non-invasively, the mechanisms of human brain function. Conducting multi-modal comparisons helps to construct a more rounded understanding of how signals in the two modalities co-vary and what this may mean in terms of studying a particular behaviour, cognition or clinical population.

An overview of the technical and neurophysiological basis of MEG is given in chapter one of this thesis. The MEG signal is assumed to arise from post-synaptic current flow in pyramidal cells of the cortex (Hämäläinen et al., 1993). These primary current dipoles reflect mass coherent activity from thousands of neurons, and give rise to magnetic field components that can be measured at the scalp using MEG. This theory is supported by a body of literature comparing MEG with invasive recordings at different spatial scales. For example, one study compared MEG with simultaneous electrophysiology in monkey cortex during stimulation of primary somatosensory cortex (Zhu et al., 2009). The authors found that the intensity and latency of the MEG signal in response to stimulation was best correlated with local field potentials (LFPs), that are believed to reflect summed excitatory and inhibitory post-synaptic potentials.

The idea that cerebral blood flow could be related to cellular activity was first recorded in the late 1800's (Sandrone et al., 2014). From the first fMRI scan using blood as an endogenous contrast agent (Ogawa, Lee, Kay, & Tank, 1990), the blood oxygenation level dependent (BOLD) response has become one of the most common

image contrasts used in fMRI. The BOLD response depends on differences in blood flow and oxygenation when a region of the brain is in an activated compared to a baseline state. The activated state is associated with increased cerebral blood flow (CBF), increased cerebral blood volume (CBV) and a decrease in cerebral metabolic rate of oxygen ($CMRO_2$). The net effect is greater uniformity of magnetic field around the vessels and thus increased image contrast (Ogawa et al., 1990).

The relationship between BOLD and cellular activation (neurovascular coupling) has been modelled, but the mechanism is yet to be fully understood. Using simultaneous invasive electrophysiology and BOLD-fMRI in monkey cortex, Logothetis et al, (2001) found that the BOLD response best correlated with LFP recordings in the gamma band, rather than firing rates or spiking (i.e. multi-unit activity - MUA). Negative correlations between low frequency LFPs and BOLD, along with positive correlations between high frequency LFPs and BOLD have also been shown in invasive studies (Mukamel et al., 2005). In one example, the authors showed that the BOLD-LFP coupling varies according to frequency band, with positive BOLD-LFP correlations in the gamma band and negative correlations in the beta band (Conner, Ellmore, Pieters, DiSano, & Tandon, 2011). Previous studies have also specifically investigated the correspondence between the BOLD and MEG signals, and these generally mirror the findings from invasive electrophysiology (Singh, Barnes, Hillebrand, Forde, & Williams, 2002; Zumer, Brookes, Stevenson, Francis, & Morris, 2010). However, a number of studies have also shown nonlinearity in the relationship between synaptic activity and hemodynamic responses (Devonshire et al., 2012; Hewson-Stoate, Jones, Martindale, Berwick, & Mayhew, 2005; Sheth et al., 2004), suggesting that a monotonic increase in BOLD signal area or magnitude does not necessarily correspond to an in increase in neuronal activity.

3.2.2 Measuring resting-state connectivity in MEG and fMRI

Given the popularity of resting-state connectivity in both the MEG and fMRI fields during recent years, relatively few studies have specifically investigated the relationship between resting-state connectivity as measured in fMRI and MEG. That said, a number of studies have shown that RSNs derived in fMRI and MEG show good spatial concordance. In one of the first examples, de Pasquale and colleagues (2010) showed using a seed-based approach that the dorsal attention network (DAN) and default mode network (DMN) are most prevalent in the theta-beta ranges and show a similar topography to RSNs obtained using the same seed regions in fMRI. Spatial similarities between eight fMRI RSNs and independently generated MEG RSNs in the beta band was also shown using the ICA analysis applied in the previous chapter (Brookes et al., 2011b). In terms of whole brain connectivity, there is also evidence, from both fMRI and MEG, for the presence of a hub of increased connectivity in occipital and parietal regions at rest (Grayson et al., 2014; Tewarie et al., 2014). The findings in the previous experimental chapter are consistent with this notion in MEG.

The suggestion that BOLD RSNs have frequency specific relationships with RSNs measured from MEG is consistent with the framework for the function of oscillations proposed by Donner and Siegel (2011), in which it is suggested that functional integration is associated with diverse local and long-range cortical interactions in the beta band. It should be noted that it is possible that networks in the beta-band are biased by increased signal-to-noise ratio (SNR) in that band (Hall, Robson, Morris, & Brookes, 2014). Hipp and Siegel (2015) found the strongest relationship with fMRI connectivity in the alpha and beta bands, but following correction for SNR a more broadband relationship emerged. This notwithstanding, it may be the case that fMRI RSNs are best represented by some combination of band-limited MEG connectivity.

Although similarities exist between the spatial patterns of resting-state connectivity in MEG and fMRI, there are also some differences between the two modalities. In the paper by de Pasquale et al (2010), MEG RSNs were generated using seed regions derived from fMRI RSNs, and though they showed spatial similarities, the correlation was confined in the MEG to the hemisphere ipsilateral to the seed. Strong connectivity between homologous regions in opposite hemispheres is often reported in fMRI (Guo et al., 2013; Salvador, Suckling, Schwarzbauer, & Bullmore, 2005). Conversely, this type of homotopic connectivity is rarely reported in MEG (Tewarie et al., 2014). One of the difficulties in directly comparing MEG with fMRI connectivity is inherent disparity in spatial resolution between the techniques. Using high-field MRI, it is possible to detect activity on a sub-mm scale (Yacoub, Harel, & Ugurbil, 2008), whereas MEG is limited at best to 2-3mm (Hämäläinen et al., 1993) and in practice may not perform this well, particularly for deeper sources. One way to overcome these differences in spatial smoothness is to use the atlas based reconstruction described in the previous chapter (Hillebrand et al., 2012) to provide a common spatial framework from both the FMRI and MEG datasets.

3.2.3 Aims

The first aim of the present study was to replicate the MEG findings shown in the previous chapter in a larger independent cohort. Specifically, we wanted to determine whether the presence of increased connectivity structures in occipital and parietal areas is robust across datasets and validate the pipeline choices made on the basis of the previous results.

The second aim was to compare the connectivity matrices derived from MEG data with connectivity matrices derived from fMRI in the same cohort. We wanted to build

on previous work to determine how we can use MEG connectivity to best predict fMRI connectivity.

3.3 Methods and Materials

3.3.1 Participants

The data presented were collected at Cardiff University as part of the UK MEG Partnership (UKMP). The UKMP is a collaborative, multi-site project whose aims include development of a national normative database of resting-state and task related MEG data. We scanned 88 individuals (27 male/61 female) with a mean age of 25.5 (range 18-55). All participants were right-handed, had normal or corrected-to-normal vision, and had no personal history of neurological or neuropsychiatric disorder. The study was approved by the relevant ethics committee and all volunteers gave written informed consent prior to participation.

3.3.2 Stimuli and procedure

The scan session was one hour long. Here we report only on the 5 minute eyes-open resting data that was acquired as either the first or second protocol (counterbalanced across participants with eyes-closed rest recording). Subjects were seated upright in the MEG scanner inside a magnetically shielded room. During the eyes-open rest recording, participants were instructed to maintain fixation on a red fixation spot. The visual fixation point was displayed on a Sanyo PLC-XP41 projector (1024 pixels x 768 pixels resolution, 60Hz refresh rate). All stimulus delivery was controlled by Matlab software.

3.3.3 MEG recordings and pre-processing

As in the previous chapter, MEG recordings were made over the whole head using a CTF-Omega 275 channel system. Data were sampled continuously at 1200Hz and analysed in synthetic third order gradiometer mode. Eye movements and blinks were monitored using vertical and horizontal electrooculogram (EOG) recordings. To achieve MEG/MRI co-registration, electromagnetic coils were placed at fixed distances from anatomical landmarks (left and right preauricular, nasion) prior to the MEG recording, and localised inside the scanner before and after each task. The fiduciary locations were marked manually on the anatomical MRI. Offline, data were downsampled to 600Hz and 1-150Hz band-pass filter was applied. Each dataset was parsed into 2 second intervals and visually inspected to remove trials including gross muscle, eyeblinks and eye movement artefacts.

3.3.4 MRI recordings and pre-processing

Anatomical MRIs for each participant were acquired on a 3T system using an FSPGR sequence with 1mm isotropic voxel resolution. Additionally, five minutes of resting-state fMRI data were acquired using a BOLD EPI sequence of 150 volumes (TR/TE = 2000ms/35ms, flip angle = 90deg, acquisition matrix = 64x64, slice thickness = 3.4mm). Data were pre-processed using AFNI (Cox, 1996). For fMRI processing, the data was despiked and time-shifted to 0. Volumes were aligned using rigid-body transformations and then transformed into MNI space. The data was blurred with a Gaussian spatial filter with FWHM=4mm and then segmented to calculate the average timeseries for cerebrospinal fluid (CSF), white matter (WM) and grey matter (GM) masks. In the final pre-processing step, noise confounds were removed using a GLM with the following regressors: motion, motion derivatives and motion censor (euclidean distance >0.3), average timeseries across WM and CSF tissue masks,

bandpass filter (0.01-0.1Hz). The fMRI data for three subjects were excluded due to excessive motion, and the remaining 85 participants were included in subsequent analysis.

3.3.5 Combined analysis

The combined analysis pipeline is presented in Figure 3-1. For the MEG analysis, we followed the pipeline validated in the previous chapter. This involves atlas-guided beamforming in 6 frequency bands, with selection of the voxel with maximum percentage change in each ROI as the region representative. This is followed by estimation of functional connectivity using amplitude envelope correlation, with leakage correction, across these virtual sensors in each of the 90 AAL regions. In order to enable direct comparison between MEG and fMRI data, we calculated fMRI timeseries using an average over voxels in each of the same 90 AAL regions used in the MEG source reconstruction. We then cross-correlated these timeseries to generate an fMRI connectivity matrix. In order to quantify the relationship between MEG and fMRI connectivity, we used a partial least squares (PLS) regression to determine which combination of MEG correlation matrices best explained the fMRI connectivity pattern. We vectorised the mean MEG connectivity matrices for each frequency band and combined these to form the predictor variable matrix. We also included the squared, cubed and fourth powers of each frequency band in attempts to capture more variance in the fMRI data. The fMRI connectivity matrix was also

vectorised and used as the response variable in the regression model.

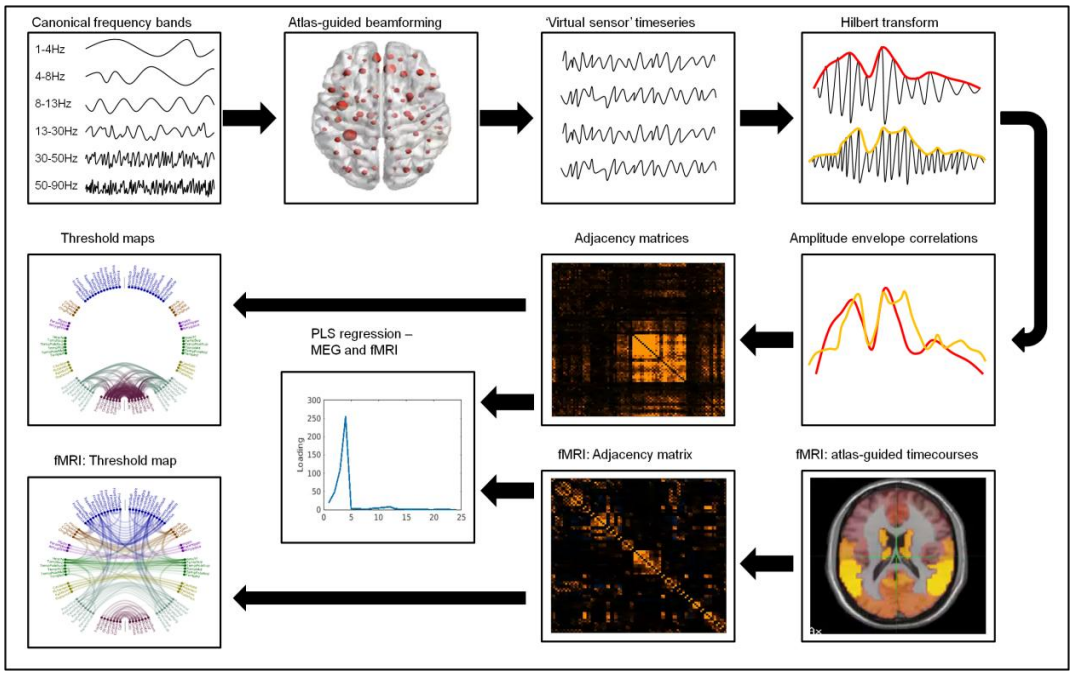

Figure 3-1. Diagrammatic representation of the analysis steps. The MEG pipeline is the same as that validated in the previous chapter of this thesis. For fMRI, we use an average timecourse in each region to ensure ease of correspondence with MEG connectivity matrices.

3.4 Results

3.4.1 Replication of MEG connectivity matrices

In order to further validate the connectivity pipeline chosen in the previous chapter, we first wanted to replicate the connectivity patterns seen in the MEG data in this larger independent cohort. The connectivity matrices derived using the voxel of maximum change as the ROI representative for each region with symmetric orthogonalisation of the virtual sensor timecourses are shown in Figure 3-2. The clearest spatially resolved connectivity structure corresponds to occipito-parietal regions in the alpha, beta and theta bands. The delta and theta bands also show an

area of increased connectivity corresponding to frontal regions. As before, there is no clear structure in either the low- or high-gamma bands.

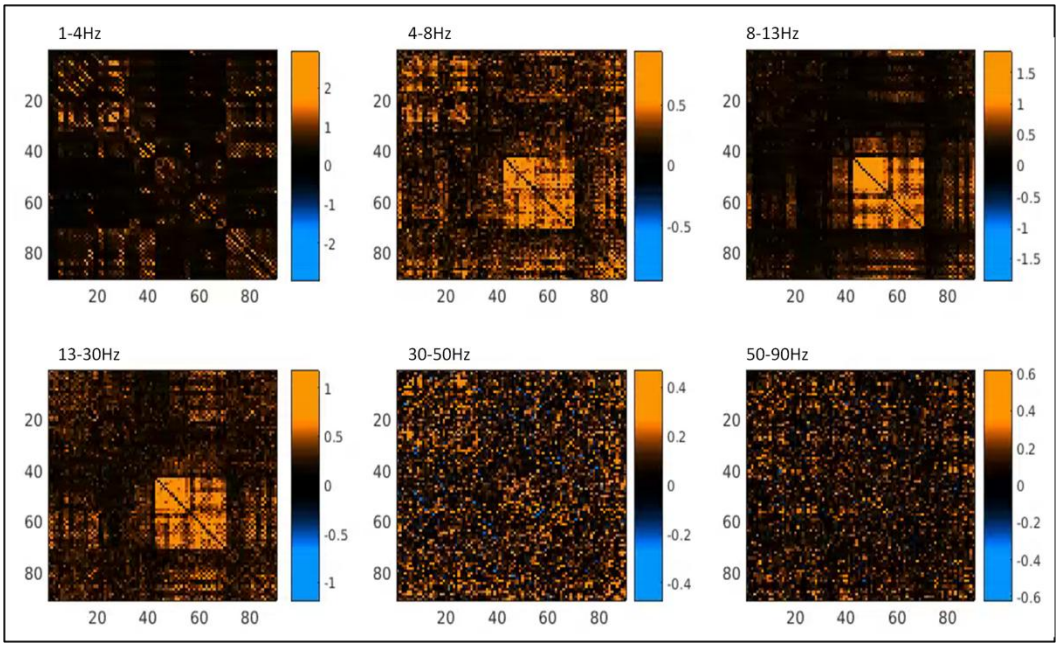

Figure 3-2. Average whole-brain connectivity matrices for each of the six frequency bands studied. The 90 AAL regions are plot along both the X and Y axes, and each element in the matrix represents the amplitude coupling between the two given regions. Stronger orange colouration indicates stronger connectivity between regions.

3.4.2 Comparison with fMRI

The fMRI connectivity matrix was derived using correlations between the average timecourse for each AAL region, and is shown in Figure 3-3. The strongest spatially resolved connectivity in the fMRI matrix can be seen in the off-diagonal elements, corresponding to homologous regions in the two hemispheres. There is also an area of increase connectivity around frontal regions, but the occipito-parietal connectivity hub that is dominant in the MEG theta-beta ranges is less evident in the fMRI data.

We used PLS regression to calculate predictor loadings of mean MEG connectivity in each frequency band to the fMRI connectivity matrix. The mean fMRI connectivity can be predicted to some degree by a combination of the mean MEG adjacency

matrices (Figure 3-3). Connectivity in the delta band dominates the MEG prediction of fMRI connectivity, with some contribution from alpha, theta and beta bands. There is residual connectivity in the fMRI matrix that cannot be accounted for by a combination of MEG connectivity, particularly coupling between homologous regions across hemispheres.

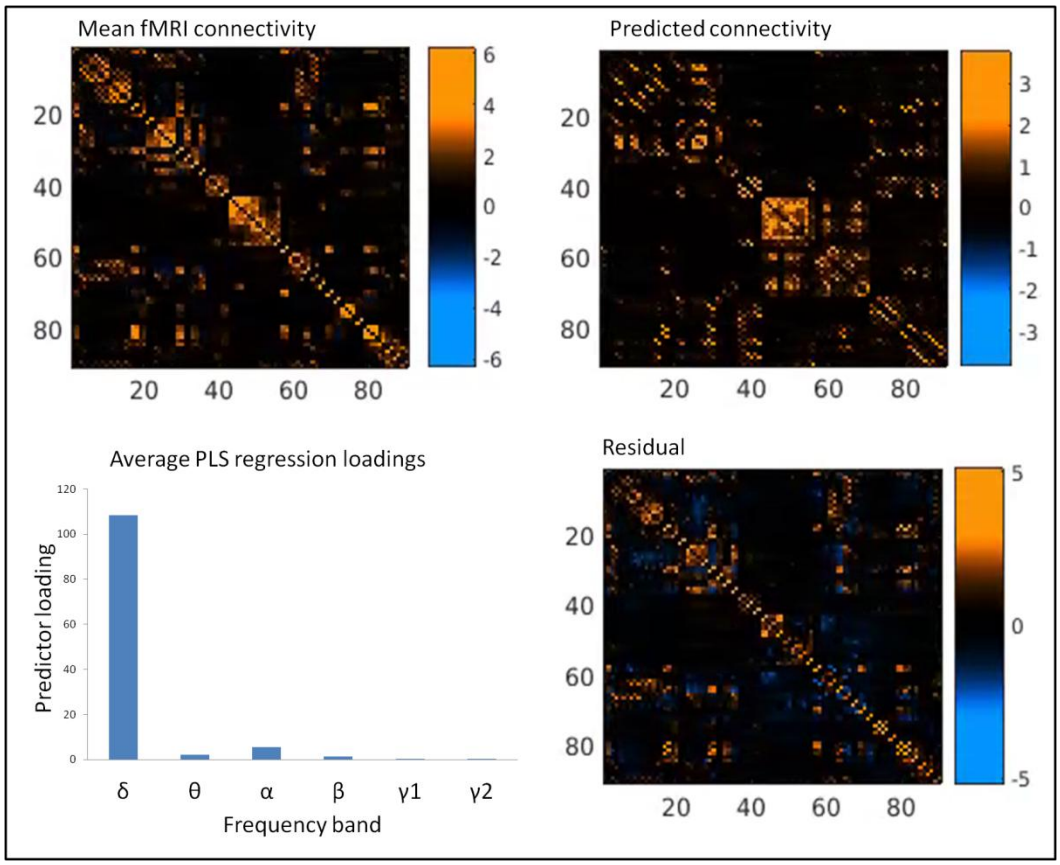

Figure 3-3. **Top left:** BOLD fMRI connectivity matrix. Stronger orange colouration indicates stronger coupling between two regions. **Top right:** Combination of MEG connectivity that best predicts observed connectivity in fMRI. **Bottom left:** PLS regression loadings for each of the MEG frequency bands to fMRI connectivity. Mean connectivity in each frequency band as well as the connectivity squared, cubed and to the fourth power are combined into a single bin to represent the total contribution of the frequency band. This pattern is mostly dominated by the delta band, with some contribution from alpha, theta and beta bands. **Bottom right:** Residual fMRI connectivity that cannot be explained with combination of MEG variables. The dominant structure here is the off-diagonal elements representing connectivity between homologous regions in the two hemispheres.

As well as comparing the mean connectivity across subjects, we also wanted to investigate the specific relationship between MEG and fMRI connectivity values for individuals. For each MEG frequency band, we computed a correlation across subjects between the z-score in that frequency band and the corresponding fMRI z-score, across the whole connectivity matrix. This measure gives an indication of consistency at the single subject level between band-limited MEG connectivity and fMRI connectivity values. At the group level (above) we found the greatest concordance between connectivity in the delta and alpha bands with fMRI, and prior studies show greatest correspondence between fMRI and beta band connectivity (Brookes et al., 2011b; de Pasquale et al., 2010). Given these priors, we expected the best intra-individual correspondence in one or more of these three bands. The cross-modality correlation matrices in the delta, alpha and beta bands are plotted in Figure 3-4. There is no discernible relationship between individual variability in band-limited MEG and fMRI connectivity in any frequency band when comparing across the whole matrix. However, there is a small but significant correlation between the global (i.e. mean) connectivity for each subject in fMRI and the beta-band ($r=0.25$, $p=0.01$). The same global correlation in the delta band narrowly misses significance (delta: $r=0.2$, $p=0.057$; alpha: $r=0.15$, $p=0.1$.). There was no relationship between fMRI connectivity and connectivity in the theta, low gamma and high gamma bands (see Appendix B for these plots).

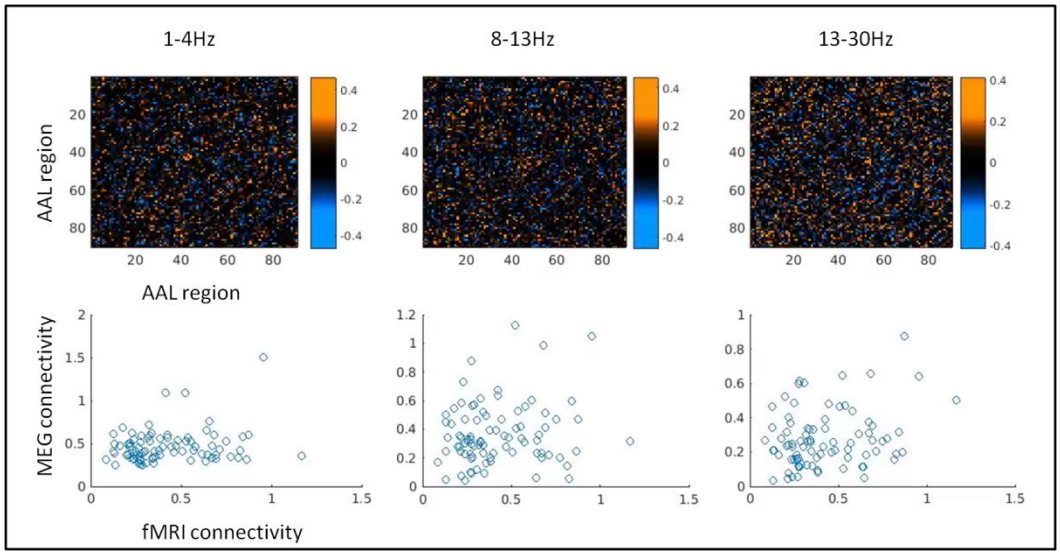

Figure 3-4. **Top:** Correlation between band-limited MEG connectivity and fMRI across subjects. Each point in this matrix represents the correlation, across subjects, between the z-score of the corresponding connection in (L-R) delta, alpha and beta bands with fMRI. There is no clear pattern of correlation between connectivity in any band with fMRI. **Bottom:** Correlation between global connectivity (i.e. mean of the connectivity matrix) for each participant in fMRI (X) and MEG connectivity (Y) in the delta, alpha and beta bands. The correlation values in each case are low but statistical testing indicates a small but significant positive correlation between global connectivity in fMRI and the beta band (r=0.25, p=0.01).

As an additional visual comparison, we thresholded the matrices in order to reduce noise and aid contrast between modalities. As in the previous chapter, we used a bootstrapping procedure with 10,000 iterations to build a distribution for each frequency band and the BOLD-fMRI. A connection was considered supra-threshold if it occurred within the strongest 5% of connections for 95% of iterations. The thresholded connectivity maps for each MEG frequency band and fMRI are plotted in Figure 3-5. For the MEG, the delta band is dominated by a pattern of connections within and to/from frontal regions. In the theta, alpha and beta bands, the strongest pattern of connectivity can be seen in posterior regions, particularly occipital and parietal cortex. There are no connections in the low- or high-gamma bands above the threshold. The strong homotopic connectivity previously observed in the

unthresholded fMRI matrices continues to dominate the fMRI map across frontal, temporal, parietal and occipital cortex as well as deeper structures.

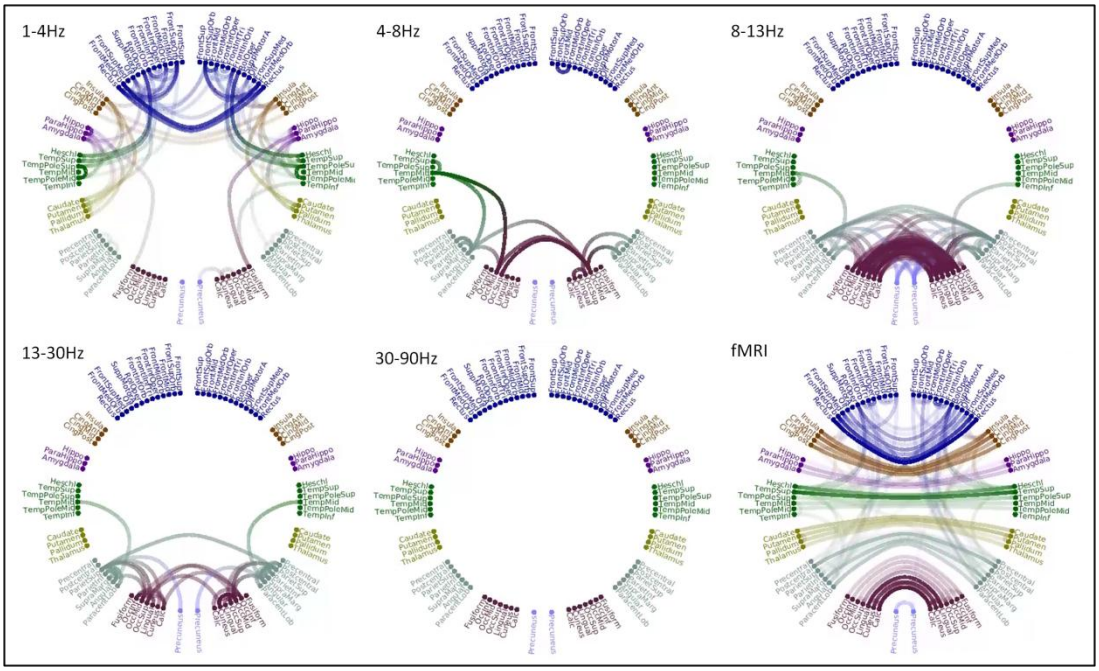

Figure 3-5. Thresholded connectivity maps for all MEG frequency bands and fMRI. Low and high gamma frequency bands have been combined as there were no supra-threshold connections in either band. The threshold was defined to include only the connections occurring within the strongest 5% of connectivity for 95% of 10,000 bootstrap iterations. The AAL regions range from frontal (top) to occipital (bottom) around each circle. Plots are weighted so that stronger connections appear more opaque.

3.5 **Discussion**

In the current work, we sought to replicate the connectivity patterns of resting-state MEG observed in the previous chapter using the described connectivity pipeline and compare this pattern to BOLD-fMRI connectivity in the same participants. Both the unthresholded and thresholded MEG connectivity matrices are consistent with the findings in the previous cohort. The fMRI connectivity matrices were dominated by homotopic connectivity that cannot be accounted for by a linear combination of the

MEG data. The spatial distribution of mean connectivity in the delta and alpha bands showed the best correspondence with the mean fMRI connectivity matrix.

The mean connectivity matrices generated from the MEG data are spatially consistent with those generated during validation of the pipeline in the previous chapter. In particular, a region of increased connectivity in occipital and parietal areas is visible in the theta-beta bands. As before, this is in line with a number of studies demonstrating presence of this cortical hub in MEG connectivity (Cabral, Kringelbach, & Deco, 2014; Tewarie et al., 2014). Following thresholding, we see fewer frontal theta connections relative to the previous cohort, and no supra-threshold gamma band connections. Here we used a large cohort of 88 participants, compared to 21 subjects in the previous chapter, and therefore may expect better SNR in connectivity estimations. Frontal theta rhythms are known to have greater susceptibilty to contamination from eye movement artefacts (Gasser, Sroka, & Möcks, 1985), and the gamma band is prone to contamination from muscle artefact (Muthukumaraswamy, 2013). Taken together, it is reasonable that we see less of these 'noisy' connections in the present work.

We find that the pattern of MEG connectivity in the delta band describes the highest amount of variance in fMRI connectivity, but that global connectivity in the beta band shows best correspondence with global fMRI connectivity. This is somewhat inconsistent with previous studies suggesting that networks in the alpha and beta bands show best correspondence with fMRI connectivity (Brookes et al., 2011b; de Pasquale et al., 2010; Tewarie et al., 2016; Tewarie et al., 2014). However, on inspection of the spatial pattern of the group-level matrices, the dominant occipito-parietal connectivity that is typically found in both alpha and beta bands as well as in fMRI (Buckner et al., 2009; Tewarie et al., 2016; Tewarie et al., 2014) is less visible in

this data. Instead, the most consistent spatial pattern of connectivity between fMRI and MEG in the present study is connectivity of frontal regions. A recent study showed that regional contribution of MEG to fMRI connectivity varied by frequency band, with greatest correspondence between fMRI and MEG connectivity in the delta band occurring over frontal regions (Tewarie et al., 2016). Further, the relationship between MEG and BOLD matrices may be affected by the 1/f spectral power density in MEG. Hipp and Siegel (2015) show that following SNR correction, correlation between fMRI and electrophysiology emerges across the 1-128Hz range. It may be the case that correspondence between delta connectivity and fMRI in the present findings be explained in part by increased SNR in this frequency band.

There is some variance in the fMRI connectivity matrices that is not explained using a linear combination of MEG connectivity. The most striking of these is the finding of strong homotopic connectivity in the fMRI matrices that is not evident in the MEG. Previous studies have shown strong coupling between homologous regions in resting-state fMRI (Owen et al., 2013) so this finding is consistent with existing literature. However, the reason for this difference between modalities is unclear and could occur for a number of reasons. Firstly, it is possible that homologous regions are coupled in frequencies slower than those we studied. A study has shown that MEG oscillations at frequencies less than 1Hz synchronise over long distances, and particularly in bilateral homologous regions (Liu, Fukunaga, de Zwart, & Duyn, 2010). So the high-pass filter of 1Hz applied during pre-processing may have attenuated homotopic connectivity in our MEG data. Further, given the relative spatial resolutions of the two techniques, it is perhaps unsurprising that fMRI can distinguish connectivity in deep structures such as the insula and thalamus where MEG may be limited (Hillebrand & Barnes, 2002). Connectivity between some ROIs may have been artificially inflated due to smoothing of the fMRI data. As a fairly standard pre-

processing step BOLD-fMRI data is smoothed (Lindquist, 2008), thus creating the possibility that signal is smeared across the boundary line between two ROIs and appears as part of the timecourse for both regions. This may be considered analogous to the signal leakage problem in MEG, but will only affect connectivity between midline structures in fMRI. Lastly, it is also important to consider the possibility that such strong homotopic coupling arises as a result of physiological or vascular artefact. Although we removed noise regressors from our BOLD-fMRI data, there are a number of non-neural confounds that may remain poorly controlled, such as CO2 concentration and vasomotion (Murphy, Birn, & Bandettini, 2013). A study using CBF from SPECT imaging found the strongest correlations between homologous cortical regions (Melie-Garcia, Sanabria-Diaz, & Sanchez-Catasus, 2013). Given that CBF represents one component in the BOLD response, homologous connectivity could represent a change to this component rather than an increase in coupling of neuronal activity per se. However, a recent study showed that MEG connectivity is also not infallible and may be affected by some of the same artefacts related to CO2 concentration (Driver & Whittaker, 2016). Monitoring physiology during recordings would allow further investigation about the relative contribution of these non-neural signals to both MEG and BOLD-fMRI connectivity.

We estimate a single connectivity measure based on the correlation of entire MEG and fMRI timecourses. This assumption of stationarity leads to some level of inherent bias towards slow changes over a long timeframe. The loadings of the MEG to fMRI connectivity could also change with a dynamic approach to estimating amplitude coupling in MEG, of which a number of techniques have been proposed in recent years (O'Neill et al., 2015; O'Neill et al., 2017; Woolrich et al., 2013). These approaches utilise the full temporal resolution of MEG to build a picture of varying connectivity across the recording length. Lastly, our approach assumes that the best

fit to fMRI data can be obtained with a combination of amplitude-coupling estimates in band-limited MEG connectivity. In the past year, Tewarie et al (2016) introduce a framework that characterises the relationship between MEG and fMRI connectivity in terms of multiple connectivity estimates from multiple frequency bands, with linear and non-linear interactions. Thus, the fit between MEG and fMRI connectivity here may have been improved by adding further parameters to our MEG prediction model, such as phase-coupling estimates, non-linear interactions between frequency bands and cross-frequency coupling.

3.6 **Conclusion**

In this chapter, we were able to replicate from the previous chapter the basic pattern of connectivity during resting-state recordings for each of the six frequency bands studied, in a larger independent cohort. We additionally compared MEG connectivity with BOLD-fMRI connectivity in the same subjects. We saw best correspondence between MEG and BOLD in the delta band, driven by frontal connectivity. Strong homotopic connectivity in the fMRI matrices could be due to slow fluctuations or physiological artefact.

4 The effects of AMPA receptor blockade on resting-state MEG recording

4.1 Abstract

PharmacoMEG is an emerging branch of research that combines MEG with pharmacological intervention. This approach not only enables the study of drug compounds non-invasively in humans, but also allows investigation into the complex neurochemical dynamics underlying the MEG signal. Glutamate is the primary excitatory neurotransmitter in the human brain, thus the ionotropic NMDA and AMPA receptors of the glutamatergic system are of fundamental importance to healthy brain function. Neuroimaging studies in humans have previously been conducted using various drugs that interact with NMDA glutamate receptors, but no such studies have investigated AMPA receptor signalling. The recent approval of Perampanel (Fycompa ©) for use in humans provides a means to specifically study the role of AMPA receptors in the pharmacological basis of neuroimaging signals. Twenty male subjects participated in this placebo-controlled crossover study in which we recorded ten minutes of wakeful rest before and after dosage with 6mg perampanel and a placebo. Here, we report the effects of perampanel on both spectral power and frequency in the resting-state. We additionally apply the connectivity pipeline validated in previous chapters of this thesis in order to investigate the effects of changes to endogenous glutamate levels on amplitude coupling.

4.2 Introduction

4.2.1 A brief background on glutamatergic neurotransmission

The MEG signal arises from synchronous activity within neuronal assemblies, in particular the summed post-synaptic potentials of cortical pyramidal cells (Lopes de Silva, 2010). MEG data are therefore influenced by a complex interplay of neurochemical systems. Activity across the frequency range typically measured using MEG (0->100Hz) can be selectively modified by pharmacological agents acting on neurotransmitters including γ-Aminobutyric acid (GABA; Hall et al.2011; Saxena et al., 2013), serotonin (Muthukumaraswamy et al., 2013b) and dopamine (Moran, Symmonds, Stephan, Friston, & Dolan, 2011), among others. Whereas GABA is the primary inhibitory neurotransmitter in the human brain, glutamate is the primary excitatory neurotransmitter. Ionotropic glutamate receptors, particularly N-methyl-D-aspartate (NMDA) and α-amino-3-hydroxy-5-methyl-4-isoxazolepropionic acid (AMPA) subtypes, are of fundamental importance in neuronal signaling. Both AMPA and NMDA receptors co-exist on most excitatory synapses within the central nervous system, but crucially possess differing kinetic properties that, coupled together, define the timecourse of synaptic transmission (Traynelis et al., 2010). Activation of the AMPA receptor is a rapid process whereby channels allowing influx of sodium ions open and close within 2-3ms (Dingledine, Borges, Bowie, & Traynelis, 1999). NMDA receptors, however, are more permeable to calcium ions and possess a slower rise time (~20ms), with a several hundred millisecond delay in closing (Dingledine et al., 1999). Voltage-dependent regulation of the glutamate receptors by endogenous ions not only defines the timecourse of synaptic transmission but is also thought to be key in synaptic plasticity (Traynelis et al., 2010). Furthermore, dysfunction in glutamatergic systems is implicated in many neurological and neuropsychiatric

disorders including schizophrenia (Goff & Coyle, 2014; Olney & Farber, 1995), mood disorder (Sanacora, Treccani, & Popoli, 2012) and Alzheimer's disease (Hynd, Scott, & Dodd, 2004).

4.2.2 Pharmacological intervention with MEG

There have been various neuroimaging studies of compounds acting on GABA and NMDA receptors (among others) using both fMRI (Downey et al., 2016; Licata, Lowen, Trksak, MacLean, & Lukas, 2011; Northoff et al., 2005) and EEG/MEG (Lozano-Soldevilla, ter Huurne, Cools, & Jensen, 2014; Sanacora et al., 2014; Saxena et al., 2013; Shaw et al., 2015). But there are, to our knowledge, no neuroimaging studies to-date that have used a selective AMPA receptor drug as, until recently, such a compound was not available for use in humans. Perampanel is a new anti-epileptic drug (approved 2012) that acts as a non-competitive antagonist of the AMPA receptors, and so reduces the actions of glutamate at the synapse. The compound is highly-selective, and at therapeutic doses displays no affinity to the other ionotropic glutamate receptors (NMDA or kainate; Rogawski & Hanada, 2013). This drug has been licensed in the USA and EU since 2012 as an adjunctive medication in the treatment of refractory partial-onset epileptic seizures.

Conducting non-clinical intervention studies with pharmacoMEG not only enables study of the actions of pharmacological agents non-invasively in humans, but also helps to develop understanding of the neurotransmission dynamics underlying the MEG signal (Muthukumaraswamy, 2014). Using a task-free paradigm enables us to investigate the effects of different compounds on both oscillatory power and functional connectivity, across a variety of frequency bands, within one recording. Previous animal studies suggest that both low and high frequency oscillations are affected by AMPA receptor activity. For example, an EEG study in conscious rats

demonstrated dose-dependent increases in power across the 1-30Hz spectrum following administration of two AMPA antagonists (Sebban, Tesolin-Decros, Ciprian-Ollivier, Perret, & Spedding, 2002). At higher frequencies, Oke et al (2010) showed that application of the AMPA antagonist SYM-2206 to slice preparations taken from rat visual cortex almost abolished both low (~50Hz) and high (~80Hz) gamma oscillations. Furthermore, concurrent increases in low frequency oscillatory power (1-4Hz and 7-13Hz) and decreases in high frequency power (30-60Hz) have been found in a task-driven study following administration of AMPA antagonists to the visual cortex of monkeys in vivo (Herrero, Gieselmann, Sanayei, & Thiele, 2013).

To the best of our knowledge, no human neuroimaging studies have specifically investigated the effects of AMPA receptor mediation on functional connectivity. However, studies using compounds that act on monoamine neurotransmitter systems have shown that it is possible to detect drug-related changes to functional connectivity, typically in low frequency ranges, using a range of methods (Franzen et al., 2013; Muthukumaraswamy et al., 2013b). Furthermore, a number studies have found altered patterns of connectivity across cortical and subcortical regions following administration of the NMDA receptor antagonist, ketamine (Anticevic et al., 2015; Driesen et al., 2013; Muthukumaraswamy & Shaw, 2015; Scheidegger et al., 2012). It is worth noting here that ketamine is known to increase extracellular glutamate concentration (Stone et al., 2012), but has a complex mechanism of action (Tyler, Yourish, Ionescu, & Haggarty, 2017) so results should be interpreted with caution.

4.2.3 Aims

Therefore, the present study aimed to investigate the actions of glutamate in the human brain, by utilising the interaction between perampanel and AMPA receptors

at the synapse. Firstly, we describe the oscillatory profile of perampanel during task-free MEG recordings in a group of healthy volunteers. Based on previous in-vivo (Herrero et al., 2013; Sebban et al., 2002) and in-vitro work (Oke et al., 2010), we expected to see an increase in power in low frequency bands, coupled with a decrease in power of gamma band activity. Further, we reconstruct source locations of drug-effects and investigate drug-related changes to broadband functional connectivity, using the method validated in previous chapters. It is difficult to make predictions regarding this final aim given the lack of existing literature.

4.3 Methods

4.3.1 Participants

Twenty healthy volunteers (mean age 22.9 years, SD 3.75; mean weight 75.6 kg, SD 8.2) participated in the study. Inclusion criteria were that participants be males between 18 and 45 years old, non-smokers, with a body mass index of 18-30 kg/m^2. Exclusion criteria included personal history of neuropsychiatric or neurological disorder, current recreational or prescription drug use, ongoing health problems (including liver and cardiovascular function) and contraindications for MEG/MRI. Participants were additionally screened for alcohol misuse with the Alcohol Use Disorders Identification Test (AUDIT; Saunders, Aasland, Babor, De la Fuente, & Grant, 1993); all participants scored below the threshold for alcohol dependence (≥16; mean score 7.1, SD 3.9). Participants were required to abstain from alcohol for 72 hours prior to study sessions, and from use of illicit substances and 'legal highs' for 7 days prior. All procedures were approved by the UK National Research Ethics Service (South East Wales), and a description of task-related MEG activity from the

same recording days is available elsewhere (Muthukumaraswamy, Routley, Droog, Singh, & Hamandi, 2016).

4.3.2 Design and Procedure

Participants were scanned on two separate days in a single-blind, placebo-controlled crossover design. Study sessions were separated by a minimum period of 14 days to allow for drug washout. Each session took place at approximately the same time of day, and session order (drug/placebo) was counterbalanced across participants. During each study session, a 'pre-dose' MEG recording was obtained, following which participants orally ingested a capsule containing either 6mg of Perampanel (Fycompa ©) or an unmarked vitamin E placebo. A further 'post-dose' MEG recording was obtained two hours after ingestion, at which time Perampanel is expected to have reached peak plasma level (Templeton, 2010). As part of each MEG scan a 10-minute resting recording was obtained, during which time participants were instructed to remain relaxed but alert with their eyes open and fixated on a red circle presented at the centre of the screen. The fixation point was displayed on a Sanyo PLC-XP41 projector with a screen resolution of 1024x768 and refresh rate of 60Hz. All recordings were made with participants lying supine in the scanner. Just prior to each MEG recording, participants completed a battery of psychological questionnaires including the Subjective High Assessment Scale (SHAS; Schuckit, 1980) and Biphasic Alcohol Effects Scale (BAES; Martin, Earleywine, Musty, Perrine, & Swift, 1993) to measure subjective drug experience, and the State Hostility Scale (SHS; Anderson, Deuser, & DeNeve, 1995) to quantify experience of potential side effects.

4.3.3 MEG recordings

As in all previous experiments, whole-head MEG recordings were made using a CTF-Omega 275 channel system, sampled at 1200Hz and analysed in third-order

gradiometer mode. Eye movements and blinks were monitored using vertical and horizontal electrooculogram (EOG) recordings. For this study, we also recorded an electrocardiogram (ECG) and electromyograms (EMGs) from the frontalis and temporalis for additional physiological monitoring following drug dose.

For source localisation, a 1mm isotropic FSPGR anatomical MRI scan was obtained, either on a different day to that of the MEG recording or from previous study participation at CUBRIC. To achieve MEG/MRI co-registration, electromagnetic coils were placed at fixed distances from anatomical landmarks (10mm anterior to left and right tragus, 10mm superior to nasion) and localised immediately before and after each recording. Fiduciary locations were later manually marked on the anatomical MRI.

4.3.4 Sensor-level analysis

Offline, the data were downsampled to 600Hz, and divided into 2 second epochs. Each epoch was visually inspected and those containing gross muscle artefacts (e.g. jaw clenches) were removed from subsequent analysis. To complete pre-processing we applied independent component analysis to the data and rejected artefacts including eye movements and cardiac noise, based on topography and waveform patterns of each component. This additional pre-processing step was not included in previous chapters but was used in this sensor-space analysis as this is more sensitive to noise contamination than beamformed source estimates. For the following analysis, the frequency bands used were: delta (1-4Hz), theta (4-8Hz), alpha (8-13Hz), beta (13-30Hz), low gamma (30-50Hz) and high gamma (50-100Hz). These bandings are consistent with similar previous work (Nutt et al., 2015).

We examined the power spectra of various frequency bands in sensor space, using the FieldTrip toolbox (Oostenveld et al., 2011) in a pipeline similar to that described

previously (Nutt et al., 2015). The pre-processed data were first converted to planar gradient formation and frequency analysis was conducted using Hanning-windowed fast Fourier transforms. The gradients over both planar directions were then combined to obtain a single positive-valued number under each sensor. In this sensor configuration, sources can be assumed to lie directly underneath local maxima on field maps, thus allowing the results of this analysis to be more easily interpretable (Bastiaansen & Knosche, 2000). Difference images were then created by subtracting the pre-dose spectra from the post-dose spectra for each condition (drug/placebo) and participant, according to the frequency bands defined above. Statistical differences between the drug and placebo conditions were determined used Monte-Carlo permutation testing of t-statistics on these difference images (5000 permutations, cluster-based multiple comparisons correction applied).

Visual inspection of the power spectra indicated that there may be a drug-related slowing of alpha oscillations. So, in addition to changes in oscillatory power we also chose to selectively examine the effects of perampanel on alpha frequency. We used an approach to peak frequency estimation with quality control that has previously been described for gamma oscillations (Magazzini et al., 2016). Here, the single trial spectra were averaged separately for each condition and time-point (pre-placebo, post-placebo, pre-drug and post-drug) and the channel with greatest alpha power in each case selected. Single-trial spectra in the peak channel were then resampled (with replacement) using 10,000 iterations of bootstrapping, re-averaged, and peak alpha frequency for each participant was defined as the mode of the bootstrapped distribution in the 8-13Hz range. To control for data quality, we used the distribution of peak frequency estimations generated by the bootstrapping, and included data for any participant only when at least 50% of bootstrap iterations occurred within a frequency window of ±1Hz around the bootstrapped mode, for all four conditions. In

this study, no participants were excluded using this criterion. Differences in peak frequency were then analysed using a 2x2 repeated measures ANOVA, using factors drug (placebo and perampanel) and time (pre-dose and post-dose).

4.3.5 Connectivity analysis

We additionally investigated drug-related changes in source space connectivity patterns. Here, we used an amplitude coupling approach that assesses temporal interactions between the amplitude envelopes of brain sources, as described in previous chapters. A brief description of the pipeline, including the parameters chosen based on the comparison in chapter 2, follows: We first applied an atlas-guided beamformer in the frequency bands delta (1-4Hz), theta (4-8Hz), alpha (8-13Hz), beta (13-30Hz), low gamma (30-50Hz) and high gamma (50-90Hz) to derive source-space signals. The voxel with maximum percentage change in each ROI of the AAL atlas was chosen as representative 'node' for that region. Once the timeseries were estimated for each of the 90 AAL-atlas nodes, we applied symmetric orthogonalisation to correct for source leakage (Colclough et al., 2015). These orthogonalised virtual-sensor timeseries were then converted to amplitude envelopes via the analytic function (Matlab: hilbert). We then cross-correlated the envelopes to generate an amplitude coupling connectivity matrix for each participant and recording, and converted the matrices to normalised z-scores for statistical analysis.

In order to compare between drug conditions, we first sum along the rows of each z matrix to derive a measure of 'connection strength', representing in a single metric how strongly connected each node is to the other nodes. As in the sensor space analysis, we create difference scores for each participant by subtracting the pre-dose connection strength measures from the post-dose measures for both perampanel

and placebo. We then conduct a randomisation test (10,000 permutations) on the difference, perampanel – placebo, for each node strength , with omnibus correction for multiple comparisons across the 90 nodes (Nichols & Holmes, 2002).

4.4 Results

4.4.1 Subjective experience of drug

The behavioural measures indicate changes to subjective experience following dosage of the drug, particularly increased feelings of drowsiness or sedation. Descriptive statistics for all scales can be found in Appendix C, along with group averages for the individual scale items on the BAES (Appendix D) and SHAS (Appendix E). In the BAES, there was an average 13.5 point increase on the sedative subscale following perampanel dosage (compared to 0.6 point increase on placebo), with the greatest increase seen on the 'sedated' item (2.75 point increase, maximum score per item is 5 points). Similarly, in the SHAS, many items increased by an average of 10 points or more following drug dose (maximum score per item is 100), with the greatest increase reported in feelings of sleepiness and concentration (31.1 and 24.8 point average change, respectively). As well as somnolence, perampanel has significant association with adverse events of dizziness and irritability (Zaccara, Giovannelli, Cincotta, Verrotti, & Grillo, 2013). Reports of dizziness on the SHAS were increased by 18.9 points following perampanel administration in this study, but there was no increase on the 'irritable' item of the SHS.

A series of 2x2 ANOVAS revealed significant drug-time interactions in both the sedative scale of the BAES (Figure 4-1a; $F(1,19)=28.4$, $p<0.01$), and the SHAS (Figure 4-1c; $F(1,19)=23.7$, $p<0.01$). There were no significant interaction effects in the

stimulant scale of the BAES (Figure 4-1b; F(1,19)=0.8, p=0.37), or the SHS (Figure 4-1d; F(1,19)=2.4, p=0.14). All participants were able to correctly identify the session order following completion of the study.

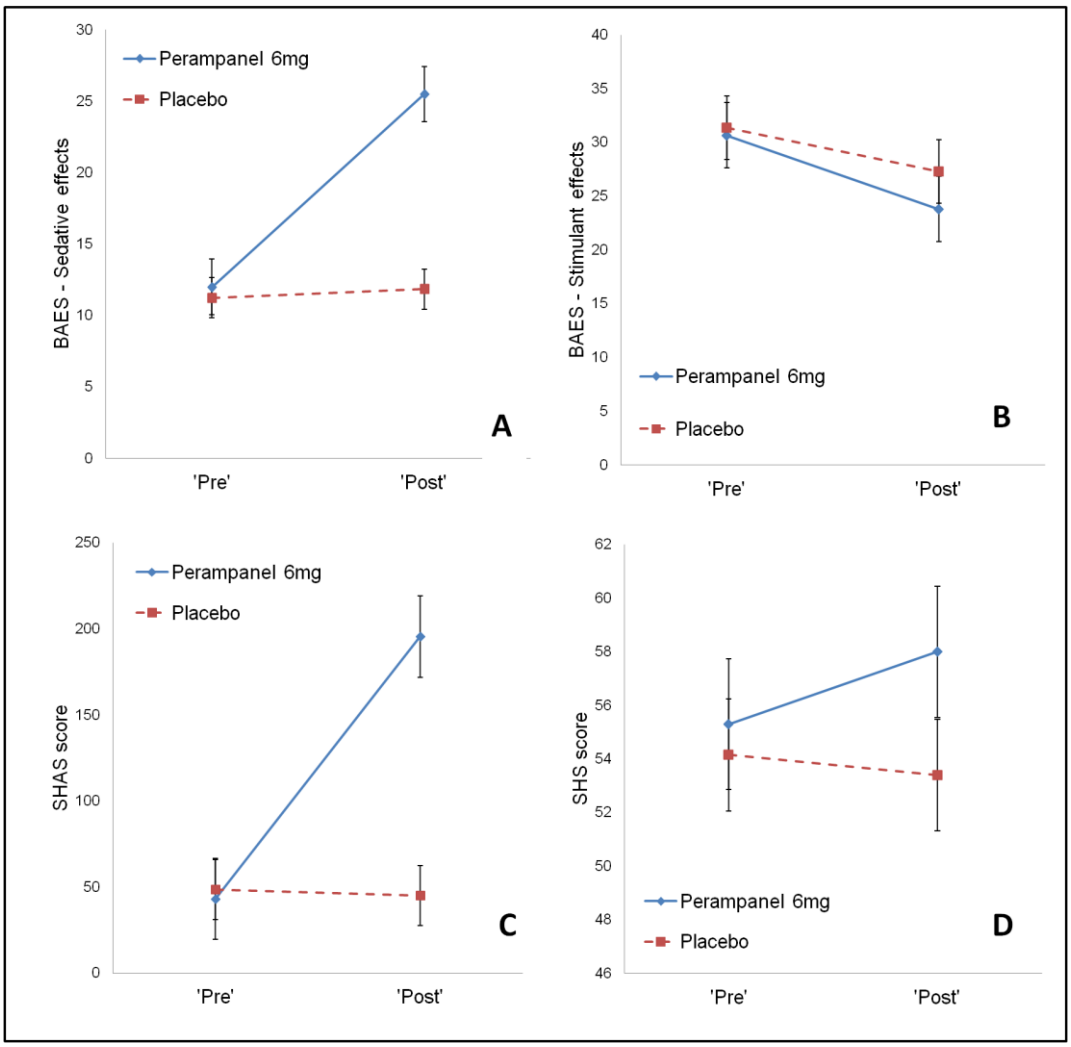

Figure 4-1. Differences in mean scores on psychometric scales between 'pre' and 'post' timepoints for drug and placebo, for the BAES (A and B), SHAS (C) and SHS (D). Significant interaction terms (p<0.01) are denoted using '*'.

4.4.2 Power and frequency changes in sensor space

Following artefact rejection from the original trials, there were comparable trial numbers left in each condition: Placebo pre-dose = 293 (std=8.1), placebo post-dose = 292 (std=6.4), drug pre-dose = 294 (std=4.5), drug post-dose = 293 (std=8.9) indicating preserved data quality following drug administration. A repeated measures

ANOVA confirmed that there was no significant drug*time interaction in trial number (F=(1,19)=0.137, p=0.71)

Drug-induced changes in power were observed in almost all frequency bands. In the lower bands (δ – β) we found a significant increase (p<0.01) in power focused around posterior sensors. There were no significant changes to power in the low-gamma range, but a significant decrease in power (p<0.01) over central parietal sensors in the high-gamma range. Figure 4-2 topographically shows the drug-related effects on the power spectrum in each frequency band.

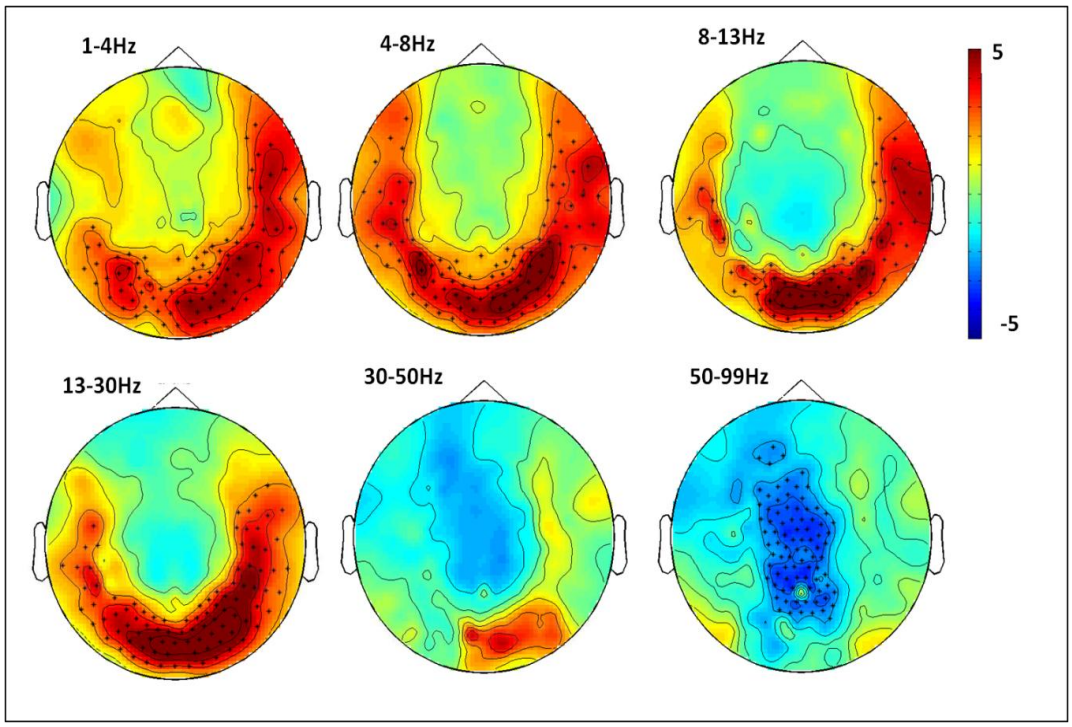

Figure 4-2. Contrast performed on drug-placebo difference spectra, in the frequency bands: δ, θ, α, β, low γ, high γ. Red indicates a relative increase in power following drug and blue indicates relative decrease. Units are t-statistics and significant sensor clusters (p<0.01, corrected for multiple comparisons) are marked on the sensor plots using '*'.

The broadband effects of perampanel on oscillatory power at single sensor locations around the head are shown in Figure 4-3a. Inspection of these plots indicates that in addition to increasing power at low frequencies and decreasing power at higher

frequencies, perampanel may also cause frequency slowing in the alpha band. Subsequent analysis of peak frequency using the quality-control bootstrapping procedure (Magazzini et al., 2016) confirmed this. The drug*time interaction term of the 2x2 repeated measured ANOVA was significant ($F(1,19)=5.444$, $p=0.03$). Inspection of the graphs indicates that this change is mostly due to a reduction in alpha frequency following 6mg dose of perampanel (Figure 4-3b;).

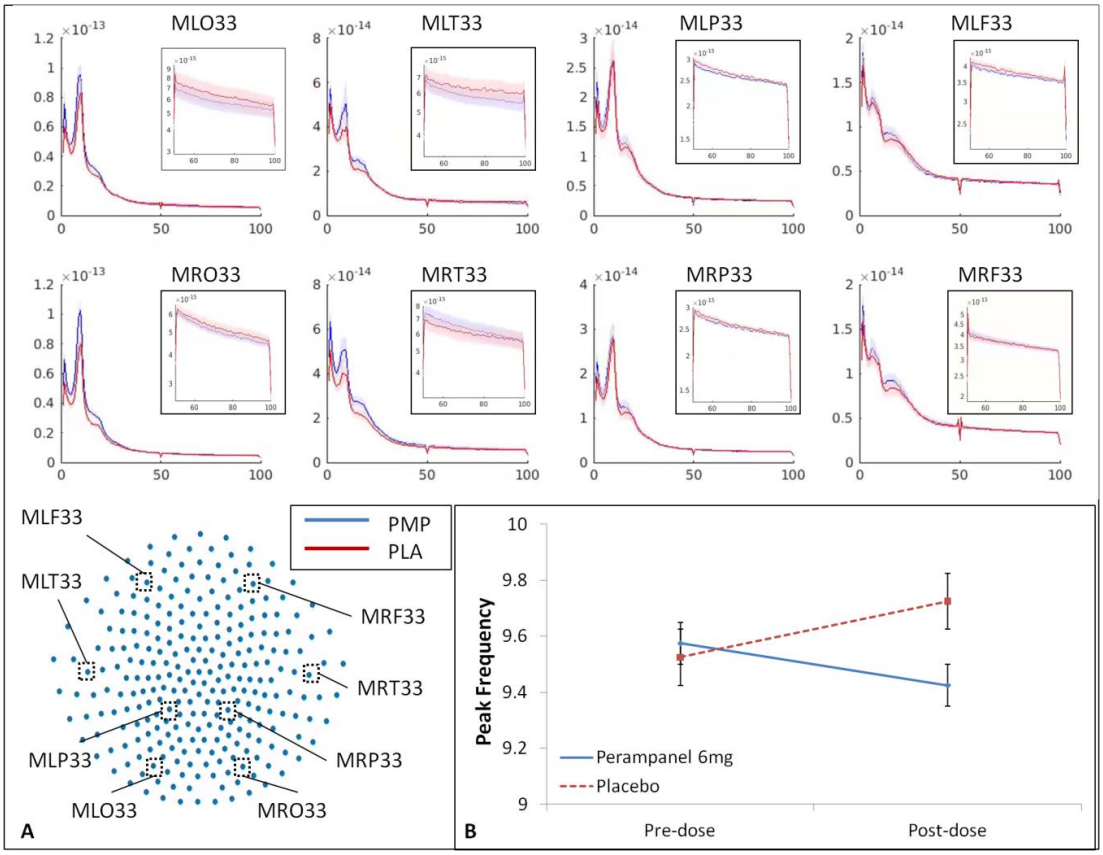

Figure 4-3. (A). Power-Frequency plots for post-dose conditions at single sensors in the occipital, temporal, parietal and frontal regions. Frequency is plot on the x-axis and power on the y-axis. Sensor locations are shown in the bottom-left schematic. Shaded bars are standard error. Inset plots show 50-100Hz on a log-scale. (B). Changes to peak frequency in the alpha (8-13Hz) band, for pre-dose and post-dose drug and placebo conditions. Bars show standard error. The drug*time interaction of the 2x2 ANOVA conducted on this data was significant.

4.4.3 Source –space connectivity

Following source estimation, we assessed drug-related changes to connectivity in each of the frequency bands. The average adjacency matrices (90x90 regions) for each frequency band are shown in Figure 4-4a. In both the drug and placebo conditions, the connectivity shows most structure in the alpha and beta ranges, with a 'hub' region of increased connectivity in occipital and parietal areas. Stronger orange colouration in the post-drug matrices indicates that amplitude coupling is increased across the low frequency ranges following perampanel dose. We conducted statistical testing based on the previously described 'connection strength' measure, which gives an indication of how connected a region is to all other regions. The only connectivity increases that survive statistical testing with multiple comparisons correction can be seen in the alpha and beta bands (Figure 4-4b). In both cases, these changes localise mainly to connections to/from parietal regions. For the alpha band, significantly increased connection strength is observed following drug dose in the left superior parietal lobule ($p=0.04$). For the beta band, this increase is observed for the left postcentral gyrus ($p<0.01$), right inferior parietal gyrus ($p<0.01$) and left caudate ($p=0.04$).

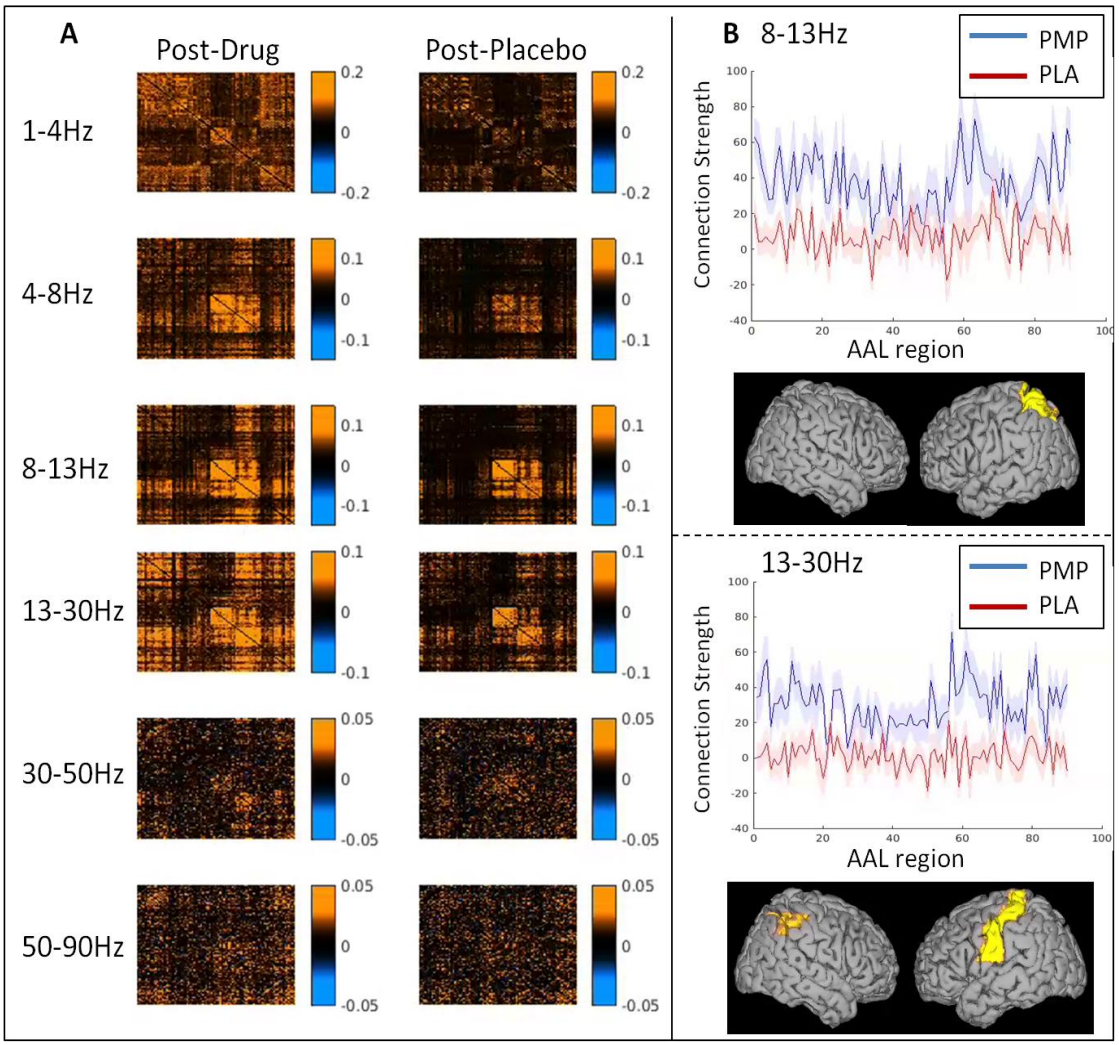

Figure 4-4. (A). Post-dose connectivity matrices for each of the frequency bands studied. Each point in the plot indicates the group-averaged correlation of one AAL region with another (90x90). (B). For alpha (8-13Hz; top) and beta (13-30Hz; bottom), difference scores (post dose - pre dose) for z-corrected mean connection strength for all AAL regions. Regions where drug-related connectivity increases survive statistical testing, with multiple comparisons correction, are plot on MNI template brains below.

4.4.4 Subsequent re-analysis: Connectivity matrix thresholding

The work contained in this chapter, presented above, is currently under review for publication. Subsequent to submission of the manuscript, we have further developed the connectivity pipeline to include thresholding of connectivity matrices prior to calculation of group-level statistics. The thresholding procedure, previously described in chapter two of this thesis, includes pooling across all subjects and conditions to

select the strongest 5% of connections within the matrix. This is combined with a bootstrapping approach (10,000 iterations) to sub-select only those connections which appear in the strongest 5% for 95% of iterations. The thresholded maps for the alpha and beta bands, that previously showed connectivity changes following perampanel, are shown in Figure 4-5a. The pooled thresholded matrices are consistent with previous chapters in terms of spatial pattern: Connectivity in the alpha band is largely dominated by occipital connections, whilst in the beta band we observe increased connectivity with parietal and temporal areas. In the beta band, there is increased connectivity in thresholded matrices for perampanel compared to placebo, but this pattern is more mixed in the alpha band (Figure 4-5b). A t-test on the global connectivity (i.e. mean connectivity of all asked nodes) between perampanel and placebo is significant for the beta band ($t(19)=3.20$, $p=0.004$) but not significant for the alpha band ($t(19)=1.28$, $p=0.2$). However, a randomisation test on the connection strength in these matrices between perampanel and placebo no longer yields any significant areas of connectivity in either frequency band. The threshold used is conservative so it is possible that true connectivity is masked, but even if this is the case, it may be for a number of reasons.

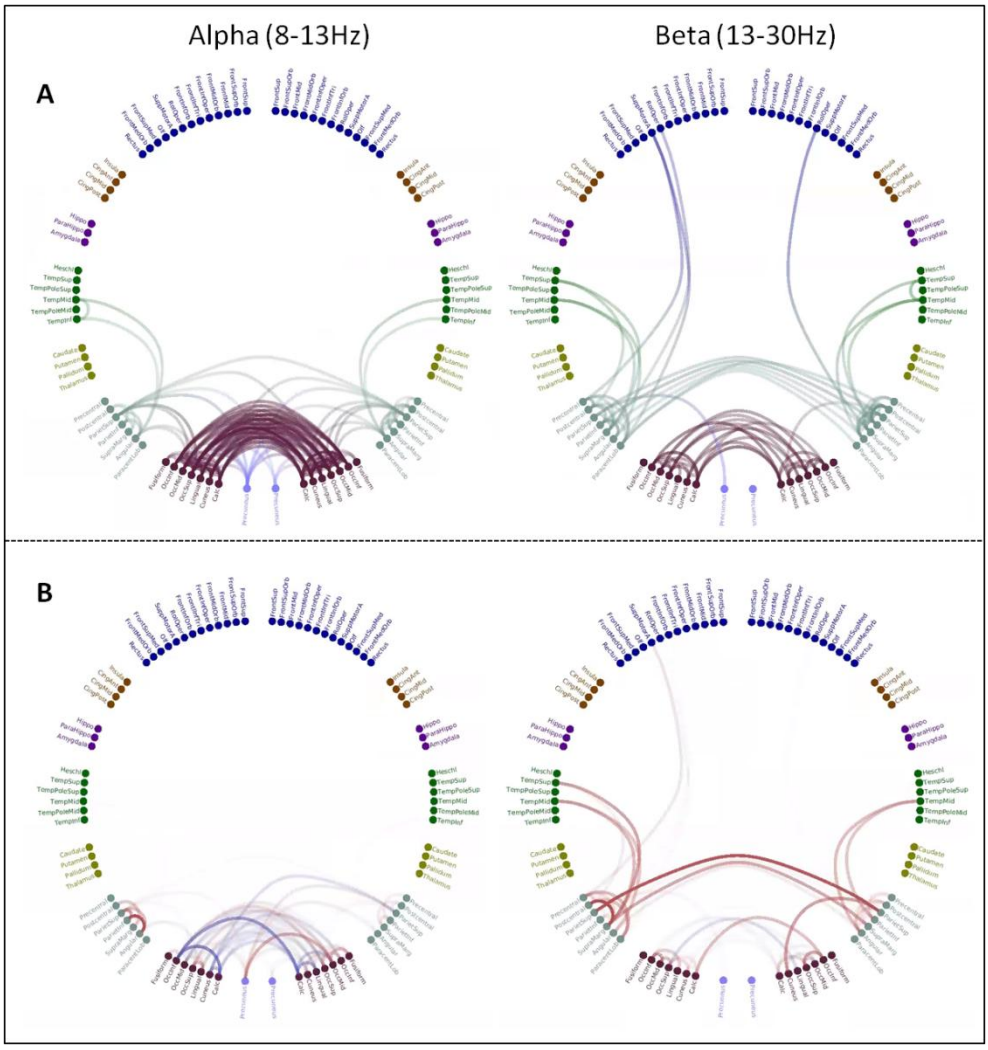

Figure 4-5. **(A)** Thresholded connectivity maps. The threshold was set to show only those connections occurring in the strongest 5% for 95% of bootstrap iterations. Stronger colouration is indicative of a stronger connection. **(B)** Comparison of node-node connectivity differences between perampanel and placebo (t-statistics). Red lines indicate a relative increase in t-value with perampanel relative to placebo and blue lines indicate a relative decrease.

A region could have a high connection strength value driven by moderate connections to lots of other regions, or a single strong connection to one region. It is therefore possible that some of the regions with significantly different non-thresholded connection strength between conditions failed to survive the thresholding procedure. This is the case for the left caudate in the beta band (Figure 4-6).

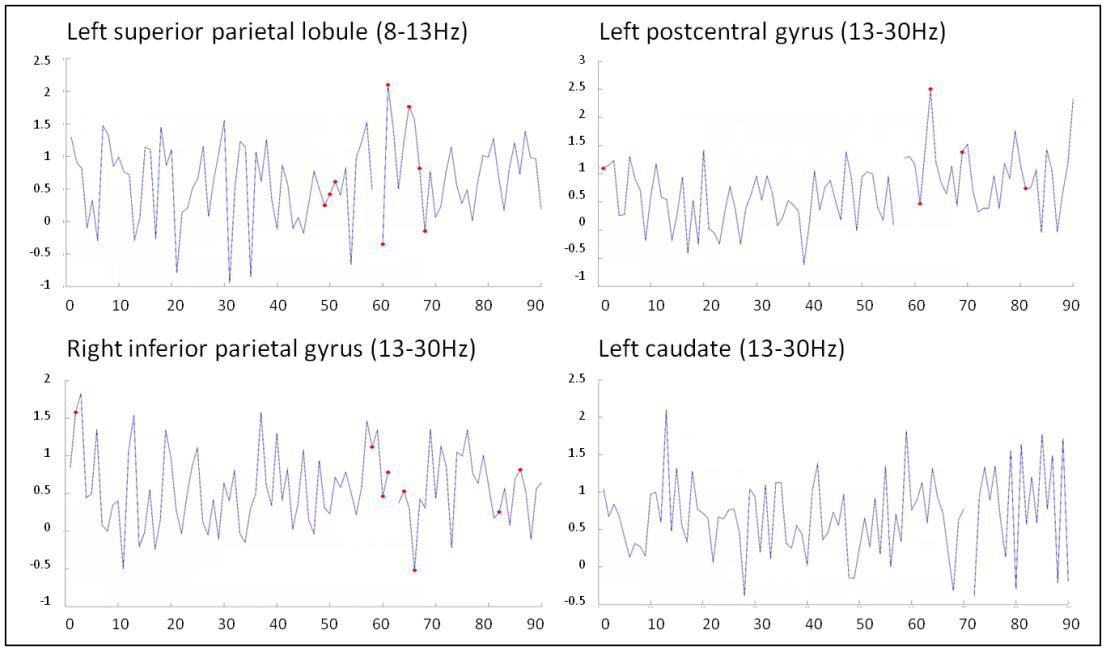

Figure 4-6. Average connectivity (correlation values) between each of the previously significant regions with all other regions in the connectivity matrix. The non-thresholded connectivity values are plot by the solid blue line, and those which survived the thresholding procedure are plot as red circles.

Nevertheless, five supra-threshold connections are found in the left postcentral gyrus (beta band), and eight connections survive in both the left superior parietal lobule (alpha band) and right inferior parietal gyrus (beta band). Figure 4-6 also highlights that the connections with the highest average correlation value in the non-thresholded maps do not necessarily fall consistently within the strongest subset of connections, and thus do not survive the present threshold. Indeed, in each case, there seem to be a number of sub-threshold connections that have an equivalent or higher average correlation value compared to the supra-threshold connections. It may be the case that these non-stable connections, perhaps occurring in only a subset of participants, were driving the previously observed statistical differences between perampanel and placebo.

4.5 **Discussion**

We report here, for the first time, the impact of the AMPA antagonist perampanel on signal power across 1-100Hz in resting-state EEG/MEG recordings in humans. We predicted that perampanel would increase MEG power in low frequency bands and decrease power in higher bands, and this hypothesis was supported. Following perampanel administration, we saw an increase in posterior power in lower frequency bands, but decreased power in the high gamma range over parietal sensors. Further, we also investigated the effect of perampanel on functional connectivity in source space. We found selective increases in functional connectivity following drug dose. Analysis of psychometric scales confirmed increased subjective ratings of intoxication following the dose of perampanel compared to placebo.

Participants reported feeling more intoxicated following perampanel dose compared to placebo, and on completion of the study all were able to correctly guess their session participation order. The significant effect of perampanel on the SHAS is consistent with these subjective reports, and findings of significant drug effects in the sedative but not stimulant scale of the BAES is consistent with the drug's mechanism of action. In some cases perampanel can have psychiatric side effects including increased aggression and hostility (FDA, 2012). However, the results of the SHS suggest that there were no such side effects in the present study, likely due to only a single administration of the drug. Although the experiment was run under single-blind conditions the subjective effects that participants experienced effectively unblinded them from the intervention. This is a common issue in many psychopharmacology experiments. That said, given the basic physiological measures reported here (as opposed to clinical responses), and the similar data quality

between conditions, we would argue that the effective unblinding is unlikely to have affected our central results.

To the best of our knowledge this is the first human neuroimaging study of the effects of a selective AMPA compound and, as such, the results cannot be compared to previous human studies. However, our results are consistent with previous animal work showing suppression or near elimination of gamma oscillations and increase in low frequency oscillations following administration of AMPA antagonists (Herrero et al., 2013; Oke et al., 2010; Sebban et al., 2002). It becomes more difficult to compare the connectivity analyses to previous literature given the lack of previous studies. It is worthwhile to note that the regions showing increases in connectivity following perampanel dose appear distinct from those which showed a straightforward power increase in the sensor analysis. Generally speaking, we found that connectivity was higher in parietal regions in each recording. This is reflective of previously documented fMRI connectivity hubs in parietal regions, including the inferior parietal cortex and postcentral gyrus (Buckner et al., 2009; Tomasi & Volkow, 2011). There is some evidence that focal epilepsies are associated with reductions in connectivity in various networks, including those recruiting parietal regions (e.g. sensorimotor networks; Liao et al., 2010; Luo et al., 2012b). So, the increase in connectivity following perampanel dose may point to a possible correlate of the seizure controlling mechanism of the drug.

Interestingly, NMDA antagonists (e.g. ketamine) seem to exhibit almost the opposite pattern of effects from the present study. Compounds of this type increase fast- and decrease slow background rhythms in both in-vivo mouse recordings (Lazarewicz et al., 2009) and human EEG (Hong et al., 2009). A recent MEG study showed that ketamine reduced posterior alpha power and increased parietal gamma power

(Muthukumaraswamy & Shaw, 2015), thus again supporting the idea of differential receptor effects. Furthermore, AMPA and NMDA signaling pathways have been shown to have differential effects on fMRI signals in rodents (Gsell et al., 2006). Taken together, these findings suggest that it is too simplistic to consider generic glutamate effects on oscillatory activity, but rather the separation of specific receptors, AMPA and NMDA, is critical to understanding the generation of EEG/MEG signals and the nature of oscillatory coupling across brain regions.

The similarities of the perampanel oscillatory modulations to those of tiagabine reported by Nutt et al. (2015) is clear for some frequency bands (see Figure 4-7). Both drugs increase slow wave activity and decrease faster rhythms, thus shifting the brain to a less excitable state, but have marked differences in their mechanism of action. Whereas perampanel decreases the actions of glutamate at the synapse via allosteric blockade of AMPA receptors, tiagabine is a GABAergic drug that is thought to potentiate GABAergic inhibition by blocking reuptake (Meldrum, 1996). However, both drugs are most commonly used as an adjunctive treatment for refractory partial seizures in epilepsy, so the similarities in spectral power changes may, again, reflect the seizure-controlling mechanisms of both compounds.

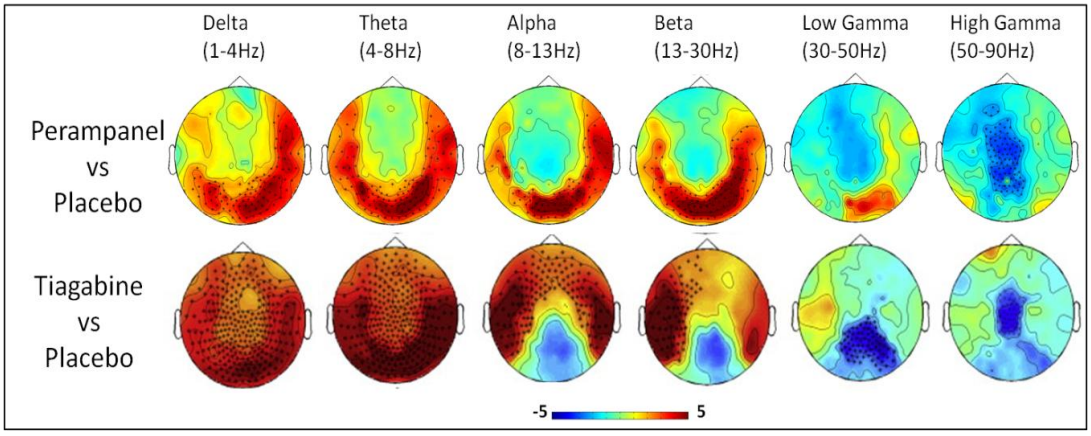

Figure 4-7. The spectral profile of perampanel shows similarities to tiagabine, with both increasing power in lower frequencies (1-30Hz) and decreasing power in higher

frequencies (30-100Hz). A full description of the tiagabine results can be found in a previous publication (Nutt et al., 2015).

We chose to complete the second MEG recording two hours after dosage, as a single dose <8mg is expected to have reached maximum blood plasma level by this time (Templeton, 2010), but with a range from 30 minutes to 2 hours, it is possible that we missed the peak for some participants. This being said, the combined effects of fast absorption rate and long terminal half-life of perampanel suggests that we would be unlikely to be more than 50ng/ml from peak concentration for any given participant. Measuring plasma concentrations following dosage with the drug might have ensured the post-dose timepoints were collected at the optimum time. Additionally, collecting multiple post dose timepoints as has been done previously (Magazzini et al., 2016; Muthukumaraswamy et al., 2013c; Nutt et al., 2015) would give a more comprehensive picture of the full effects of the pharmokinetic profile on oscillatory activity, though the terminal half life range from 53-123 hours means that collecting data over the full range would be difficult in practical terms. Furthermore, it would be interesting to study the oscillatory effects of perampanel at sustained doses, for example in epilepsy patients prior to commencement of perampanel and again at steady-state dose. However such studies in patient populations present practical difficulties through disease heterogeneity and variable concomitant medications.

4.6 **Conclusion**

The results reported here demonstrate that perampanel has widespread effects on MEG spectral power at rest. These results, taken with previous work on NMDA receptor antagonists, highlight the sensitivity of MEG to specific receptor-level changes within the glutamatergic system. Given these results, caution should be

exercised in analyses comparing medicated patient groups with un-medicated controls. We also show that non-thresholded connectivity matrices seem sensitive to drug-related changes in connectivity in specific regions, but following thresholding only global connectivity changes in the beta band maintain statistical significance. Given that the thresholding procedure relies on commonly strong connections among all participants, it is possible that non-stable connectivity in a subgroup of participants drive the differences observed in the non-thresholded maps.

5 Assessing changes to MEG spectral power and functional connectivity in Juvenile Myoclonic Epilepsy

5.1 Abstract

Juvenile Myoclonic Epilepsy (JME) is one of the most common idiopathic generalised epilepsies, and is characterised by myoclonic jerks. Patients also commonly experience generalised tonic-clonic seizures and in some cases, absence seizures. A growing body of evidence implicates a frontal thalamcortical network in generation of epileptiform activity in this syndrome. A number of studies have investigated background changes in power and connectivity between JME patients and healthy controls, but the findings may be confounded by the presence of interictal paroxysms. Non-invasive neurophysiological techniques such as MEG are ideally suited to studying background oscillatory activity in epilepsy as they allow for identification and removal of epileptoform activity. It has previously been shown that generalised epilepsy patients exhibit disrupted connectivity across a broad range of frequency bands, but often these studies do not distinguish between common syndromes. Here, we examine resting-state MEG data in a homogenous group of 25 JME patients and 25 age- and gender- matched controls. We use the pipeline established in previous chapters of this thesis with the aim of investigating whether JME patients show dysfunction in whole brain connectivity across a range of frequencies.

5.2 Introduction

5.2.1 Brief background on Juvenile Myoclonic Epilepsy

Juvenile myoclonic epilepsy (JME) is a sub-classification of idiopathic generalised epilepsy (IGE), characterised by myoclonic jerks, generalised tonic-clonic seizures (GTCS) and absence seizures (ILAE, 1989). The syndrome has an estimated prevalence of 0.1-0.2 per 1000 and accounts for up to 18% of all IGE diagnoses, making it one of the most common syndromes in that classification (Camfield, Striano, & Camfield, 2013). Symptoms typically first appear during childhood or adolescence, though age of onset range between 8 and 36 years is reported (Delgado-Escueta & Enrile-Bacsal, 1984). More recently, the IGE classification has additionally come to be known as genetic generalised epilepsies due to evidence of a genetic component in the aetiology (Berg et al., 2010).

The hallmark seizure of JME is myoclonic jerks, which are most frequent in the morning and exacerbated by sleep deprivation (Panayiotopoulos, 2010). The classic EEG feature in JME is a 4-6Hz generalised spike-wave (GSW) or polyspike-wave activity. Almost all patients with JME will have at least one GTCS, and a smaller number also experience absence seizures (Camfield et al., 2013). Related syndromes include juvenile absence epilepsy (JAE) and IGE with GTCS only. An EEG study of interictal power ('background' activity with no paroxysms present) suggests that JME is associated with increased global power in the delta and alpha bands that are most pronounced in frontal regions (Tikka, Goyal, Umesh, & Nizamie, 2013).

Though JME is classified as a generalised epilepsy, focal discharges are reported in some patients (Jayalakshmi, Srinivasa Rao, & Sailaja, 2010). Consistent with this notion, an increasing body of neuroimaging work indicates the involvement of a frontal thalamocortical network in JME (see reviews by Anderson & Hamandi, 2011; Koepp, Woermann, Savic, & Wandschneider, 2013). A MEG and EEG study of seven IGE patients

found that spike-wave and single spike activity localised most consistently to frontal and subcortical/thalamic areas (Stefan, Paulini-Ruf, Hopfengärtner, & Rampp, 2009). This is consistent with work suggesting that JME patients show altered structural connectivity in mesial frontal areas (Vollmar et al., 2012), though other studies have also found more widespread structural changes in IGE/JME (Focke et al., 2014).

5.2.2 Studying functional connectivity in JME

Given that epilepsy is fundamentally a disorder of aberrant neural synchrony, the study of connectivity is gaining pace and is expected to be a valuable tool in further understanding the many facets of the disorder (see reviews by Engel et al., 2013b; Hamandi et al., 2016; Pittau & Vulliemoz, 2015). Previous work has focused on studying interactions between different brain areas during epileptic paroxysms such as GSW (Lee et al., 2014; Moeller et al., 2011; Vaudano et al., 2009). Whilst specific thalamocortical networks are implicated in generation of GSW (Blumenfeld, 2005), a recent MEG study suggests that epileptic activity in JME is associated with both local and global increases in connectivity (Lee et al., 2015).

However, it is also important to understand background activity, between seizures, in order to elucidate the way in which the brain is kept in an enduring seizure prone state. Few studies have specifically examined the interictal connectivity profile in JME. Functional magnetic resonance imaging (fMRI) studies have revealed altered connectivity, particularly decreases in integration of the default mode network (DMN), in both IGE (McGill et al., 2012; Wang et al., 2011) and temporal lobe epilepsy (Pittau, Grova, Moeller, Dubeau, & Gotman, 2012). Given the indirect nature of the technique, studies using fMRI alone are limited by inability to distinguish true background activity from recordings containing paroxysmal discharges. Nevertheless, disrupted DMN connectivity has also been shown in concurrent EEG-fMRI studies of absence epilepsy

(Luo et al., 2011; Masterton, Carney, & Jackson, 2012), as well as increased connectivity in the basal ganglia network in IGE (Luo et al., 2012a).

Results from MEG and EEG connectivity studies specific to JME are mixed. One EEG study found increased connectivity in the 1-10Hz range coupled with decreased connectivity in the 10-25Hz range, primarily in cortical regions related to sensorimotor function (Clemens et al., 2013). However, another study using sensor space MEG analysis found that JME patients exhibit increased connectivity (phase synchronisation) across the entire scalp for all frequency bands (Niso et al., 2015). More generally, some studies have investigated functional connectivity in heterogenous groups of IGE patients, or in those who experience GSW discharges. In JAE, patients exhibit increased connectivity in the 5-14Hz range compared to controls (Chavez, Valencia, Navarro, Latora, & Martinerie, 2010), somewhat consistent with the JME results from Niso et al (2015) who found greatest connectivity increases in the 8-20Hz range. A recent MEG graph-theory study found global increases in interictal connectivity at source level in IGE patients compared to controls, with the most pronounced effects occurring in mesio-frontal, temporal and motor areas (Elshahabi et al., 2015). This is consistent with sensor-space JME results from Niso et al (2015) but provides additional information about areas underlying connectivity changes. However, only one patient in the study by Elshahabi et al (2015) had a specific diagnosis of JME, so it remains to be seen whether source-localised connectivity in a homogenous group will exhibit similar patterns.

5.2.3 Aims

The present study aims to build on previous EEG and MEG work investigating changes to spectral power and functional connectivity during the interictal period in JME patients. We will apply the analysis pipeline validated in previous chapters of this thesis to estimate whole-brain connectivity during interictal periods and compare to the

connectivity pattern of neurotypical control subjects. It is hoped that better understanding of background activity will contribute to further elucidating the mechanisms by which patients with JME remain in an enduring seizure-prone state.

5.3 Methods

5.3.1 Participants

The patient data presented were collected as part of a number of projects conducted at CUBRIC involving epilepsy patients. Some of the structural imaging data and task MEG data from these patients has been published (Caeyenberghs et al., 2015; Hamandi, Singh, & Muthukumaraswamy, 2011; Perry, Brindley, Muthukumaraswamy, Singh, & Hamandi, 2014), but the resting-state MEG data have not been reported previously. Healthy control subjects are taken from the first phase of the '100 Brains' genetic neuroimaging project (for a full description, see Brealy, 2015). All studies were approved by NHS ethics and research and development committees and participants gave written informed consent prior to participation.

We analysed rest data from 25 patients (19F/6M, mean age 27.5, range 18-47). Twenty-five control subjects were matched to patients for age and gender (19F/6M, mean age 26.5, range 18-47). Each of the patients included in this analysis had a diagnosis of IGE with sub-classification to JME, and an overview of clinical characteristics can be seen in Table 6. A more extended clinical information table can be found in the appendices.

Seizure type	**MJ 100%**

	GTCS 100%
	ABS 48%
Age at onset (MJ)	15 ± 4years
AEDs	LEV 52%, VPA 40%, LTG 28%, TPM 16%, ZNM 12%, CLB 8%
Status	Refractory 76%
	Controlled 24%

Table 6. Clinical information for the 25 JME patients included in this analysis. Abbreviations: MJ - myoclonic jerks, GTCS - generalised tonic clonic seizures, ABS - absence seizures, AEDs - anti-epileptic drugs, LEV - levetiracetam, VPA - valproate, LTG - lamotrigine, TPM - topiramate, ZNM - zonisamide, CLB - clobazam.

5.3.2 Stimuli and procedure

Subjects were seated upright in the MEG scanner inside a magnetically shielded room. For the 5 minute eyes-open rest recording, subjects were instructed to maintain their gaze on a fixation spot in the centre of the screen. The visual fixation point was displayed on a Mitsubishi Diamond Pro 2070 monitor (1024 pixels x 768 pixels resolution, 100Hz refresh rate). All stimulus delivery was controlled by Matlab software.

5.3.3 MEG recordings

Resting-state MEG data were acquired as a continuous recording, using a CTF-Omega 275 channel system sampled at either 600Hz or 1200Hz. Consistent with previous experiments, all recordings were later downsampled to 600Hz for analysis and the data were analysed in synthetic third order gradiometer mode. For MEG/MRI co-registration, electromagnetic coils were placed at fixed distances from anatomical landmarks (left/right preauricular and nasion) prior to the MEG recording, and localised inside the

scanner before and after each task. The fiduciary locations were later marked manually on the anatomical MRI.

5.3.4 Analysis

For pre-processing, the data were cut into 2 second epochs and visually inspected to remove artefacts. Given the aims of the present study to characterise the background connectivity profile in JME, any trials containing interictal spiking activity in the patient datasets were also discarded.

As in previous chapters, we used an atlas-based source reconstruction to derive virtual sensors in each of the 90 regions of the AAL atlas. We first considered group differences in oscillatory power. For this purpose, we used the percentage change in the Hilbert envelope (herein referred to as 'activation') that is calculated for each region prior to generation of the connectivity matrices. Given that we use the voxel of maximum change as the ROI representative in subsequent steps, the activation measure represents the maximally active voxel within a region, for each person and frequency band. We additionally extracted kurtosis values for each representative voxel in order to determine whether any inherent differences in data smoothness remained in the patient data relative to control subjects, even after removal of epileptic spiking events. Kurtosis is a mathematical operator that measures the susceptibility of a given data distribution to outliers, and is used in automatic localisation algorithms for epileptic foci (e.g. SAM(g2); Robinson, Nagarajan, Mantle, Gibbons, & Kirsch, 2004). In this case, we apply a simple kurtosis measure (matlab implementation) to the envelope data from each virtual sensor to derive an index of data 'spikiness'.

The connectivity analysis pipeline used is consistent with that reported in previous chapters. Briefly, this includes generation of whole-brain amplitude-amplitude

connectivity matrices using the voxel of maximum change for each of the 90 AAL regions, with multivariate leakage correction applied.

5.4 Results

5.4.1 Spectral characteristics

Following artefact rejection, there were no significant differences in the number of remaining trials between controls (mean=146, std=4.6) and patients (mean=142, std=11.9; t(48)=1.65, p=0.1).

In order to determine whether there were any differences between patients and controls in activation, we examined the percentage change in power for each of the 90 AAL regions (Figure 5-1). In the theta and alpha bands, there were a small number of areas around occipital and parietal regions where average activation seemed to trend towards an increase for patients compared to controls. We formally tested differences in activation using a randomisation test (10,000 permutations of the mean), and found that only the right angular gyrus (region 66) in the theta band differed significantly between patients and controls (t=2.764, p=0.02). We also compared kurtosis values for each of the 90 AAL regions, but found no significant differences between patients and controls on this measure (see Appendix G for figure).

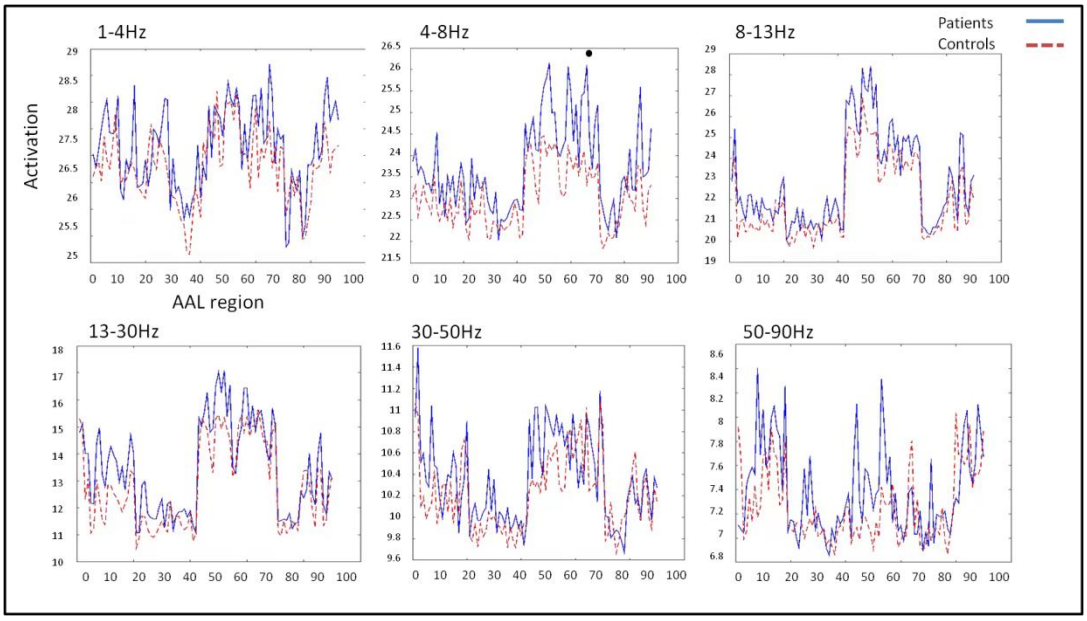

Figure 5-1. Average activation (percentage change) in each of the 90 AAL regions, for patients (in blue) and controls (in red). Activation in the right angular gyrus in the theta band (4-8Hz) was significantly higher for patients compared to controls, marked with a black circle on the plot.

5.4.2 Functional Connectivity

For the next stage of the analysis, we assessed functional connectivity using a pipeline validated in previous chapters of this thesis. The unthresholded connectivity matrices for patients and controls are plotted in Figure 5-2a. The matrices for both patients and controls exhibit the same spatial structure as shown previously; namely a hub of increased connectivity across occipital and parietal areas that is strongest in the alpha band, but also evident in other bands. Patients also appear to have widespread increases in connectivity relative to controls, particularly in the theta-beta bands (Figure 5-2b).

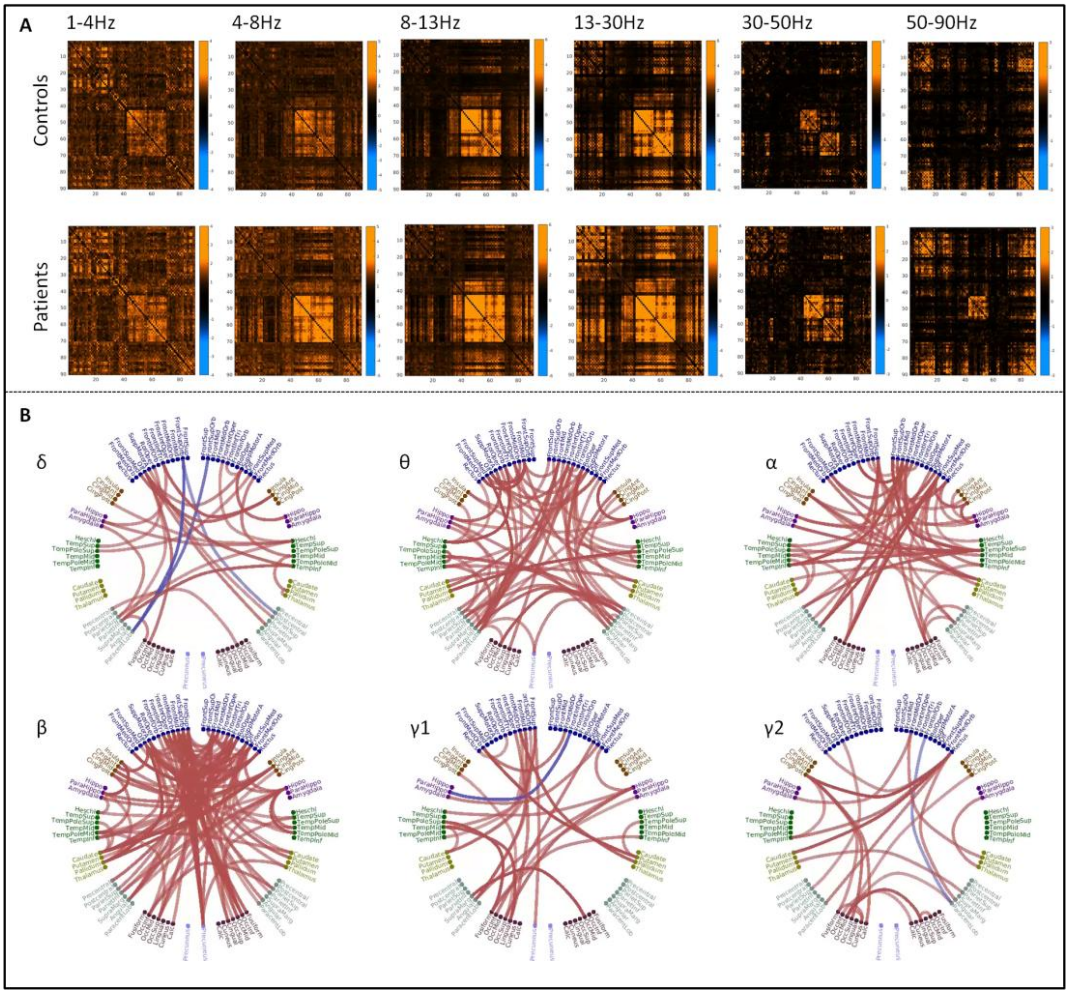

Figure 5-2. **(A)**Unthresholded connectivity matrices for patients (top) and controls (bottom), for each of the frequency bands studied. Stronger orange colouration is indicative of increased functional connectivity. **(B)** Differences in unthresholded node-

node connectivity between patients and controls. Lines plotted are t-statistics, p=0.05 (uncorrected). Red indicates a relative increase in patients and blue is a relative decrease.

To compare global connectivity differences between patients and controls, we computed the mean connectivity across all AAL regions in the unthresholded matrices for each participant (Figure 5-3). Using a between-subjects t-test, we found significant differences in global connectivity in the theta ($t(48)=2.87$, $p<0.01$), alpha ($t(48)=2.28$, $p=0.02$), and beta ($t(48)=2.26$, $p=0.02$) frequency bands. There were no significant group differences in the delta ($t(48)=1.84$, $p=0.07$), low gamma ($t(48)=1.66$, $p=0.1$) or high gamma ($t(48)=1.01$, $p=0.3$) frequency bands.

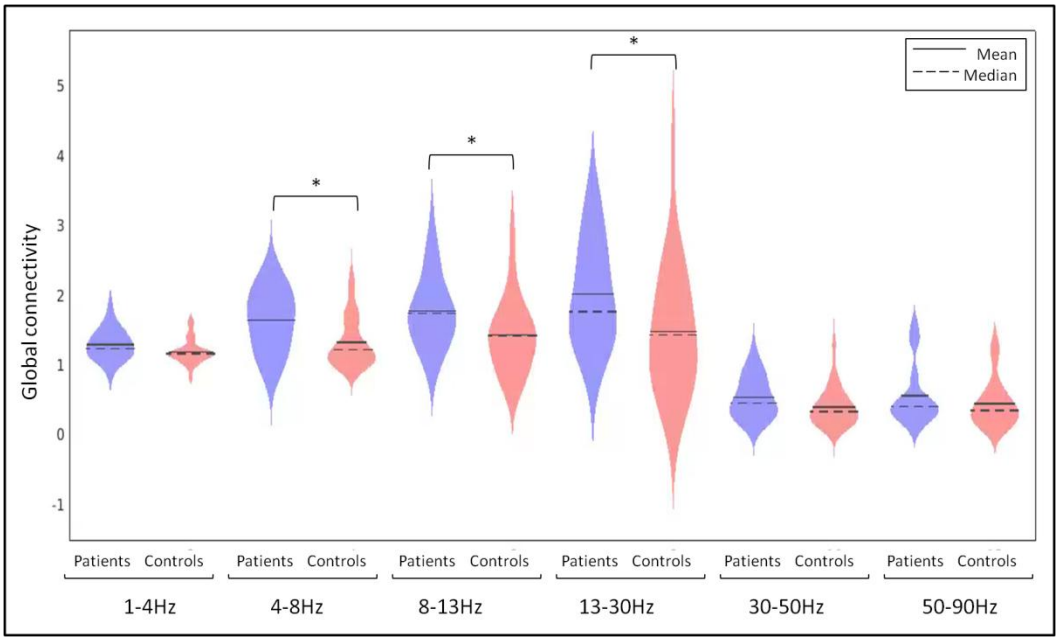

Figure 5-3. Global connectivity for patients and controls across delta-high gamma frequency bands, computed by taking a single value for each participant of the average unthresholded connectivity matrix in each band. Statistically significant differences are present in the theta, alpha and beta ranges (denoted '*').

We then pooled the matrices from all participants and thresholded the data in order to retain only the strongest and most consistent connections, consistent with the approach in previous chapters. The threshold was set to include the top 5% of connections

occurring for 95% of 10,000 bootstrap iterations. The remainder of the results herein are grouped by frequency band and the thresholded connectivity in the delta band is plotted in Figure 5-4. The pattern of connectivity following thresholding is consistent with previous chapters, with the greatest number of connections in frontal and temporal areas. However, there are no significant differences between patients and controls in single connections after omnibus correction, connectivity strength or global connectivity.

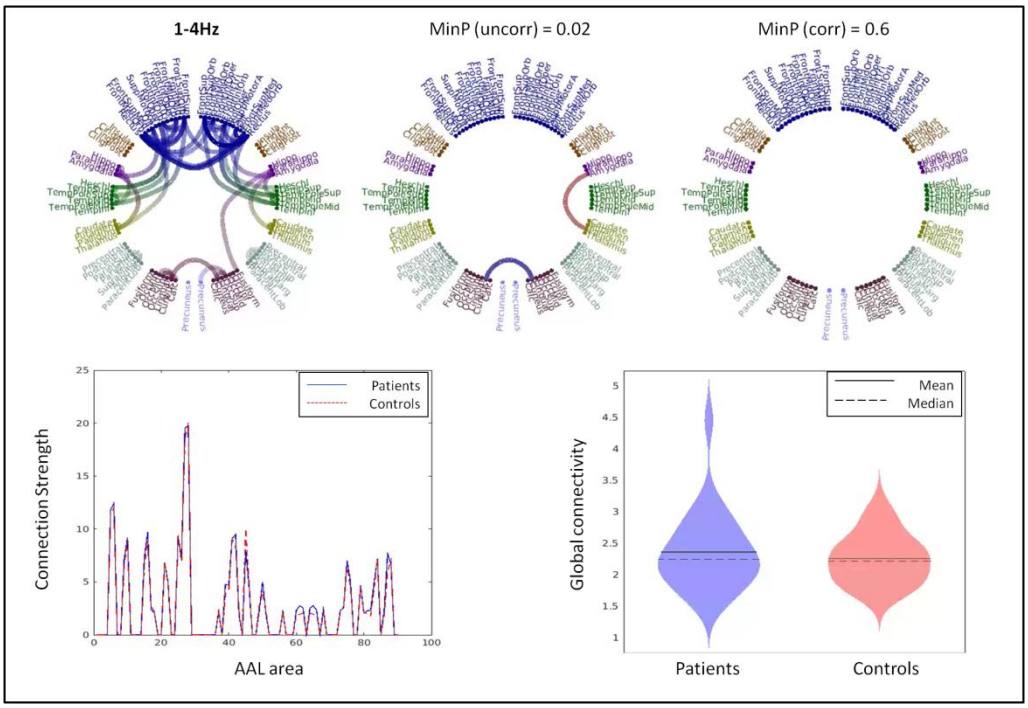

Figure 5-4. **Top Left:** Thresholded delta connectivity. **Top Middle:** Node-node connectivity (t-statistics) in thresholded maps at p=0.05, uncorrected. **Top Right:** No single connections survive statistical testing with omnibus correction. **Bottom right:** Thresholded connection strength for patients and controls, no significant differences. **Bottom left:** Thresholded global connectivity for patients and controls (t(48)=0.72, p=0.4).

The thresholded connectivity in the theta band is shown in Figure 5-5. The connections are concentrated in occipital and parietal areas with some projections to the temporal lobe. Again, statistical testing of node-node connectivity and connection strength using

randomisation testing (10,000 permutations) yields no significant differences between patients and controls. As in the unthresholded maps, global connectivity in the thresholded matrices is higher in patients compared to controls, though this difference now narrowly misses out on statistical significance (t(48=1.92, p=0.06).

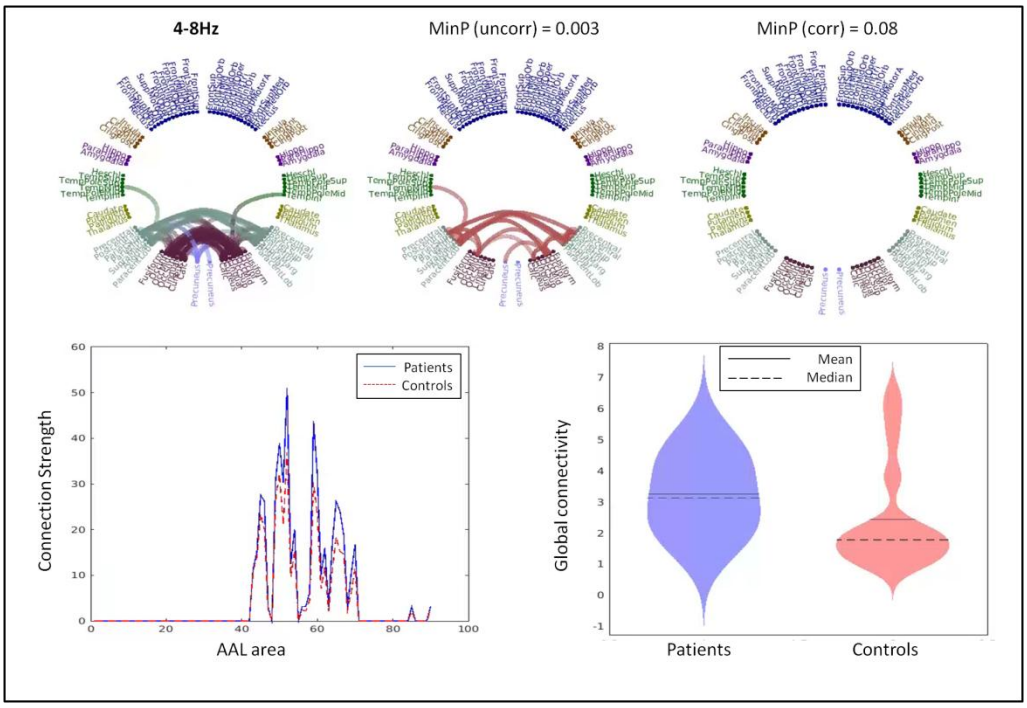

Figure 5-5. **Top left:** Thresholded theta connectivity. **Top middle:** Node-node connectivity in thresholded map (t-statistics, p=0.05 uncorrected). There are no statistical differences between patients and controls in single connections following omnibus correction (**top right**) or connection strength (**bottom left**). **Bottom right:** Patients still exhibit higher global connectivity values following thresholding, but this difference is no longer statistically significant (t(48)=1.92, p=0.06).

Thresholded connectivity in the alpha and beta bands also shows a pattern consistent with previous chapters (Figure 5-6 and Figure 5-7). However, similarly to the other frequency bands, there are no statistically significant differences between patients and controls in these thresholded matrices at the level of single connections or connection strength, or global connectivity value.

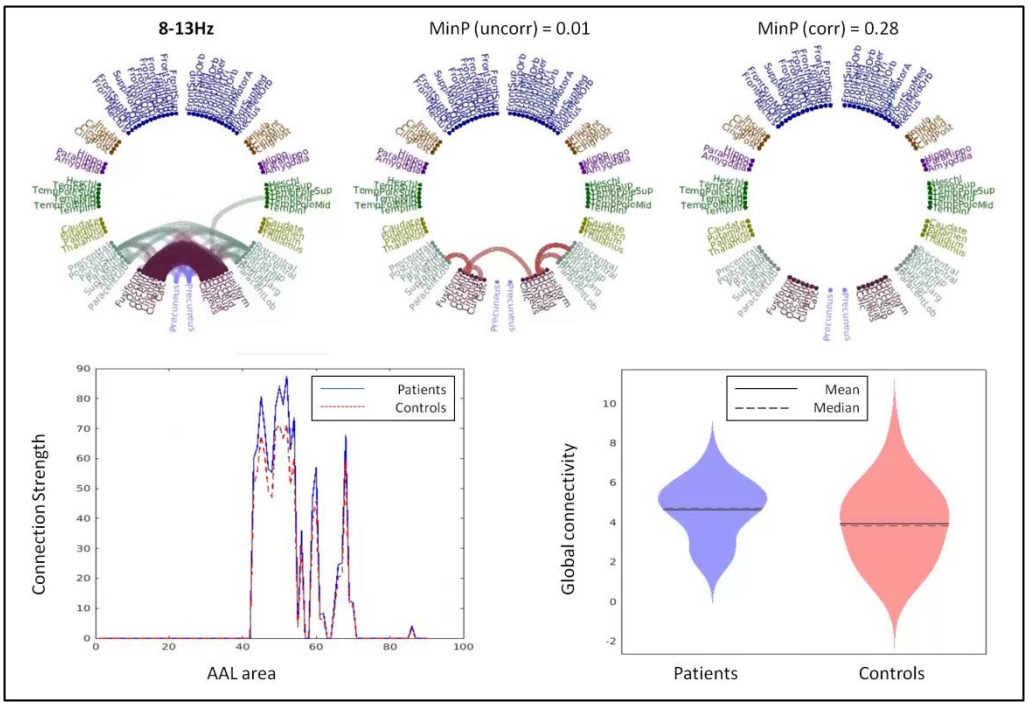

Figure 5-6. **Top left:** Thresholded alpha connectivity. **Top middle:** Single connections in the thresholded map plot as t-statistics, p=0.05 (uncorrected). As before, there are no statistically significant group differences in single connections with omnibus correction (**top right**), connection strength (**bottom left**) or global connectivity ((t(48)=1.48, p=0.1); **bottom right**).

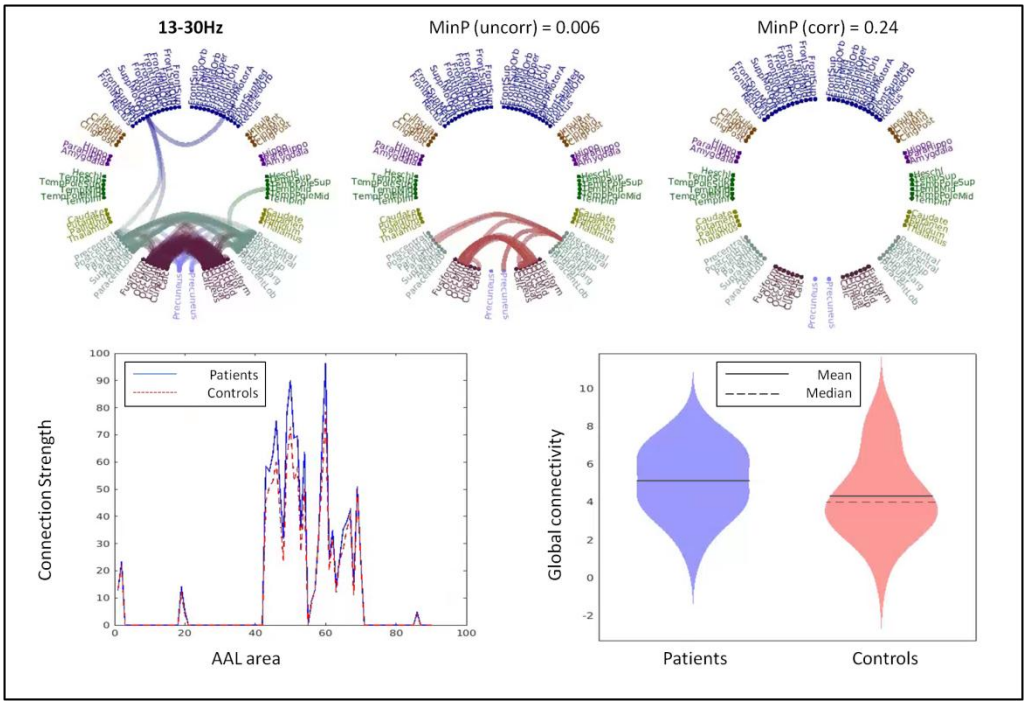

Figure 5-7. **Top left:** Thresholded beta connectivity. **Top middle:** Node-node connectivity (t-statistics) in the thresholded maps, p=0.05 (uncorrected). As before, there are no statistically significant group differences in single connections with omnibus correction (**top right**), connection strength (**bottom left**) or global connectivity ((t(48)=1.49, p=0.1); **bottom right**).

The thresholded maps for both gamma bands are plotted in Figure 5-8. It is notable that a number of connections survive thresholding in this cohort in both the low and high gamma bands. For the low gamma band the pattern bears similarity to the spatial distribution of thresholded beta connectivity and may represent frequency leakage from the higher SNR band. In the high gamma band the remaining connections are largely focused in frontal and temporal regions that are known to be sensitive to contamination by muscle artefact (Muthukumaraswamy, 2010). Further, given that thresholded gamma connections were not observed in any chapter previously using the same pipeline we suspect that, in both cases, this suprathreshold connectivity is artefactual and the gamma bands were not analysed further.

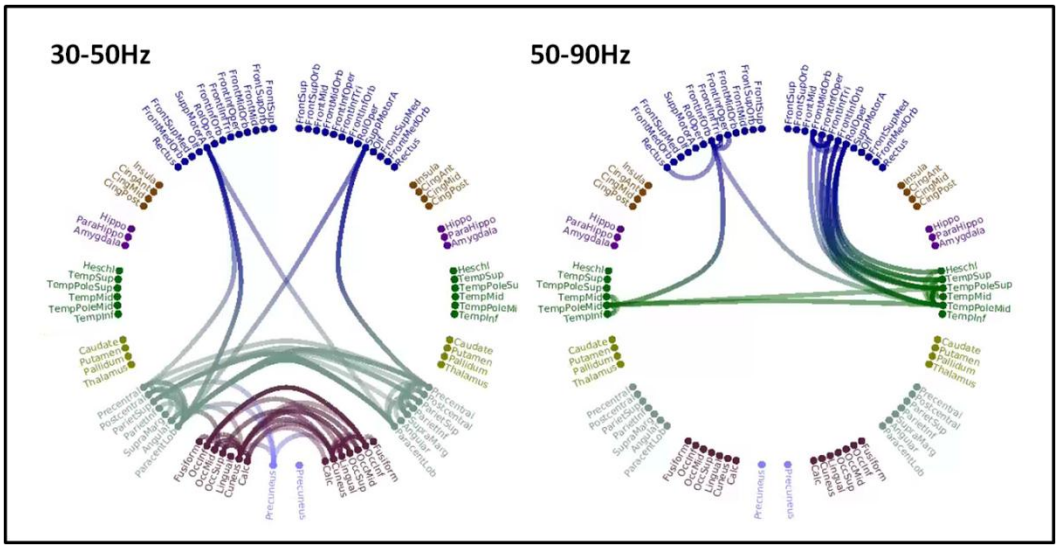

Figure 5-8. Thresholded connectivity for low-gamma (**left**) and high-gamma (**right**). This connectivity is presumed to reflect non-neural artefact and was not analysed further.

5.5 **Discussion**

Here we aimed to investigate source-space differences in spectral properties and connectivity between a group of JME patients and age- and gender- matched control subjects. We found that patients exhibit significantly higher source activation in the right

angular gyrus in the theta band, but that there are no differences between patients and controls in source-level kurtosis. Patients show increases in functional connectivity relative to controls across the 4-30Hz range prior to thresholding, but these findings are not preserved in the thresholded matrices.

The only statistically significant difference in source activation between patients and controls was in the right angular gyrus in the theta band. This finding is somewhat consistent with findings of disruption to areas involved in the default mode network in generalised epilepsies (McGill et al., 2012; Wang et al., 2011), and also in a previous paper using data from the same patients showing abnormalities in a structural network involving parietal areas (Caeyenberghs et al., 2015). The lack of group differences in beta activation is consistent with a previous paper from our group in which no significant differences in baseline beta amplitude (during the inter-trial interval of a visual task) were found between JME patients and controls (Hamandi et al., 2011). However, it is important to note that SNR is comparably high on the lateral surface (Goldenholz et al., 2009) as well as in low frequency bands due to the power-law distribution of oscillatory frequency. Therefore, we cannot rule out the possibility that this finding could be attributed to relatively increased SNR in this region and frequency band.

The JME patients included here form a sub-set of a larger group of patients in the study published by Caeyenberghs et al (2015). In that study, the authors find that JME patients exhibit hyperconnectivity in a structural network involving primary motor, parietal and subcortical regions, but no differences between patients and controls on global measures of structural connectivity (Caeyenberghs et al., 2015). Here, we do not find region-specific changes to functional connectivity but do observe an overall increase in global functional connectivity for patients relative to controls prior to thresholding, as well as increased power in an ROI in the right parietal lobe. It is possible that structural

changes in this cortical-subcortical network are related to changes in functional connectivity but further work is required to elucidate the nature and direction of this relationship. Our findings of increased connectivity in a number of frequency bands in the unthresholded matrices are consistent with previous electrophysiological work on functional connectivity in IGE (Elshahabi et al., 2015; Niso et al., 2015).

Nonetheless, we find no statistically significant group differences in connectivity following matrix thresholding that may be for a number of reasons aside from an absence of a true difference between groups. It is possible that our analysis was lacking in power to detect a between-groups effect, though other studies have detected statistically significant differences with similar or fewer participant numbers (Elshahabi et al., 2015; Niso et al., 2015). However, given the connections surviving in the gamma bands, it may be the case that SNR in this cohort is generally low. An additional consideration is in the choice of thresholding procedure, which selects only connections that are commonly strong among all groups. Therefore, this approach may not be suitable in cases where there are plausible differences in the spatial patterns of connectivity between groups as well as connectivity strength. For example, in this instance, structural and functional changes in frontal areas are commonly implicated in JME (Holmes, Quiring, & Tucker, 2010; Tae et al., 2006) and yet very few frontal connections survive thresholding.

Some previous studies have suggested that epileptoform activity drives altered connectivity patterns in epilepsy. For example, one fMRI study found that areas involved in GSW do not show interictal changes in connectivity (Moeller et al., 2011). Other studies show correlations between interictal paroxyms and increased network connectivity (Zhang et al., 2010), or increased connectivity in data containing GSW compared to non-GSW data (Zhang et al., 2014). In the current study, we manually

inspected the data to remove suspected epileptoform activity as well as physiological artefacts. Therefore, it is unlikely that any differences between patients and controls can be attributed to interictal paroxysms, and a more likely to reflect a difference in the baseline connectivity profile.

Although we used a fairly homogenous group of JME patients, there was variation among the cohort in seizure frequency, controlled or refractory status, duration of epilepsy and a variety of anti-epileptic medications. So, it is likely that even in this group, there are a number of factors that may have influenced the results. For example, we already show in the previous chapter that AEDs can affected the connectivity profile, and other studies also highlight drug-related changes to power and connectivity. Lamotrigine has been shown to decrease delta and theta power, and the level of LTG related power decrease was correlated with initial (untreated) power (Clemens, Piros, Bessenyei, & Hollody, 2007). Further, when compared with unmedicated patients, IGE patients treated with valproate show more 'normalised' functional connectivity (Clemens et al., 2014). So ,it may be the case that differences in power or connectivity were masked and/or exacerbated by a number of uncontrolled variables in the current cohort.

5.6 **Conclusion**

Relative to controls, patients show increased activation in the right angular gyrus in the theta band that may be consistent with the notion of disruption to the DNM in JME. The JME patients exhibit increases in global connectivity compared to controls in the theta-beta bands, but these differences are not preserved following matrix thresholding. This may be due in part to the use of a thresholding procedure that is potentially insensitive

to differences between groups in the spatial profile of the connectivity matrix. The findings of the present study are consistent with previous work and add to the growing body of literature implicating pathology in theta band oscillations in JME.

6 General discussion

6.1 Thesis rationale and main findings

The work contained within this thesis is an investigation of the resting-state in MEG, and more specifically functional connectivity measured using amplitude coupling. We first sought to establish reproducibility and suitability of a full connectivity analysis pipeline for a variety of applications in resting-state MEG. These included a comparison of MEG and fMRI derived connectivity and an examination of the neural activity underlying the MEG signal using pharmacological intervention, as well as the application of this technique in the non-invasive study of epilepsy.

6.1.1 MEG RSNs measured using both ICA and atlas-based correlation of amplitude envelopes are robust over repeated recordings

In the first experimental chapter, we assessed the repeatability of connectivity in resting-state MEG recordings from 21 participants using two analysis techniques. For the first technique, we extracted biologically plausible RSNs using an ICA approach to assess amplitude coupling and found a number of robust networks in the beta band, consistent with the seminal paper on the approach (Brookes et al., 2011b). Focusing on the sensorimotor and visual networks, we found some degree of individual variability in network strength but estimates for each individual were consistent over repeated recording. Using the second technique, we instead estimated whole brain amplitude coupling using an atlas-based approach (Hillebrand et al., 2012). Not surprisingly, the alpha and beta band connectivity in the atlas-based approach showed the highest degree of repeatability. This is consistent with previous work demonstrating that corrected amplitude envelope correlation provides a stable estimate of connectivity over multiple recordings (Colclough et al., 2016; Garces et al., 2016). Given that the atlas-based approach inherently minimises signal leakage

that could give rise to spurious correlation (Schoffelen & Gross, 2009) and offers an entirely data driven approach to connectivity analysis, we selected this pipeline for subsequent chapters.

6.1.2 Varying minor parameters of the analysis pipeline has little effect on connectivity estimates

We chose to vary two minor parameters in the atlas-based pipeline, namely the choice of ROI representative and the orthogonalisation method, in order to determine the effects of these changes on the stability of connectivity estimates. Regardless of condition, we saw the greatest spatial structure in connectivity in the alpha and beta bands, consistent with a number of similar studies (Hillebrand et al., 2012; Tewarie et al., 2016; Tewarie et al., 2014). There was little difference between choosing the voxel of maximum change or conducting a PCA to determine those voxels within each ROI that explain 95% of the temporal variance, so we opted for the voxel of maximum change as the more parsimonious and computationally efficient choice. Symmetric orthogonalisation (Colclough et al., 2015) led to more spatially resolved matrices compared to pairwise orthogonalisation (Hipp et al., 2012), so we elected to use the former for subsequent analyses. Following selection of the most appropriate pipeline, we also replicated the same pattern of connectivity in an independent cohort in the second experimental chapter.

6.1.3 Using a linear combination of band-limited MEG connectivity gives a moderate estimate of BOLD-fMRI connectivity

After choosing our preferred MEG connectivity technique, we also wanted to see how MEG connectivity in the resting state would compare to fMRI resting-state connectivity in the same cohort. One of the key advantages of the atlas-based approach is that it enables ease of comparison between modalities (Hillebrand et al.,

2012). To generate fMRI connectivity matrices on the same spatial scale as MEG, we created a single BOLD timeseries for each AAL region by taking an average over all voxels in the ROI. We compared connectivity patterns among the two modalities using a regression approach and found that activity in the delta band had the greatest loading to the fMRI connectivity map. There was some variance in the fMRI connectivity that could not be explained by a linear combination of the MEG frequency bands, and this corresponded to connectivity between homologous areas in the two hemispheres. Although some MEG studies do report observing this homotopic connectivity (Hipp et al., 2012; Liu et al., 2010), this often occurs in frequencies <1Hz. We routinely filter MEG data with a high pass filter at 1Hz during pre-processing prior to analysis, so this may explain why the homotopic connectivity effects are not strong in this analysis.

6.1.4 Changes to endogenous glutamate levels affect power and connectivity in the resting-state

We next applied the validated pipeline in a pharmacoMEG experiment, where we also studied changes to spectral power following administration of a single 6mg oral dose of the selective AMPA antagonist, Perampanel. As well as probing the possible mechanisms of therapeutic action of these anti-epileptic drugs, this type of intervention study may help to better understand the complex biochemical dynamics underlying the MEG signal. We found widespread drug-related changes to spectral power, with increases in posterior regions across low frequencies (1-30Hz) and a decrease in the high gamma range (50-90Hz). We additionally observed drug-related changes in global connectivity in the beta band that survived matrix thresholding. These findings are completely novel in humans, but are consistent with invasive animal work (Sebban et al., 2002). Our findings related to spectral power show some similarities to the profile of another anti-epileptic medication that may hint at the

seizure controlling mechanisms of these compounds (Magazzini et al., 2016; Nutt et al., 2015). Both animals and human studies using drugs that act primarily on NMDA receptors in the glutamate system show a largely opposite pattern of results (Lazarewicz et al., 2009; Muthukumaraswamy & Shaw, 2015; Shaw et al., 2015). Taken together, this suggests that MEG may be differentially sensitive to the effects of activity of multiple receptor types as well as discrete neurotransmitter systems.

6.1.5 JME patients show altered patterns of connectivity during resting-state recordings compared to healthy controls

In the final experimental chapter, we investigated resting-state changes in a group of patients with JME compared to age- and gender- matched controls. We found significantly increased source activation in patients relative to controls in the right angular gryus in the theta band. It is possible that this finding links with work exploring disruption to the default mode network in generalised epilepsies (McGill et al., 2012; Wang et al., 2011), but it is important to recognise the possibility that this outcome could also be caused due to increased SNR from the combination of location on the lateral surface (Goldenholz et al., 2009) and low frequency band.

We also saw widespread increases in connectivity in low frequencies in patients relative to controls, with a notable increase in connectivity structure around frontal regions in patients. This is consistent with the general implication of frontal regions in JME (Holmes et al., 2010; Jayalakshmi et al., 2010), as well as a number of studies that have specifically shown increased connectivity in networks recruiting frontal regions (Clemens et al., 2013; Lee et al., 2015). However, these changes did not survive matrix thresholding and significance testing. We suggest that the thresholding procedure used could have masked true connectivity differences, and may not be

appropriate for scenarios where the spatial pattern of connectivity differs between groups.

6.2 Towards the use of functional connectivity as a 'biomarker'

6.2.1 Stability of estimates over time

Functional connectivity is shown to be affected in many circumstances including neuropsychiatric disease (Greicius, 2008) and pharmacological interventions (Muthukumaraswamy, 2014). But in order for functional connectivity to be a valid marker of group differences, it must be shown to be reproducible in healthy participants using multiple analysis techniques and over repeated recording sessions. A number of studies have demonstrated the repeatability of RSNs using a variety of techniques in fMRI (Damoiseaux et al., 2006) and MEG (Colclough et al., 2016; Garces et al., 2016). Further, the work contained in this thesis shows that a reproducible connectivity estimate is affected following manipulation of glutamate using pharmacoMEG and in the JME syndrome of IGE (chapters 2, 4 and 5 respectively).

However, assessing stability in the absence of disease or disorder goes only one step towards full understanding of functional connectivity as a biomarker. In order for any technique to be a valuable clinical tool, it is important to establish the ability to draw conclusions based on data from one person (Lee, Smyser, & Shimony, 2013; Liuzzi et al., 2016). Although we show in chapter 2 that global connectivity estimates vary little between individuals, we cannot claim that the analysis technique is robust or diagnostic on a single-subject level. It is also unwise to draw conclusions about mid-length or longer term repeatability of RSNs based on the current study of scans only one week apart. Previous work from our group has shown that oscillatory activity in

the cortex is repeatable over multiple recording sessions (Muthukumaraswamy, 2010), but changes with age (Gaetz, Roberts, Singh, & Muthukumaraswamy, 2012). A recent MEG study also indicates that connectivity both within and between RSNs changes during development up to age 34 (Schafer, Morgan, Ye, Taylor, & Doesburg, 2014), but less is known about changes to RSNs across the full lifespan. It is plausible that there are ongoing changes to various aspects of functional connectivity with age (e.g. strength or spatial extent and pattern) but more longitudinal repeatability work or studies with a wider age range of subjects is required to delineate this possibility further. Recently a large (N=652) normative MEG database, spanning the age-ranges from 18 to 88, has been released by the Cambridge MEG group (https://camcan-archive.mrc-cbu.cam.ac.uk/dataaccess/). The validated pipelines I have outlined in this thesis could easily be used to assess age-related changes within this dataset.

6.2.2 The biological importance of functional connectivity

Although spontaneous statistical dependencies between regions, or 'functional connectivity', are now a well-established phenomenon, the physiological processes underlying this coupling are yet to be fully elucidated. The presumption that the MEG signal arises from post-synaptic potentials of pyramidal neurons (Lopes de Silva, 2010) indicates that any coupling changes measured by this technique at the macroscopic level are likely to reflect microscopic changes to the excitation-inhibition balance. For example, a recent modelling study by Gao, Peterson, and Voytek (2017) demonstrates that it is possible to infer the cortical excitation-inhibition balance using invasive electrophysiological data. The results of that study are consistent with the alterations to the MEG spectral profile following AMPA receptor blockade in chapter 4 of this thesis. Furthermore, increased connectivity in JME patients reported in chapter four of this thesis, as well as in previous literature, could indicate that

functional connectivity represents underlying physiological processes related to balancing excitability across the cortex. In the same vein, there is yet no agreed mechanistic account of the functional role that functional networks perform in mammalian cortex. Postulated theories are numerate, with many centred around capabilities related to information transfer and cognitive processing. For example, fMRI studies suggest that the default mode network is presumed to be involved in memory retrieval and manipulation (Greicius et al., 2003), and gamma band oscillatory networks are believed to have a role in attention and information flow regulation (Sejnowski & Paulsen, 2006). Further, there is a suggestion that oscillatory networks may have evolved as a mechanism to minimise energy expenditure during computational processing (Laughlin & Sejnowski, 2003). Based on these observations, one could speculate that inter-regional dependencies at rest reflect a 'baseline' state of excitability, or the maintenance of a state of preparedness to receive and process input. In this scenario, excitatory synaptic drive could be maintained at a higher basic level in a subset of regions that perform as a hub to the rest of the cortex. When the system is perturbed by pharmacological manipulation or disease state (e.g. epilepsy) this state of preparedness is interrupted, which can lead to pathologically increased or decreased connectivity across a wide range of regions. The fact that functional coupling typically manifests most clearly in the alpha and beta bands and across a consistent set of posterior regions could be seen as further evidence for this notion, especially given the theorised involvement of oscillatory activity at these frequencies in routing information transfer (Jensen & Mazaheri, 2010). Nevertheless, this could also merely be a manifestation of the increased SNR in these frequency bands and at these locations, so this interpretation should be taken with caution.

Within the remit of non-invasive electrophysiology alone, there are multiple ways in which the brain can become functionally connected (Schölvinck, Leopold, Brookes, &

Khader, 2013). This includes coupling between the amplitude of activity in different areas as studied in this thesis, but also fixed relationships between the phase of oscillations. There is some suggestion that phase synchronisation specifically is the most biologically plausible mechanism of long-range integration (Canolty & Knight, 2010; Varela, Lachaux, Rodriguez, & Martinerie, 2001). However, a recent framework suggests that both phase and amplitude coupling represent distinct intrinsic coupling modes that can co-exist from moment to moment in the brain (Engel, Gerloff, Hilgetag, & Nolte, 2013). In this framework, Engel et al. (2013) suggest that the function of spontaneous amplitude coupling is to modulate cortical excitability as a mechanism to assist sensory and cognitive processing. It may be argued that our results somewhat support this hypothesis, with changes to connectivity related to situations with known altered excitability observed in both chapters 3 and 4. However it is unclear from this resting-state work whether these connectivity fluctuations subserve sensory or cognitive performance. Further, the model is tailored to amplitude coupling at very low frequencies such as those measured in BOLD (<1Hz), so it remains to be seen whether this account also provides a reasonable explanation for amplitude coupling in higher frequencies.

Another facet in understanding the basis of functional connectivity relates to the association between functional coupling measured with different techniques. In chapter three, we show using a regression analysis that coupling in the delta and alpha bands have the strongest loading to fMRI connectivity. This finding is consistent with the suggestion that low frequencies engender long-range integration in the brain (Donner & Siegel, 2011; von Stein & Sarnthein, 2000), but somewhat inconsistent with other studies that show most similarity between fMRI and beta band connectivity (Brookes et al., 2011a; Brookes et al., 2011b). However, this

discrepancy may be explained by the fact that the strong parietal-occipital structure that dominates alpha and beta connectivity is less present in our fMRI data.

6.3 Relating neurotransmission to neuroimaging signals

6.3.1 Studying excitation and inhibition with MEG

GABA and glutamate respectively are the primary inhibitory and excitatory neurotransmitters present in the human brain and are intrinsically related to the excitation/inhibition balance(Isaacson & Scanziani, 2011). Studies relating the MEG signal to neurotransmitters have focused on GABA. For example, in visual task paradigms, GABA concentration has been linked to modulations of visual gamma frequency and gamma amplitude (Magazzini et al., 2016; Muthukumaraswamy et al., 2013c), though a larger study failed to replicate the link between GABA and gamma frequency (Cousijn et al., 2014). At rest, pharmaco-MEG work has shown that generally, increased GABA action is associated with increased low frequency power and decreased gamma power, though this pattern does vary according to mechanism of action (Nutt et al., 2015). To our knowledge, no previous studies have conducted this kind of work regarding the glutamate system. In chapter 4, we use the selective AMPA antagonist Perampanel in a pharmacoMEG intervention to show that transiently decreasing the actions of glutamate at the synapse is associated with increased power in delta-beta oscillations and decreased power in the high-gamma range. Our findings are consistent with previous invasive animal recordings (Oke et al., 2010; Sebban et al., 2002), and also consistent with the results of Nutt et al. (2015) in terms of net inhibition relating to increased low- and decreased high-frequency oscillatory power.

6.3.2 Functional connectivity and neurovascular coupling

A number of fMRI studies have related GABA and glutamate function to BOLD responses. In general, studies of GABA show that increased GABA concentration is related to decreases in both task-driven and resting-state BOLD responses (for a review, see Duncan, Wiebking, & Northoff, 2014). Given that oscillatory activity in the gamma band is shown to have the closest correlation with BOLD activity (Zumer et al., 2010), these findings are consistent with the MEG-GABA literature. As in MEG, fewer fMRI studies have specifically investigated the actions of glutamate. For example, in studies using fMRI combined with magnetic resonance spectroscopy, a positive correlation has been shown between glutamate concentration and activity in nodes of the default mode network (Enzi et al., 2012; Kapogiannis, Reiter, Willette, & Mattson, 2013). The findings in chapter 4 are consistent with these reports, as we show a decrease in gamma power related to decreased glutamatergic action. It follows that a decrease in oscillatory power in the gamma range should be associated with a decrease in local BOLD activity (Zumer et al., 2010). It should be noted that neurotransmitter concentration is not necessarily related to the hemodynamic response in a linear fashion over time (Forman et al., 1998), so changes to BOLD could represent changes to neurovascular coupling rather than neuronal activity per se. Nonetheless, these types of comparison offer a good method for assessing both neurovascular coupling and the microscale activity underlying neuroimaging methods.

There is some implication from the results in chapter 4 that further than the effects of different neurotransmitter systems, MEG may be sensitive to differential effects of receptor types in the glutamate system. For example, a previous study using the NMDA receptor antagonist ketamine showed drug-related decreases in delta, alpha

and beta activity along with an increase in theta and gamma power (Muthukumaraswamy & Shaw, 2015). Conversely in chapter 4 of this thesis, using an AMPA-receptor antagonist we show drug-related increases in low-frequency and decreases in high-frequency oscillatory power. The two receptors are known to have distinct physiological properties that may relate to these differential effects (Dodt, Frick, Kampe, & Zieglgänsberger, 1998; Kidd & Isaac, 2000). Further, a study in rodents showed that whilst an AMPA receptor antagonist significantly decreased both BOLD and evoked potentials to forepaw stimulation, administration of a NMDA receptor antagonist significantly decreased BOLD but only moderately decreased the electrophysiological response (Gsell et al., 2006). This indicates that electrophysiological measures may be more sensitive to differential receptor effects than BOLD-fMRI. Taken together with the findings of Muthukumaraswamy and Shaw (2015), our results indicate that it is possible to observe these same differential receptor effects non-invasively in humans using MEG. However, more work and replication of the effects seen in chapter 4 are necessary to delineate this possibility further.

6.4 Imaging functional connectivity in epilepsy using MEG

Epilepsy is one of the most common serious neurological conditions (WHO, 2017). Though it has been known for some time that epileptic seizures are associated with massive hypersynchrony in the brain, substantial heterogeneity in aetiology, seizure types and co-morbidities means that it is difficult to elucidate the true nature of the disorder. Recent research has led to the suggestion of epilepsy as a network disorder (see review by Hamandi et al., 2016), and subsequent re-organisation of diagnostic guidelines to accommodate for this (ILAE, 1989; Scheffer et al., 2017). Some models

even suggest that terminology relating to a 'seizure onset zone' is unhelpful and places too much emphasis on focal features of the disorder (Spencer, 2002). Indeed, there is evidence to suggest that there are networks involved in seizure generation and propagation in a variety of focal and generalised epilepsies including medial temporal lobe epilepsy (Bartolomei, Wendling, Bellanger, Régis, & Chauvel, 2001), absence seizures (Amor et al., 2009) and the focus of chapter 5, JME (Lee et al., 2014).

However, background activity and connectivity in both JME and other epilepsies has received less research attention, despite the potential for this work to uncover phenomenon related to transition to seizure. In chapter 5, we show global connectivity increases for JME patients relative to controls in theta-beta bands. We further highlight that only global connectivity differences in the theta band come close to statistical significance following thresholding. These findings are consistent with a recent EEG study in JME that found increased functional connectivity in the 1-10Hz range during interictal recordings, with a further increase in delta connectivity preictally (Clemens et al., 2013). In focal epilepsies, there is some evidence that activity in low frequency rhythms, particularly delta and theta, is associated with epileptic foci (Panet-Raymond & Gotman, 1990a, 1990b; Vanrumste, Jones, Bones, & Carroll, 2005).

However, there are a number of considerations to be made in this type of patient study, many of which relate to heterogeneity of the disease. Most of the prior studies mentioned in chapter 5 group together multiple IGE syndromes, making it difficult or inappropriate to tease apart findings in relation to specific sub-groups. The patient group reported in chapter 5 of this thesis all had a specific diagnosis of JME, but this still does not make the sample homogenous. All patients were medicated with anti-

epileptic drugs (AEDs), though the type and dosage of medication was variable (for summary see chapter 5, full clinical characteristics can be found in Appendix F). Many of these medications have been shown to impact electrophysiology signals (Clemens et al., 2007; Clemens et al., 2014; Specchio et al., 2008). Further, some patients were well controlled using AEDs but others were drug-refractory, and seizure frequency and time since diagnosis also varied among participants. There is some evidence that any one of these factors could impact on neuroimaging measures (Deppe et al., 2008; Fernando-Dongas, Radtke, VanLandingham, & Husain, 2000; Kim et al., 2007). In this case, the sample size was too small for meaningful sub-groups to be separated, but future studies could investigate the effects of these uncontrolled variables on functional connectivity.

6.5 Methodological developments and future directions

6.5.1 Complexity in functional connectivity

Estimating functional connectivity from the information dense MEG signal is a process with many options, not all of which could be covered within this thesis. The basic building blocks of band-limited amplitude and phase connectivity can give rise to more complex regulatory processes such as cross-frequency coupling (Canolty & Knight, 2010). This can occur when either the phase or amplitudes of oscillations in different frequency bands becomes coupled, but is more commonly used to refer to the process by which the phase of one oscillation becomes coupled to the amplitude of another (Canolty & Knight, 2010). Using MEG, Florin and Baillet (2015) show that cross-frequency coupling of low-frequency phase to high-frequency amplitude oscillations represents a plausible mechanism of local to global integration in the resting-state. Further, dysfunction of cross-frequency coupling has been implicated in

a variety of conditions including traumatic brain injury (Antonakakis et al., 2016), depression (Noda et al., 2017) and epilepsy (Amiri, Frauscher, & Gotman, 2016). A recent study using both phase- and amplitude-coupling measures showed that incorporation of multiple frequency bands, cross-frequency terms and non-linear interactions provides a significantly better estimate of similarity between MEG and fMRI connectivity than using linear and band-limited terms alone (Tewarie et al., 2016). This finding is particularly relevant to the results of moderate prediction of fMRI from band-limited MEG connectivity reported in chapter 3 of this thesis. Introducing additional complexity into the model may help to gain a better understanding of the interaction between coupling in different frequency bands, neurovascular coupling and the mechanistic importance of these processes.

6.5.2 Dynamic functional coupling

Along with the richness and complexity of coupling 'type', there is an increasing acceptance that the assumption of temporal stationarity in functional connectivity estimates is likely to be an oversimplification (Allen et al., 2014; de Pasquale et al., 2010; Honey, Kotter, Breakspear, & Sporns, 2007). Of the non-invasive imaging techniques, MEG is ideally suited to study dynamic, non-stationary connectivity processes due to the higher temporal resolution and more direct measure of neuronal activity relative to techniques such as BOLD fMRI. For example, O'Neill et al. (2015) show that when assessing amplitude envelope correlation over smaller time windows (3-6 seconds) within a MEG recording it is possible to distinguish multiple transient sub-networks that form and dissolve rapidly. The additive effect of these transient sub-networks over the whole recording is a spatial pattern of connectivity that appears remarkably similar to established beta-band RSNs (O'Neill et al., 2015). Another method uses a hidden Markov model to infer a number of discrete

microstates that reoccur transiently throughout the recording period (Baker et al., 2014). Future work could apply these dynamic techniques (e.g. those in Baker et al., 2014; Brookes et al., 2016; O'Neill et al., 2015) in order to further investigate resting-state connectivity in epilepsy, or use in conjunction with pharmacoMEG to study dynamic properties of the biochemical interactions underlying the MEG signal.

6.6 Conclusions

In summary, this thesis set out to validate a connectivity pipeline for resting-state MEG and use this in a number of applications relating to the resting-state in health and epilepsy. We show that it is possible, using an atlas-based approach, to obtain reliable estimates of band-limited static connectivity, and that these estimates in the delta and alpha bands relate most closely to fMRI connectivity. Furthermore, we go on to demonstrate that resting-state MEG is sensitive to specific AMPA-receptor mediated changes to spectral power and connectivity. Finally, we show that the JME patients show global connectivity changes in the theta and beta bands. These findings have implications regarding the use of MEG as a tool to study investigate neurovascular coupling and neurochemical dynamics, as well as the study of JME as a network epilepsy. The main limitation of the analysis contained herein is in the stationary nature of temporal and spatial connectivity inferences, over a period of minutes. Recent methodological developments mean that it is now possible to characterise dynamic connectivity on a much shorter timescale using MEG, and this should be the focus of future work.

References

Aarabi, A., Wallois, F., & Grebe, R. (2008). Does spatiotemporal synchronization of EEG change prior to absence seizures? *Brain Res, 1188*, 207-221. doi: 10.1016/j.brainres.2007.10.048

Adjamian, P., Holliday, I. E., Barnes, G. R., Hillebrand, A., Hadjipapas, A., & Singh, K. D. (2004). Induced visual illusions and gamma oscillations in human primary visual cortex. *European Journal of Neuroscience, 20*(2), 587-592.

Alarcon, G., Guy, C. N., Binnie, C. D., Walker, S. R., Elwes, R. D., & Polkey, C. E. (1994). Intracerebral propagation of interictal activity in partial epilepsy: implications for source localisation. *J Neurol Neurosurg Psychiatry, 57*(4), 435-449.

Allen, E. A., Damaraju, E., Plis, S. M., Erhardt, E. B., Eichele, T., & Calhoun, V. D. (2014). Tracking whole-brain connectivity dynamics in the resting state. *Cereb Cortex, 24*(3), 663-676. doi: 10.1093/cercor/bhs352

Amiri, M., Frauscher, B., & Gotman, J. (2016). Phase-Amplitude Coupling Is Elevated in Deep Sleep and in the Onset Zone of Focal Epileptic Seizures. *Front Hum Neurosci, 10*, 387. doi: 10.3389/fnhum.2016.00387

Amor, F., Baillet, S., Navarro, V., Adam, C., Martinerie, J., & Quyen Mle, V. (2009). Cortical local and long-range synchronization interplay in human absence seizure initiation. *Neuroimage, 45*(3), 950-962. doi: 10.1016/j.neuroimage.2008.12.011

Anderson, C. A., Deuser, W. E., & DeNeve, K. M. (1995). Hot temperatures, hostile affect, hostile cognition, and arousal: Tests of a general model of affective aggression. *Personality and Social Psychology Bulletin, 21*(5), 434-448.

Anderson, J., & Hamandi, K. (2011). Understanding juvenile myoclonic epilepsy: Contributions from neuroimaging. *Epilepsy Res, 94*(3), 127-137. doi: https://doi.org/10.1016/j.eplepsyres.2011.03.008

Anticevic, A., Corlett, P. R., Cole, M. W., Savic, A., Gancsos, M., Tang, Y., . . . Krystal, J. H. (2015). N-methyl-D-aspartate receptor antagonist effects on prefrontal cortical connectivity better model early than chronic schizophrenia. *Biol Psychiatry, 77*(6), 569-580. doi: 10.1016/j.biopsych.2014.07.022

Antonakakis, M., Dimitriadis, S. I., Zervakis, M., Micheloyannis, S., Rezaie, R., Babajani-Feremi, A., . . . Papanicolaou, A. C. (2016). Altered cross-frequency coupling in resting-state MEG after mild traumatic brain injury. *International Journal of Psychophysiology, 102*, 1-11. doi: https://doi.org/10.1016/j.ijpsycho.2016.02.002

Arbabshirani, M., Kiehl, K., Pearlson, G., & Calhoun, V. (2013). Classification of schizophrenia patients based on resting-state functional network connectivity. *Frontiers in Neuroscience, 7*(133). doi: 10.3389/fnins.2013.00133

Baker, A. P., Brookes, M. J., Rezek, I. A., Smith, S. M., Behrens, T., Probert Smith, P. J., & Woolrich, M. (2014). Fast transient networks in spontaneous human brain activity. *Elife, 3*, e01867. doi: 10.7554/eLife.01867

Bartolomei, F., Bosma, I., Klein, M., Baayen, J. C., Reijneveld, J. C., Postma, T. J., . . . Stam, C. J. (2006). Disturbed functional connectivity in brain tumour patients: Evaluation by graph analysis of synchronization matrices. *Clinical Neurophysiology, 117*(9), 2039-2049.

Bartolomei, F., Wendling, F., Bellanger, J.-J., Régis, J., & Chauvel, P. (2001). Neural networks involving the medial temporal structures in temporal lobe epilepsy. *Clinical Neurophysiology, 112*(9), 1746-1760.

Bastiaansen, M. C., & Knosche, T. R. (2000). Tangential derivative mapping of axial MEG applied to event-related desynchronization research. *Clin Neurophysiol, 111*(7), 1300-1305.

Beghi, E. (2017). Epilepsy: New classification of seizures and epilepsies [mdash] an advance? *Nat Rev Neurol, 13*(6), 324-325. doi: 10.1038/nrneurol.2017.70

Berg, A. T., Berkovic, S. F., Brodie, M. J., Buchhalter, J., Cross, J. H., van Emde Boas, W., . . . Scheffer, I. E. (2010). Revised terminology and concepts for organization of seizures and epilepsies: report of the ILAE Commission on Classification and Terminology, 2005-2009. *Epilepsia, 51*(4), 676-685. doi: 10.1111/j.1528-1167.2010.02522.x

Berger, H. (1929). Über das Elektrenkephalogramm des Menschen. *Archiv für Psychiatrie und Nervenkrankheiten, 87*(1), 527-570. doi: 10.1007/BF01797193

Berkes, P., Orbán, G., Lengyel, M., & Fiser, J. (2011). Spontaneous Cortical Activity Reveals Hallmarks of an Optimal Internal Model of the Environment. *Science, 331*(6013), 83-87. doi: 10.1126/science.1195870

Biswal, B., Zerrin Yetkin, F., Haughton, V. M., & Hyde, J. S. (1995). Functional connectivity in the motor cortex of resting human brain using echo-planar mri. *Magnetic Resonance in Medicine, 34*(4), 537-541. doi: 10.1002/mrm.1910340409

Blumenfeld, H. (2005). Cellular and network mechanisms of spike-wave seizures. *Epilepsia, 46 Suppl 9*, 21-33. doi: 10.1111/j.1528-1167.2005.00311.x

Braeutigam, S. (2013). Magnetoencephalography: Fundamentals and Established and Emerging Clinical Applications in Radiology. *ISRN Radiology, 2013*, 529463. doi: 10.5402/2013/529463

Braun, U., Plichta, M. M., Esslinger, C., Sauer, C., Haddad, L., Grimm, O., . . . Meyer-Lindenberg, A. (2012). Test-retest reliability of resting-state connectivity network characteristics using fMRI and graph theoretical measures. *Neuroimage, 59*(2), 1404-1412. doi: DOI 10.1016/j.neuroimage.2011.08.044

Brealy, J. A. (2015). *The Relationship Between Variation in Genes, GABA, Structure and Gamma Oscillations in the Visual and Auditory System of Healthy Individuals and Psychiatric Disorder (Doctoral Dissertation). .* Cardiff University.

Brookes, M. J., Hale, J. R., Zumer, J. M., Stevenson, C. M., Francis, S. T., Barnes, G. R., . . . Nagarajan, S. S. (2011a). Measuring functional connectivity using MEG: methodology and comparison with fcMRI. *Neuroimage, 56*(3), 1082-1104. doi: 10.1016/j.neuroimage.2011.02.054

Brookes, M. J., Liddle, E. B., Hale, J. R., Woolrich, M., Luckhoo, H., Liddle, P. F., & Morris, P. G. (2012). Task induced modulation of neural oscillations in electrophysiological brain networks. *Neuroimage, 63*, 1918-1930.

Brookes, M. J., Tewarie, P. K., Hunt, B. A. E., Robson, S. E., Gascoyne, L. E., Liddle, E. B., . . . Morris, P. G. (2016). A multi-layer network approach to MEG connectivity analysis. *Neuroimage, 132*, 425-438. doi: http://doi.org/10.1016/j.neuroimage.2016.02.045

Brookes, M. J., Woolrich, M., Luckhoo, H., Price, D., Hale, J. R., Stephenson, M. C., . . . Morris, P. G. (2011b). Investigating the electrophysiological basis of resting state networks using magnetoencephalography. *Proc Natl Acad Sci U S A, 108*(40), 16783-16788. doi: 10.1073/pnas.1112685108

Brunel, N., & Wang, X. J. (2003). What determines the frequency of fast network oscillations with irregular neural discharges? I. Synaptic dynamics and excitation-inhibition balance. *J Neurophysiol, 90*(1), 415-430. doi: 10.1152/jn.01095.2002

Buckner, R. L., Sepulcre, J., Talukdar, T., Krienen, F. M., Liu, H., Hedden, T., . . . Johnson, K. A. (2009). Cortical Hubs Revealed by Intrinsic Functional Connectivity: Mapping, Assessment of Stability, and Relation to Alzheimer's Disease. *The Journal of Neuroscience, 29*(6), 1860-1873. doi: 10.1523/jneurosci.5062-08.2009

Buzsaki, G., & Wang, X. J. (2012). Mechanisms of gamma oscillations. *Annu Rev Neurosci, 35*, 203-225. doi: 10.1146/annurev-neuro-062111-150444

Cabral, J., Kringelbach, M. L., & Deco, G. (2014). Exploring the network dynamics underlying brain activity during rest. *Progress in Neurobiology, 114*, 102-131. doi: https://doi.org/10.1016/j.pneurobio.2013.12.005

Caeyenberghs, K., Powell, H. W., Thomas, R. H., Brindley, L., Church, C., Evans, J., . . . Hamandi, K. (2015). Hyperconnectivity in juvenile myoclonic epilepsy: a network analysis. *Neuroimage Clin, 7*, 98-104. doi: 10.1016/j.nicl.2014.11.018

Camfield, C. S., Striano, P., & Camfield, P. R. (2013). Epidemiology of juvenile myoclonic epilepsy. *Epilepsy & Behavior, 28, Supplement 1*, S15-S17. doi: https://doi.org/10.1016/j.yebeh.2012.06.024

Canolty, R. T., & Knight, R. T. (2010). The functional role of cross-frequency coupling. *Trends Cogn Sci, 14*(11), 506-515. doi: 10.1016/j.tics.2010.09.001

Chavez, M., Valencia, M., Navarro, V., Latora, V., & Martinerie, J. (2010). Functional modularity of background activities in normal and epileptic brain networks. *Phys Rev Lett, 104*(11), 118701.

Cicchetti, D. V. (1994). Guidelines, criteria, and rules of thumb for evaluating normed and standardized assessment instruments in psychology (Vol. 6, pp. 284-290). US: American Psychological Association.

Clemens, B., Piros, P., Bessenyei, M., & Hollody, K. (2007). Lamotrigine decreases EEG synchronization in a use-dependent manner in patients with idiopathic generalized epilepsy. *Clin Neurophysiol, 118*(4), 910-917. doi: 10.1016/j.clinph.2006.11.016

Clemens, B., Puskás, S., Besenyei, M., Kovács, N. Z., Spisák, T., Kis, S. A., . . . Fekete, I. (2014). Valproate treatment normalizes EEG functional connectivity in successfully treated idiopathic generalized epilepsy patients. *Epilepsy Res, 108*(10), 1896-1903. doi: https://doi.org/10.1016/j.eplepsyres.2014.09.032

Clemens, B., Puskás, S., Besenyei, M., Spisák, T., Opposits, G., Hollódy, K., . . . Emri, M. (2013). Neurophysiology of juvenile myoclonic epilepsy: EEG-based network and graph analysis of the interictal and immediate preictal states. *Epilepsy Res, 106*(3), 357-369. doi: http://doi.org/10.1016/j.eplepsyres.2013.06.017

Cohen, D. (1968). Magnetoencephalography: evidence of magnetic fields produced by alpha-rhythm currents. *Science, 161*(3843), 784-786.

Cohen, D. (1972). Magnetoencephalography: detection of the brain's electrical activity with a superconducting magnetometer. *Science, 175*(4022), 664-666.

Colclough, G. L., Brookes, M. J., Smith, S. M., & Woolrich, M. W. (2015). A symmetric multivariate leakage correction for MEG connectomes. *Neuroimage, 117*, 439-448. doi: http://dx.doi.org/10.1016/j.neuroimage.2015.03.071

Colclough, G. L., Woolrich, M. W., Tewarie, P. K., Brookes, M. J., Quinn, A. J., & Smith, S. M. (2016). How reliable are MEG resting-state connectivity metrics? *Neuroimage, 138*, 284-293. doi: http://dx.doi.org/10.1016/j.neuroimage.2016.05.070

Colgin, L. L. (2013). Mechanisms and functions of theta rhythms. *Annu Rev Neurosci, 36*, 295-312. doi: 10.1146/annurev-neuro-062012-170330

Conner, C. R., Ellmore, T. M., Pieters, T. A., DiSano, M. A., & Tandon, N. (2011). Variability of the Relationship between Electrophysiology and BOLD-fMRI across Cortical Regions in Humans. *The Journal of Neuroscience, 31*(36), 12855-12865. doi: 10.1523/JNEUROSCI.1457-11.2011

Cornwell, B. R., Johnson, L. L., Holroyd, T., Carver, F. W., & Grillon, C. (2008). Human hippocampal and parahippocampal theta during goal-directed spatial navigation predicts performance on a virtual Morris water maze. *J Neurosci, 28*(23), 5983-5990. doi: 10.1523/jneurosci.5001-07.2008

Cousijn, H., Haegens, S., Wallis, G., Near, J., Stokes, M. G., Harrison, P. J., & Nobre, A. C. (2014). Resting GABA and glutamate concentrations do not predict visual gamma frequency or amplitude. *Proceedings of the National Academy of Sciences, 111*(25), 9301-9306. doi: 10.1073/pnas.1321072111

Cox, R. W. (1996). AFNI: software for analysis and visualization of functional magnetic resonance neuroimages. *Comput Biomed Res, 29*(3), 162-173.

Damoiseaux, J. S., Rombouts, S. A. R. B., Barkhof, F., Scheltens, P., Stam, C. J., Smith, S. M., & Beckmann, C. F. (2006). Consistent resting-state networks across healthy subjects. *Proc Natl Acad Sci U S A, 103*(37), 13848-13853. doi: 10.1073/pnas.0601417103

de Pasquale, F., Della Penna, S., Snyder, A. Z., Lewis, C., Mantini, D., Marzetti, L., . . . Corbetta, M. (2010). Temporal dynamics of spontaneous MEG activity in brain networks. *Proc Natl Acad Sci U S A, 107*(13), 6040-6045. doi: 10.1073/pnas.0913863107

de Tisi, J., Bell, G. S., Peacock, J. L., McEvoy, A. W., Harkness, W. F. J., Sander, J. W., & Duncan, J. S. (2011). The long-term outcome of adult epilepsy surgery, patterns of seizure remission, and relapse: a cohort study. *The Lancet, 378*(9800), 1388-1395. doi: 10.1016/S0140-6736(11)60890-8

Delgado-Escueta, A. V., & Enrile-Bacsal, F. (1984). Juvenile myoclonic epilepsy of Janz. *Neurology, 34*(3), 285-294.

Deppe, M., Kellinghaus, C., Duning, T., Moddel, G., Mohammadi, S., Deppe, K., . . . Knecht, S. (2008). Nerve fiber impairment of anterior thalamocortical circuitry in juvenile myoclonic epilepsy. *Neurology, 71*(24), 1981-1985. doi: 10.1212/01.wnl.0000336969.98241.17

Deuker, L., Bullmore, E. T., Smith, M., Christensen, S., Nathan, P. J., Rockstroh, B., & Bassett, D. S. (2009). Reproducibility of graph metrics of human brain functional networks. *Neuroimage, 47*(4), 1460-1468. doi: http://doi.org/10.1016/j.neuroimage.2009.05.035

Devonshire, I. M., Papadakis, N. G., Port, M., Berwick, J., Kennerley, A. J., Mayhew, J. E. W., & Overton, P. G. (2012). Neurovascular coupling is brain region-dependent. *Neuroimage, 59*(3), 1997-2006. doi: https://doi.org/10.1016/j.neuroimage.2011.09.050

Dingledine, R., Borges, K., Bowie, D., & Traynelis, S. F. (1999). The Glutamate Receptor Ion Channels. *Pharmacological Reviews, 51*(1), 7-62.

Dodt, H. U., Frick, A., Kampe, K., & Zieglgänsberger, W. (1998). NMDA and AMPA receptors on neocortical neurons are differentially distributed. *European Journal of Neuroscience, 10*(11), 3351-3357. doi: 10.1046/j.1460-9568.1998.00338.x

Donner, T. H., & Siegel, M. (2011). A framework for local cortical oscillation patterns. *Trends Cogn Sci, 15*(5), 191-199. doi: 10.1016/j.tics.2011.03.007

Downey, D., Dutta, A., McKie, S., Dawson, G. R., Dourish, C. T., Craig, K., . . . Deakin, J. F. W. (2016). Comparing the actions of lanicemine and ketamine in depression: key role of the anterior cingulate. *European Neuropsychopharmacology, 26*(6), 994-1003. doi: 10.1016/j.euroneuro.2016.03.006

Driesen, N. R., McCarthy, G., Bhagwagar, Z., Bloch, M., Calhoun, V., D'Souza, D. C., . . . Krystal, J. H. (2013). Relationship of resting brain hyperconnectivity and schizophrenia-like symptoms produced by the NMDA receptor antagonist ketamine in humans. *Mol Psychiatry, 18*(11), 1199-1204. doi: 10.1038/mp.2012.194

Driver, I. D., & Whittaker, J. R. (2016). Arterial CO2 Fluctuations Modulate Neuronal Rhythmicity: Implications for MEG and fMRI Studies of Resting-State Networks. *36*(33), 8541-8550. doi: 10.1523/jneurosci.4263-15.2016

Drysdale, A. T., Grosenick, L., Downar, J., Dunlop, K., Mansouri, F., Meng, Y., . . . Liston, C. (2017). Resting-state connectivity biomarkers define neurophysiological subtypes of depression. *Nat Med, 23*(1), 28-38. doi: 10.1038/nm.4246

http://www.nature.com/nm/journal/v23/n1/abs/nm.4246.html#supplementary-information

Duncan, N. W., Wiebking, C., & Northoff, G. (2014). Associations of regional GABA and glutamate with intrinsic and extrinsic neural activity in humans-a review of multimodal imaging studies. *Neurosci Biobehav Rev, 47*, 36-52. doi: 10.1016/j.neubiorev.2014.07.016

Eliashiv, D. S., Elsas, S. M., Squires, K., Fried, I., & Engel, J., Jr. (2002). Ictal magnetic source imaging as a localizing tool in partial epilepsy. *Neurology, 59*(10), 1600-1610.

Elshahabi, A., Klamer, S., Sahib, A. K., Lerche, H., Braun, C., & Focke, N. K. (2015). Magnetoencephalography Reveals a Widespread Increase in Network Connectivity in Idiopathic/Genetic Generalized Epilepsy. *PLoS ONE, 10*(9), e0138119. doi: 10.1371/journal.pone.0138119

Engel, A. K., Fries, P., & Singer, W. (2001). Dynamic predictions: oscillations and synchrony in top-down processing. *Nat Rev Neurosci, 2*(10), 704-716. doi: 10.1038/35094565

Engel, A. K., Gerloff, C., Hilgetag, C. C., & Nolte, G. (2013a). Intrinsic coupling modes: multiscale interactions in ongoing brain activity. *Neuron, 80*(4), 867-886. doi: 10.1016/j.neuron.2013.09.038

Engel, J., Jr. (1996). Excitation and inhibition in epilepsy. *Can J Neurol Sci, 23*(3), 167-174.

Engel, J., Thompson, P. M., Stern, J. M., Staba, R. J., Bragin, A., & Mody, I. (2013b). Connectomics and epilepsy. *Curr Opin Neurol, 26*(2), 186-194. doi: 10.1097/WCO.0b013e32835ee5b8

Engels, M. M. A., Hillebrand, A., van der Flier, W. M., Stam, C. J., Scheltens, P., & van Straaten, E. C. W. (2016). Slowing of Hippocampal Activity Correlates with Cognitive Decline in Early Onset Alzheimer's Disease. An MEG Study with Virtual Electrodes. *Front Hum Neurosci, 10*, 238. doi: 10.3389/fnhum.2016.00238

Enzi, B., Duncan, N. W., Kaufmann, J., Tempelmann, C., Wiebking, C., & Northoff, G. (2012). Glutamate modulates resting state activity in the perigenual anterior

cingulate cortex – A combined fMRI–MRS study. *Neuroscience, 227*, 102-109. doi: https://doi.org/10.1016/j.neuroscience.2012.09.039

FDA. (2012). Fycompa Full Prescribing Information. Retrieved 16/06/, 2015, from http://www.accessdata.fda.gov/drugsatfda_docs/label/2012/202834lbl.pdf

Fernando-Dongas, M. C., Radtke, R. A., VanLandingham, K. E., & Husain, A. M. (2000). Characteristics of valproic acid resistant juvenile myoclonic epilepsy. *Seizure, 9*(6), 385-388. doi: 10.1053/seiz.2000.0432

Fingelkurts, A. A., Fingelkurts, A. A., Kivisaari, R., Pekkonen, E., Ilmoniemi, R. J., & Kahkonen, S. (2004). Enhancement of GABA-related signalling is associated with increase of functional connectivity in human cortex. *Hum Brain Mapp, 22*(1), 27-39. doi: 10.1002/hbm.20014

Fiser, J., Chiu, C., & Weliky, M. (2004). Small modulation of ongoing cortical dynamics by sensory input during natural vision. *Nature, 431*(7008), 573-578. doi: 10.1038/nature02907

Fisher, R. S., Cross, J. H., French, J. A., Higurashi, N., Hirsch, E., Jansen, F. E., . . . Zuberi, S. M. (2017). Operational classification of seizure types by the International League Against Epilepsy: Position Paper of the ILAE Commission for Classification and Terminology. *Epilepsia, 58*(4), 522-530. doi: 10.1111/epi.13670

Florin, E., & Baillet, S. (2015). The brain's resting-state activity is shaped by synchronized cross-frequency coupling of neural oscillations. *Neuroimage, 111*, 26-35. doi: https://doi.org/10.1016/j.neuroimage.2015.01.054

Focke, N. K., Diederich, C., Helms, G., Nitsche, M. A., Lerche, H., & Paulus, W. (2014). Idiopathic-generalized epilepsy shows profound white matter diffusion-tensor imaging alterations. *Hum Brain Mapp, 35*(7), 3332-3342.

Forman, S. D., Silva, A. C., Dedousis, N., Barbier, E. L., Fernstrom, J. D., & Koretsky, A. P. (1998). Simultaneous glutamate and perfusion fMRI responses to regional brain stimulation. *J Cereb Blood Flow Metab, 18*(10), 1064-1070. doi: 10.1097/00004647-199810000-00002

Fox, M. D., Snyder, A. Z., Vincent, J. L., Corbetta, M., Van Essen, D. C., & Raichle, M. E. (2005). The human brain is intrinsically organized into dynamic, anticorrelated functional networks. *Proc Natl Acad Sci U S A, 102*(27), 9673-9678. doi: 10.1073/pnas.0504136102

Franzen, J. D., Heinrichs-Graham, E., White, M. L., Wetzel, M. W., Knott, N. L., & Wilson, T. W. (2013). Atypical coupling between posterior regions of the default mode network in attention-deficit/hyperactivity disorder: a pharmaco-magnetoencephalography study. *Journal of Psychiatry & Neuroscience : JPN, 38*(5), 333-340. doi: 10.1503/jpn.120054

Frien, A., & Eckhorn, R. (2000). Functional coupling shows stronger stimulus dependency for fast oscillations than for low-frequency components in striate cortex of awake monkey. *Eur J Neurosci, 12*(4), 1466-1478.

Frien, A., Eckhorn, R., Bauer, R., Woelbern, T., & Kehr, H. (1994). Stimulus-specific fast oscillations at zero phase between visual areas V1 and V2 of awake monkey. *NeuroReport, 5*(17), 2273-2277.

Fujiwara, H., Greiner, H. M., Hemasilpin, N., Lee, K. H., Holland-Bouley, K., Arthur, T., . . . Rose, D. F. (2012). Ictal MEG onset source localization compared to intracranial EEG and outcome: improved epilepsy presurgical evaluation in pediatrics. *Epilepsy Res, 99*(3), 214-224. doi: 10.1016/j.eplepsyres.2011.11.007

Gaetz, W., Roberts, T. P., Singh, K. D., & Muthukumaraswamy, S. D. (2012). Functional and structural correlates of the aging brain: relating visual cortex (V1) gamma band responses to age-related structural change. *Hum Brain Mapp, 33*(9), 2035-2046. doi: 10.1002/hbm.21339

Gao, R., Peterson, E. J., & Voytek, B. (2017). Inferring synaptic excitation/inhibition balance from field potentials. *Neuroimage, 158*(Supplement C), 70-78. doi: https://doi.org/10.1016/j.neuroimage.2017.06.078

Garces, P., Martin-Buro, M. C., & Maestu, F. (2016). Quantifying the Test-Retest Reliability of Magnetoencephalography Resting-State Functional Connectivity. *Brain Connect, 6*(6), 448-460. doi: 10.1089/brain.2015.0416

Gasser, T., Sroka, L., & Möcks, J. (1985). The transfer of EOG activity into the EEG for eyes open and closed. *Electroencephalography and Clinical Neurophysiology, 61*(2), 181-193. doi: 10.1016/0013-4694(85)91058-2

Gloor, P. (1979). Generalized Epilepsy with Spike-and-Wave Discharge: A Reinterpretation of Its Electrographic and Clinical Manifestations1. *Epilepsia, 20*(5), 571-588. doi: 10.1111/j.1528-1157.1979.tb04840.x

Goff, D. C., & Coyle, J. T. (2014). The emerging role of glutamate in the pathophysiology and treatment of schizophrenia. *American Journal of Psychiatry*.

Goldenholz, D. M., Ahlfors, S. P., Hämäläinen, M. S., Sharon, D., Ishitobi, M., Vaina, L. M., & Stufflebeam, S. M. (2009). Mapping the Signal-To-Noise-Ratios of Cortical Sources in Magnetoencephalography and Electroencephalography. *Hum Brain Mapp, 30*(4), 1077-1086. doi: 10.1002/hbm.20571

Gray, C. M., & Singer, W. (1989). Stimulus-specific neuronal oscillations in orientation columns of cat visual cortex. *Proc Natl Acad Sci U S A, 86*(5), 1698-1702.

Grayson, D. S., Ray, S., Carpenter, S., Iyer, S., Dias, T. G. C., Stevens, C., . . . Fair, D. A. (2014). Structural and Functional Rich Club Organization of the Brain in Children and Adults. *PLoS ONE, 9*(2), e88297. doi: 10.1371/journal.pone.0088297

Greicius, M. (2008). Resting-state functional connectivity in neuropsychiatric disorders. *Curr Opin Neurol, 21*(4), 424-430. doi: 10.1097/WCO.0b013e328306f2c5

Greicius, M. D., Flores, B. H., Menon, V., Glover, G. H., Solvason, H. B., Kenna, H., . . . Schatzberg, A. F. (2007). Resting-State Functional Connectivity in Major Depression: Abnormally Increased Contributions from Subgenual Cingulate Cortex and Thalamus. *Biol Psychiatry, 62*(5), 429-437. doi: https://doi.org/10.1016/j.biopsych.2006.09.020

Greicius, M. D., Krasnow, B., Reiss, A. L., & Menon, V. (2003). Functional connectivity in the resting brain: A network analysis of the default mode hypothesis. *Proceedings of the National Academy of Sciences, 100*(1), 253-258. doi: 10.1073/pnas.0135058100

Gsell, W., Burke, M., Wiedermann, D., Bonvento, G., Silva, A. C., Dauphin, F., . . . Schwindt, W. (2006). Differential Effects of NMDA and AMPA Glutamate Receptors on Functional Magnetic Resonance Imaging Signals and Evoked Neuronal Activity during Forepaw Stimulation of the Rat. *The Journal of Neuroscience, 26*(33), 8409-8416. doi: 10.1523/jneurosci.4615-05.2006

Guo, W., Liu, F., Dai, Y., Jiang, M., Zhang, J., Yu, L., . . . Xiao, C. (2013). Decreased interhemispheric resting-state functional connectivity in first-episode, drug-naive major depressive disorder. *Prog Neuropsychopharmacol Biol Psychiatry, 41*, 24-29. doi: 10.1016/j.pnpbp.2012.11.003

Hall, E. L., Robson, S. E., Morris, P. G., & Brookes, M. J. (2014). The relationship between MEG and fMRI. *Neuroimage, 102, Part 1*, 80-91. doi: http://dx.doi.org/10.1016/j.neuroimage.2013.11.005

Hall, E. L., Woolrich, M. W., Thomaz, C. E., Morris, P. G., & Brookes, M. J. (2013). Using variance information in magnetoencephalography measures of functional connectivity. *Neuroimage, 67*, 203-212. doi: 10.1016/j.neuroimage.2012.11.011

Hall, S. D., Barnes, G. R., Furlong, P. L., Seri, S., & Hillebrand, A. (2010). Neuronal network pharmacodynamics of GABAergic modulation in the human cortex determined using pharmaco-magnetoencephalography. *Hum Brain Mapp, 31*(4), 581-594. doi: 10.1002/hbm.20889

Hall, S. D., Stanford, I. M., Yamawaki, N., McAllister, C. J., Ronnqvist, K. C., Woodhall, G. L., & Furlong, P. L. (2011). The role of GABAergic modulation in motor function related neuronal network activity. *Neuroimage, 56*(3), 1506-1510. doi: 10.1016/j.neuroimage.2011.02.025

Hämäläinen, M., Hari, R., Ilmoniemi, R. J., Knuutila, J., & Lounasmaa, O. V. (1993). Magnetoencephalography\char22{}theory, instrumentation, and applications to noninvasive studies of the working human brain. *Reviews of Modern Physics, 65*(2), 413-497.

Hämäläinen, M. S., & Ilmoniemi, R. J. (1994). Interpreting magnetic fields of the brain: minimum norm estimates. *Medical & Biological Engineering & Computing, 32*(1), 35-42. doi: 10.1007/bf02512476

Hamandi, K., Routley, B. C., Koelewijn, L., & Singh, K. D. (2016). Non-invasive brain mapping in epilepsy: Applications from magnetoencephalography. *Journal of Neuroscience Methods, 260*, 283-291. doi: http://doi.org/10.1016/j.jneumeth.2015.11.012

Hamandi, K., Singh, K. D., & Muthukumaraswamy, S. (2011). Reduced movement-related beta desynchronisation in juvenile myoclonic epilepsy: A MEG study of task specific cortical modulation. *Clinical Neurophysiology, 122*(11), 2128-2138. doi: 10.1016/j.clinph.2011.04.017

Hari, R., & Salmelin, R. (2012). Magnetoencephalography: From SQUIDs to neuroscience Neuroimage 20th Anniversary Special Edition. *Neuroimage, 61*(2), 386-396. doi: 10.1016/j.neuroimage.2011.11.074

Heinrichs-Graham, E., Kurz, M. J., Becker, K. M., Santamaria, P. M., Gendelman, H. E., & Wilson, T. W. (2014). Hypersynchrony despite pathologically reduced beta oscillations in patients with Parkinson's disease: a pharmaco-magnetoencephalography study. *J Neurophysiol, 112*(7), 1739-1747. doi: 10.1152/jn.00383.2014

Herrero, Jose L., Gieselmann, Marc A., Sanayei, M., & Thiele, A. (2013). Attention-Induced Variance and Noise Correlation Reduction in Macaque V1 Is Mediated by NMDA Receptors. *Neuron, 78*(4), 729-739. doi: 10.1016/j.neuron.2013.03.029

Hewson-Stoate, N., Jones, M., Martindale, J., Berwick, J., & Mayhew, J. (2005). Further nonlinearities in neurovascular coupling in rodent barrel cortex. *Neuroimage, 24*(2), 565-574. doi: https://doi.org/10.1016/j.neuroimage.2004.08.040

Hillebrand, A., & Barnes, G. R. (2002). A Quantitative Assessment of the Sensitivity of Whole-Head MEG to Activity in the Adult Human Cortex. *Neuroimage, 16*(3, Part A), 638-650. doi: https://doi.org/10.1006/nimg.2002.1102

Hillebrand, A., & Barnes, G. R. (2005). Beamformer analysis of MEG data. *Int Rev Neurobiol, 68*, 149-171. doi: 10.1016/s0074-7742(05)68006-3

Hillebrand, A., Barnes, G. R., Bosboom, J. L., Berendse, H. W., & Stam, C. J. (2012). Frequency-dependent functional connectivity within resting-state networks: An atlas-based MEG beamformer solution. *Neuroimage, 59*(4-2), 3909-3921. doi: 10.1016/j.neuroimage.2011.11.005

Hillebrand, A., Singh, K. D., Holliday, I. E., Furlong, P. L., & Barnes, G. R. (2005). A new approach to neuroimaging with magnetoencephalography. *Hum Brain Mapp, 25*(2), 199-211.

Hipp, J. F., Engel, A. K., & Siegel, M. (2011). Oscillatory synchronization in large-scale cortical networks predicts perception. *Neuron, 69*(2), 387-396. doi: 10.1016/j.neuron.2010.12.027

Hipp, J. F., Hawellek, D. J., Corbetta, M., Siegel, M., & Engel, A. K. (2012). Large-scale cortical correlation structure of spontaneous oscillatory activity. *Nature neuroscience, 15*(6), 10.1038/nn.3101. doi: 10.1038/nn.3101

Hipp, Joerg F., & Siegel, M. (2015). BOLD fMRI Correlation Reflects Frequency-Specific Neuronal Correlation. *Current Biology, 25*(10), 1368-1374. doi: http://dx.doi.org/10.1016/j.cub.2015.03.049

Holmes, M. D., Quiring, J., & Tucker, D. M. (2010). Evidence that juvenile myoclonic epilepsy is a disorder of frontotemporal corticothalamic networks. *Neuroimage, 49*(1), 80-93. doi: https://doi.org/10.1016/j.neuroimage.2009.08.004

Honey, C. J., Kotter, R., Breakspear, M., & Sporns, O. (2007). Network structure of cerebral cortex shapes functional connectivity on multiple time scales. *Proc Natl Acad Sci U S A, 104*(24), 10240-10245. doi: 10.1073/pnas.0701519104

Hong, L. E., Summerfelt, A., Buchanan, R. W., O'Donnell, P., Thaker, G. K., Weiler, M. A., & Lahti, A. C. (2009). Gamma and Delta Neural Oscillations and Association with Clinical Symptoms under Subanesthetic Ketamine. *Neuropsychopharmacology, 35*(3), 632-640.

Hynd, M. R., Scott, H. L., & Dodd, P. R. (2004). Glutamate-mediated excitotoxicity and neurodegeneration in Alzheimer's disease. *Neurochemistry international, 45*(5), 583-595.

ILAE. (1989). Proposal for revised classification of epilepsies and epileptic syndromes. Commission on Classification and Terminology of the International League Against Epilepsy. *Epilepsia, 30*(4), 389-399.

Isaacson, J. S., & Scanziani, M. (2011). How inhibition shapes cortical activity. *Neuron, 72*(2), 231-243. doi: 10.1016/j.neuron.2011.09.027

Jayalakshmi, S. S., Srinivasa Rao, B., & Sailaja, S. (2010). Focal clinical and electroencephalographic features in patients with juvenile myoclonic epilepsy. *Acta Neurologica Scandinavica, 122*(2), 115-123. doi: 10.1111/j.1600-0404.2009.01270.x

Jensen, O., Goel, P., Kopell, N., Pohja, M., Hari, R., & Ermentrout, B. (2005). On the human sensorimotor-cortex beta rhythm: sources and modeling. *Neuroimage, 26*(2), 347-355. doi: 10.1016/j.neuroimage.2005.02.008

Jensen, O., & Mazaheri, A. (2010). Shaping Functional Architecture by Oscillatory Alpha Activity: Gating by Inhibition. *Front Hum Neurosci, 4*, 186. doi: 10.3389/fnhum.2010.00186

Jin, S.-H., Seol, J., Kim, J. S., & Chung, C. K. (2011). How reliable are the functional connectivity networks of MEG in resting states? *J Neurophysiol, 106*(6), 2888-2895. doi: 10.1152/jn.00335.2011

Kapogiannis, D., Reiter, D. A., Willette, A. A., & Mattson, M. P. (2013). Posteromedial cortex glutamate and GABA predict intrinsic functional connectivity of the default mode network. *Neuroimage, 64*, 112-119. doi: https://doi.org/10.1016/j.neuroimage.2012.09.029

Kidd, F. L., & Isaac, J. T. R. (2000). Glutamate transport blockade has a differential effect on AMPA and NMDA receptor-mediated synaptic transmission in the developing barrel cortex. *Neuropharmacology, 39*(5), 725-732. doi: https://doi.org/10.1016/S0028-3908(99)00270-1

Kim, J. H., Lee, J. K., Koh, S.-B., Lee, S.-A., Lee, J.-M., Kim, S. I., & Kang, J. K. (2007). Regional grey matter abnormalities in juvenile myoclonic epilepsy: A voxel-based morphometry study. *Neuroimage, 37*(4), 1132-1137. doi: https://doi.org/10.1016/j.neuroimage.2007.06.025

Koelewijn, L., Hamandi, K., Brindley, L. M., Brookes, M. J., Routley, B. C., Muthukumaraswamy, S. D., . . . Singh, K. D. (2015). Resting-state oscillatory dynamics in sensorimotor cortex in benign epilepsy with centro-temporal spikes and typical brain development. *Hum Brain Mapp, 36*(10), 3935-3949. doi: 10.1002/hbm.22888

Koepp, M. J., Woermann, F., Savic, I., & Wandschneider, B. (2013). Juvenile myoclonic epilepsy — Neuroimaging findings. *Epilepsy & Behavior, 28, Supplement 1*, S40-S44. doi: https://doi.org/10.1016/j.yebeh.2012.06.035

Kopell, N., Ermentrout, G. B., Whittington, M. A., & Traub, R. D. (2000). Gamma rhythms and beta rhythms have different synchronization properties. *Proc Natl Acad Sci U S A, 97*(4), 1867-1872.

Kramer, M. A., & Cash, S. S. (2012). Epilepsy as a Disorder of Cortical Network Organization. *The Neuroscientist, 18*(4), 360-372. doi: doi:10.1177/1073858411422754

Lachaux, J. P., Rodriguez, E., Martinerie, J., & Varela, F. J. (1999). Measuring phase synchrony in brain signals. *Hum Brain Mapp, 8*(4), 194-208.

Laughlin, S. B., & Sejnowski, T. J. (2003). Communication in neuronal networks. *Science, 301*(5641), 1870-1874. doi: 10.1126/science.1089662

Lazarewicz, M. T., Ehrlichman, R. S., Maxwell, C. R., Gandal, M. J., Finkel, L. H., & Siegel, S. J. (2009). Ketamine Modulates Theta and Gamma Oscillations. *Journal of Cognitive Neuroscience, 22*(7), 1452-1464. doi: 10.1162/jocn.2009.21305

Lee, C., Im, C.-H., Koo, Y. S., Lim, J.-A., Kim, T.-J., Byun, J.-I., . . . Jung, K.-Y. (2015). Altered Network Characteristics of Spike-Wave Discharges in Juvenile Myoclonic Epilepsy. *Clinical EEG and Neuroscience, 48*(2), 111-117. doi: 10.1177/1550059415621831

Lee, C., Kim, S.-M., Jung, Y.-J., Im, C.-H., Kim, D. W., & Jung, K.-Y. (2014). Causal influence of epileptic network during spike-and-wave discharge in juvenile myoclonic epilepsy. *Epilepsy Res, 108*(2), 257-266. doi: https://doi.org/10.1016/j.eplepsyres.2013.11.005

Lee, M. H., Smyser, C. D., & Shimony, J. S. (2013). Resting-state fMRI: a review of methods and clinical applications. *AJNR Am J Neuroradiol, 34*(10), 1866-1872. doi: 10.3174/ajnr.A3263

Leopold, D. A., Murayama, Y., & Logothetis, N. K. (2003). Very Slow Activity Fluctuations in Monkey Visual Cortex: Implications for Functional Brain Imaging. *Cerebral Cortex, 13*(4), 422-433. doi: 10.1093/cercor/13.4.422

Liang, M., Zhou, Y., Jiang, T., Liu, Z., Tian, L., Liu, H., & Hao, Y. (2006). Widespread functional disconnectivity in schizophrenia with resting-state functional magnetic resonance imaging. *NeuroReport, 17*(2), 209-213.

Liao, W., Zhang, Z., Pan, Z., Mantini, D., Ding, J., Duan, X., . . . Chen, H. (2010). Altered Functional Connectivity and Small-World in Mesial Temporal Lobe Epilepsy. *PLoS ONE, 5*(1), e8525. doi: 10.1371/journal.pone.0008525

Licata, S. C., Lowen, S. B., Trksak, G. H., MacLean, R. R., & Lukas, S. E. (2011). Zolpidem reduces the blood oxygen level-dependent signal during visual system stimulation. *Progress in Neuro-Psychopharmacology and Biological Psychiatry, 35*(7), 1645-1652. doi: http://dx.doi.org/10.1016/j.pnpbp.2011.05.015

Liddle, E. B., Price, D., Palaniyappan, L., Brookes, M. J., Robson, S. E., Hall, E. L., . . . Liddle, P. F. (2016). Abnormal salience signaling in schizophrenia: The role of integrative beta oscillations. *Hum Brain Mapp*.

Lieb, J. P., Engel, J., Jr., & Babb, T. L. (1986). Interhemispheric propagation time of human hippocampal seizures. I. Relationship to surgical outcome. *Epilepsia, 27*(3), 286-293.

Lin, F.-H., Witzel, T., Ahlfors, S. P., Stufflebeam, S. M., Belliveau, J. W., & Hämäläinen, M. S. (2006). Assessing and improving the spatial accuracy in MEG source localization by depth-weighted minimum-norm estimates. *Neuroimage, 31*(1), 160-171.

Lindquist, M. A. (2008). The statistical analysis of fMRI data. *Statistical Science*, 439-464.

Liu, Z., Fukunaga, M., de Zwart, J. A., & Duyn, J. H. (2010). Large-scale spontaneous fluctuations and correlations in brain electrical activity observed with magnetoencephalography. *Neuroimage, 51*(1), 102-111. doi: https://doi.org/10.1016/j.neuroimage.2010.01.092

Liuzzi, L., Gascoyne, L. E., Tewarie, P. K., Barratt, E. L., Boto, E., & Brookes, M. J. (2016). Optimising experimental design for MEG resting state functional connectivity measurement. *Neuroimage*. doi: http://dx.doi.org/10.1016/j.neuroimage.2016.11.064

Logothetis, N. K., Pauls, J., Augath, M., Trinath, T., & Oeltermann, A. (2001). Neurophysiological investigation of the basis of the fMRI signal. *Nature, 412*(6843), 150-157. doi: http://www.nature.com/nature/journal/v412/n6843/suppinfo/412150a0_S1.html

Lopes de Silva, F. H. (2010). Electrophysiological Basis of MEG Signals. In P. Hansen, M. Kringelbach & R. Salmelin (Eds.), *MEG: An Introduction to Methods*: Oxford University Press, USA.

Lou, B., Li, Y., Philiastides, M. G., & Sajda, P. (2014). Prestimulus alpha power predicts fidelity of sensory encoding in perceptual decision making. *Neuroimage, 87*, 242-251. doi: https://doi.org/10.1016/j.neuroimage.2013.10.041

Lozano-Soldevilla, D., ter Huurne, N., Cools, R., & Jensen, O. (2014). GABAergic modulation of visual gamma and alpha oscillations and its consequences for working memory performance. *Curr Biol, 24*(24), 2878-2887. doi: 10.1016/j.cub.2014.10.017

Luckhoo, H., Hale, J. R., Stokes, M. G., Nobre, A. C., Morris, P. G., Brookes, M. J., & Woolrich, M. W. (2012). Inferring task-related networks using independent component analysis in magnetoencephalography. *Neuroimage, 62*(1), 530-541. doi: 10.1016/j.neuroimage.2012.04.046

Luo, C., Li, Q., Lai, Y., Xia, Y., Qin, Y., Liao, W., . . . Gong, Q. (2011). Altered functional connectivity in default mode network in absence epilepsy: A resting-state fMRI study. *Hum Brain Mapp, 32*(3), 438-449. doi: 10.1002/hbm.21034

10.1371/journal.pone. 0006475; Waites, A.B., Briellmann, R.S., Saling, M.M., Abbott, D.F., Jackson, G.D., Functional connectivity networks are disrupted in left temporal lobe epilepsy Ann Neurol, 59, pp. 335-343; Wise, R.J.S., Ide, K., Poulin, M.J., Tracey, I., Resting state fluctuations in arterial carbon dioxide induce significant low frequency variations in BOLD signal Neuroimage, 21, pp. 1652-1664; Yu, L., Blumenfeld, H., Theories of impaired consciousness in epilepsy Ann NY Acad Sci, 1157, pp. 48-60

Luo, C., Li, Q., Xia, Y., Lei, X., Xue, K., Yao, Z., . . . Yao, D. (2012a). Resting state basal ganglia network in idiopathic generalized epilepsy. *Hum Brain Mapp, 33*(6), 1279-1294. doi: 10.1002/hbm.21286

Luo, C., Qiu, C., Guo, Z., Fang, J., Li, Q., Lei, X., . . . Yao, D. (2012b). Disrupted Functional Brain Connectivity in Partial Epilepsy: A Resting-State fMRI Study. *PLoS ONE, 7*(1), e28196. doi: 10.1371/journal.pone.0028196

Madhavan, D., Heinrichs-Graham, E., & Wilson, T. W. (2013). Whole-brain functional connectivity increases with extended duration of focal epileptiform activity. *Neuroscience Letters, 542*, 26-29.

Magazzini, L., Muthukumaraswamy, S. D., Campbell, A. E., Hamandi, K., Lingford-Hughes, A., Myers, J. F. M., . . . Singh, K. D. (2016). Significant reductions in human visual gamma frequency by the gaba reuptake inhibitor tiagabine revealed by robust peak frequency estimation. *Hum Brain Mapp, 37*(11), 3882-3896. doi: 10.1002/hbm.23283

Martin, C. S., Earleywine, M., Musty, R. E., Perrine, M., & Swift, R. M. (1993). Development and validation of the biphasic alcohol effects scale. *Alcohol Clin Exp Res, 17*(1), 140-146.

Masterton, R. A., Carney, P. W., & Jackson, G. D. (2012). Cortical and thalamic resting-state functional connectivity is altered in childhood absence epilepsy. *Epilepsy Res, 99*(3), 327-334. doi: https://doi.org/10.1016/j.eplepsyres.2011.12.014

Mayeux, R. (2004). Biomarkers: Potential Uses and Limitations. *NeuroRx, 1*(2), 182-188.

McGill, M. L., Devinsky, O., Kelly, C., Milham, M., Castellanos, F. X., Quinn, B. T., . . . Thesen, T. (2012). Default mode network abnormalities in idiopathic generalized epilepsy. *Epilepsy & Behavior, 23*(3), 353-359. doi: https://doi.org/10.1016/j.yebeh.2012.01.013

Meeren, H. K., Pijn, J. P., Van Luijtelaar, E. L., Coenen, A. M., & Lopes da Silva, F. H. (2002). Cortical focus drives widespread corticothalamic networks during spontaneous absence seizures in rats. *J Neurosci, 22*(4), 1480-1495.

Meindl, T., Teipel, S., Elmouden, R., Mueller, S., Koch, W., Dietrich, O., . . . Glaser, C. (2010). Test-retest reproducibility of the default-mode network in healthy individuals. *Hum Brain Mapp, 31*(2), 237-246. doi: 10.1002/hbm.20860

Meldrum, B. S. (1996). Update on the Mechanism of Action of Antiepileptic Drugs. *Epilepsia, 37*, S4-S11. doi: 10.1111/j.1528-1157.1996.tb06038.x

Melie-Garcia, L., Sanabria-Diaz, G., & Sanchez-Catasus, C. (2013). Studying the topological organization of the cerebral blood flow fluctuations in resting state. *Neuroimage, 64*, 173-184. doi: 10.1016/j.neuroimage.2012.08.082

Michalareas, G., Vezoli, J., van Pelt, S., Schoffelen, J.-M., Kennedy, H., & Fries, P. (2016). Alpha-Beta and Gamma Rhythms Subserve Feedback and Feedforward Influences among Human Visual Cortical Areas. *Neuron, 89*(2), 384-397. doi: 10.1016/j.neuron.2015.12.018

Moeller, F., Maneshi, M., Pittau, F., Gholipour, T., Bellec, P., Dubeau, F., . . . Gotman, J. (2011). Functional connectivity in patients with idiopathic generalized epilepsy. *Epilepsia, 52*(3), 515-522. doi: 10.1111/j.1528-1167.2010.02938.x

Moran, R. J., Symmonds, M., Stephan, K. E., Friston, K. J., & Dolan, R. J. (2011). An in vivo assay of synaptic function mediating human cognition. *Curr Biol, 21*(15), 1320-1325. doi: 10.1016/j.cub.2011.06.053

Mosher, J. C., Leahy, R. M., & Lewis, P. S. (1999). EEG and MEG: forward solutions for inverse methods. *IEEE Transactions on Biomedical Engineering, 46*(3), 245-259.

Mukamel, R., Gelbard, H., Arieli, A., Hasson, U., Fried, I., & Malach, R. (2005). Coupling between neuronal firing, field potentials, and FMRI in human auditory cortex. *Science, 309*(5736), 951-954. doi: 10.1126/science.1110913

Murakami, S., & Okada, Y. (2006). Contributions of principal neocortical neurons to magnetoencephalography and electroencephalography signals. *J Physiol, 575*(Pt 3), 925-936. doi: 10.1113/jphysiol.2006.105379

Murphy, K., Birn, R. M., & Bandettini, P. A. (2013). Resting-state fMRI confounds and cleanup. *Neuroimage, 80*, 349-359. doi: 10.1016/j.neuroimage.2013.04.001

Muthukumaraswamy, S. (2013). High-frequency brain activity and muscle artifacts in MEG/EEG: A review and recommendations. *Front Hum Neurosci, 7*(138). doi: 10.3389/fnhum.2013.00138

Muthukumaraswamy, S. D. (2010). Functional properties of human primary motor cortex gamma oscillations. *J Neurophysiol, 104*(5), 2873-2885. doi: 10.1152/jn.00607.2010

Muthukumaraswamy, S. D. (2014). The use of magnetoencephalography in the study of psychopharmacology (pharmaco-MEG). *J Psychopharmacol, 28*(9), 815-829. doi: 10.1177/0269881114536790

Muthukumaraswamy, S. D., Carhart-Harris, R. L., Moran, R. J., Brookes, M. J., Williams, T. M., Errtizoe, D., . . . Nutt, D. J. (2013a). Broadband Cortical Desynchronization Underlies the Human Psychedelic State. *The Journal of Neuroscience, 33*(38), 15171-15183. doi: 10.1523/jneurosci.2063-13.2013

Muthukumaraswamy, S. D., Carhart-Harris, R. L., Moran, R. J., Brookes, M. J., Williams, T. M., Errtizoe, D., . . . Nutt, D. J. (2013b). Broadband cortical desynchronization

underlies the human psychedelic state. *J Neurosci, 33*(38), 15171-15183. doi: 10.1523/JNEUROSCI.2063-13.2013

Muthukumaraswamy, S. D., Myers, J. F., Wilson, S. J., Nutt, D. J., Hamandi, K., Lingford-Hughes, A., & Singh, K. D. (2013c). Elevating endogenous GABA levels with GAT-1 blockade modulates evoked but not induced responses in human visual cortex. *Neuropsychopharmacology, 38*(6), 1105-1112. doi: 10.1038/npp.2013.9

Muthukumaraswamy, S. D., Routley, B., Droog, W., Singh, K. D., & Hamandi, K. (2016). The effects of AMPA blockade on the spectral profile of human early visual cortex recordings studied with non-invasive MEG. *Cortex, 81*, 266-275. doi: http://dx.doi.org/10.1016/j.cortex.2016.03.004

Muthukumaraswamy, S. D., & Shaw, A. D. (2015). Evidence that Subanesthetic Doses of Ketamine Cause Sustained Disruptions of NMDA and AMPA-Mediated Frontoparietal Connectivity in Humans. *35*(33), 11694-11706. doi: 10.1523/jneurosci.0903-15.2015

Muthukumaraswamy, S. D., Shaw, A. D., Jackson, L. E., Hall, J., Moran, R., & Saxena, N. (2015). Evidence that Subanesthetic Doses of Ketamine Cause Sustained Disruptions of NMDA and AMPA-Mediated Frontoparietal Connectivity in Humans. *The Journal of Neuroscience, 35*(33), 11694-11706. doi: 10.1523/jneurosci.0903-15.2015

Nichols, T. E., & Holmes, A. P. (2002). Nonparametric permutation tests for functional neuroimaging: a primer with examples. *Hum Brain Mapp, 15*(1), 1-25.

Niso, G., Carrasco, S., Gudín, M., Maestú, F., del-Pozo, F., & Pereda, E. (2015). What graph theory actually tells us about resting state interictal MEG epileptic activity. *NeuroImage: Clinical, 8*, 503-515. doi: http://doi.org/10.1016/j.nicl.2015.05.008

Noda, Y., Zomorrodi, R., Saeki, T., Rajji, T. K., Blumberger, D. M., Daskalakis, Z. J., & Nakamura, M. (2017). Resting-state EEG gamma power and theta–gamma coupling enhancement following high-frequency left dorsolateral prefrontal rTMS in patients with depression. *Clinical Neurophysiology, 128*(3), 424-432. doi: https://doi.org/10.1016/j.clinph.2016.12.023

Northoff, G., Richter, A., Bermpohl, F., Grimm, S., Martin, E., Marcar, V. L., . . . Boeker, H. (2005). NMDA hypofunction in the posterior cingulate as a model for schizophrenia: an exploratory ketamine administration study in fMRI. *Schizophrenia Research, 72*(2–3), 235-248. doi: http://dx.doi.org/10.1016/j.schres.2004.04.009

Nugent, A. C., Robinson, S. E., Coppola, R., Furey, M. L., & Zarate Jr, C. A. (2015). Group differences in MEG-ICA derived resting state networks: Application to major depressive disorder. *Neuroimage, 118*, 1-12. doi: http://dx.doi.org/10.1016/j.neuroimage.2015.05.051

Nutt, D., Wilson, S., Lingford-Hughes, A., Myers, J., Papadopoulos, A., & Muthukumaraswamy, S. (2015). Differences between magnetoencephalographic (MEG) spectral profiles of drugs acting on GABA at synaptic and extrasynaptic sites: A study in healthy volunteers.

Neuropharmacology, 88(0), 155-163. doi: http://dx.doi.org/10.1016/j.neuropharm.2014.08.017

O'Neill, G. C., Bauer, M., Woolrich, M. W., Morris, P. G., Barnes, G. R., & Brookes, M. J. (2015). Dynamic recruitment of resting state sub-networks. *Neuroimage, 115*, 85-95. doi: 10.1016/j.neuroimage.2015.04.030

O'Neill, G. C., Barratt, E. L., Hunt, B. A. E., Tewarie, P. K., & Brookes, M. J. (2015). Measuring electrophysiological connectivity by power envelope correlation: a technical review on MEG methods. *Physics in Medicine & Biology, 60*(21), R271.

O'Neill, G. C., Tewarie, P. K., Colclough, G. L., Gascoyne, L. E., Hunt, B. A. E., Morris, P. G., . . . Brookes, M. J. (2017). Measurement of dynamic task related functional networks using MEG. *Neuroimage, 146*, 667-678. doi: 10.1016/j.neuroimage.2016.08.061

Ogawa, S., Lee, T. M., Kay, A. R., & Tank, D. W. (1990). Brain magnetic resonance imaging with contrast dependent on blood oxygenation. *Proc Natl Acad Sci U S A, 87*(24), 9868-9872.

Oke, O. O., Magony, A., Anver, H., Ward, P. D., Jiruska, P., Jefferys, J. G., & Vreugdenhil, M. (2010). High-frequency gamma oscillations coexist with low-frequency gamma oscillations in the rat visual cortex in vitro. *European Journal of Neuroscience, 31*(8), 1435-1445.

Olney, J. W., & Farber, N. B. (1995). Glutamate receptor dysfunction and schizophrenia. *Archives of general psychiatry, 52*(12), 998-1007.

Oostenveld, R., Fries, P., Maris, E., & Schoffelen, J.-M. (2011). FieldTrip: Open Source Software for Advanced Analysis of MEG, EEG, and Invasive Electrophysiological Data. *Computational Intelligence and Neuroscience, 2011*, 9. doi: 10.1155/2011/156869

Owen, J. P., Li, Y. O., Yang, F. G., Shetty, C., Bukshpun, P., Vora, S., . . . Mukherjee, P. (2013). Resting-state networks and the functional connectome of the human brain in agenesis of the corpus callosum. *Brain Connect, 3*(6), 547-562. doi: 10.1089/brain.2013.0175

Panayiotopoulos, C. P. (2010). *A Clinical Guide to Epileptic Syndromes and their Treatment*: Springer-Verlag London.

Panet-Raymond, D., & Gotman, J. (1990a). Asymmetry in delta activity in patients with focal epilepsy. *Electroencephalography and Clinical Neurophysiology, 75*(6), 474-481. doi: https://doi.org/10.1016/0013-4694(90)90134-6

Panet-Raymond, D., & Gotman, J. (1990b). Can slow waves in the electrocorticogram (ECoG) help localize epileptic foci? *Electroencephalogr Clin Neurophysiol, 75*(6), 464-473.

Perry, G., Brindley, L. M., Muthukumaraswamy, S. D., Singh, K. D., & Hamandi, K. (2014). Evidence for increased visual gamma responses in photosensitive epilepsy. *Epilepsy Res, 108*(6), 1076-1086. doi: https://doi.org/10.1016/j.eplepsyres.2014.04.012

Pfurtscheller, G., & Lopes da Silva, F. H. (1999). Event-related EEG/MEG synchronization and desynchronization: basic principles. *Clin Neurophysiol, 110*(11), 1842-1857.

Pfurtscheller, G., Stancák Jr, A., & Neuper, C. (1996). Event-related synchronization (ERS) in the alpha band — an electrophysiological correlate of cortical idling: A review. *International Journal of Psychophysiology, 24*(1–2), 39-46. doi: https://doi.org/10.1016/S0167-8760(96)00066-9

Pittau, F., Grova, C., Moeller, F., Dubeau, F., & Gotman, J. (2012). Patterns of altered functional connectivity in mesial temporal lobe epilepsy. *Epilepsia, 53*(6), 1013-1023. doi: 10.1111/j.1528-1167.2012.03464.x

Pittau, F., & Vulliemoz, S. (2015). Functional brain networks in epilepsy: recent advances in noninvasive mapping. *Curr Opin Neurol, 28*(4), 338-343. doi: 10.1097/wco.0000000000000221

Quraan, M. A., McCormick, C., Cohn, M., Valiante, T. A., & McAndrews, M. P. (2013). Altered Resting State Brain Dynamics in Temporal Lobe Epilepsy Can Be Observed in Spectral Power, Functional Connectivity and Graph Theory Metrics. *PLoS ONE, 8*(7), e68609. doi: 10.1371/journal.pone.0068609

Raichle, M. E. (2009). A Paradigm Shift in Functional Brain Imaging. *The Journal of Neuroscience, 29*(41), 12729-12734. doi: 10.1523/jneurosci.4366-09.2009

Raichle, M. E., MacLeod, A. M., Snyder, A. Z., Powers, W. J., Gusnard, D. A., & Shulman, G. L. (2001). A default mode of brain function. *Proceedings of the National Academy of Sciences, 98*(2), 676-682. doi: 10.1073/pnas.98.2.676

Richardson, M. P. (2012). Large scale brain models of epilepsy: dynamics meets connectomics. *J Neurol Neurosurg Psychiatry, 83*(12), 1238-1248. doi: 10.1136/jnnp-2011-301944

Robinson, S. E., Nagarajan, S. S., Mantle, M., Gibbons, V., & Kirsch, H. (2004). Localization of interictal spikes using SAM(g2) and dipole fit. *Neurol Clin Neurophysiol, 2004*, 74.

Rogawski, M. A., & Hanada, T. (2013). Preclinical pharmacology of perampanel, a selective non-competitive AMPA receptor antagonist. *Acta Neurologica Scandinavica, 197*, 19-24. doi: 10.1111/ane.12100

Romei, V., Brodbeck, V., Michel, C., Amedi, A., Pascual-Leone, A., & Thut, G. (2008). Spontaneous fluctuations in posterior α-band EEG activity reflect variability in excitability of human visual areas. *Cerebral Cortex, 18*(9), 2010-2018. doi: 10.1093/cercor/bhm229

Salvador, R., Suckling, J., Schwarzbauer, C., & Bullmore, E. (2005). Undirected graphs of frequency-dependent functional connectivity in whole brain networks. *Philosophical Transactions of the Royal Society B: Biological Sciences, 360*(1457), 937-946. doi: 10.1098/rstb.2005.1645

Sanacora, G., Smith, M. A., Pathak, S., Su, H. L., Boeijinga, P. H., McCarthy, D. J., & Quirk, M. C. (2014). Lanicemine: a low-trapping NMDA channel blocker produces

sustained antidepressant efficacy with minimal psychotomimetic adverse effects. *Mol Psychiatry, 19*(9), 978-985. doi: 10.1038/mp.2013.130

Sanacora, G., Treccani, G., & Popoli, M. (2012). Towards a glutamate hypothesis of depression: an emerging frontier of neuropsychopharmacology for mood disorders. *Neuropharmacology, 62*(1), 63-77.

Sander, J. W. A. S. (1993). Some Aspects of Prognosis in the Epilepsies: A Review. *Epilepsia, 34*(6), 1007-1016. doi: 10.1111/j.1528-1157.1993.tb02126.x

Sandrone, S., Bacigaluppi, M., Galloni, M. R., Cappa, S. F., Moro, A., Catani, M., . . . Martino, G. (2014). Weighing brain activity with the balance: Angelo Mosso's original manuscripts come to light. *Brain, 137*(2), 621-633. doi: 10.1093/brain/awt091

Saunders, J. B., Aasland, O. G., Babor, T. F., De la Fuente, J. R., & Grant, M. (1993). Development of the alcohol use disorders identification test (AUDIT). WHO collaborative project on early detection of persons with harmful alcohol consumption-II. *ADDICTION-ABINGDON-, 88*, 791-804.

Savage, N. (2014). Epidemiology: The complexities of epilepsy. *Nature, 511*(7508), S2-S3. doi: 10.1038/511S2a

Saxena, N., Muthukumaraswamy, S. D., Diukova, A., Singh, K., Hall, J., & Wise, R. (2013). Enhanced Stimulus-Induced Gamma Activity in Humans during Propofol-Induced Sedation. *PLoS ONE, 8*(3), e57685. doi: 10.1371/journal.pone.0057685

Schafer, C. B., Morgan, B. R., Ye, A. X., Taylor, M. J., & Doesburg, S. M. (2014). Oscillations, networks, and their development: MEG connectivity changes with age. *Hum Brain Mapp, 35*(10), 5249-5261. doi: 10.1002/hbm.22547

Scheffer, I. E., Berkovic, S., Capovilla, G., Connolly, M. B., French, J., Guilhoto, L., . . . Zuberi, S. M. (2017). ILAE classification of the epilepsies: Position paper of the ILAE Commission for Classification and Terminology. *Epilepsia, 58*(4), 512-521. doi: 10.1111/epi.13709

Scheffzuk, C., Kukushka, V. I., Vyssotski, A. L., Draguhn, A., Tort, A. B., & Brankack, J. (2013). Global slowing of network oscillations in mouse neocortex by diazepam. *Neuropharmacology, 65*, 123-133. doi: 10.1016/j.neuropharm.2012.09.014

Scheidegger, M., Walter, M., Lehmann, M., Metzger, C., Grimm, S., Boeker, H., . . . Seifritz, E. (2012). Ketamine decreases resting state functional network connectivity in healthy subjects: implications for antidepressant drug action. *PLoS ONE, 7*(9), e44799. doi: 10.1371/journal.pone.0044799

Schnitzler, A., & Gross, J. (2005). Functional connectivity analysis in magnetoencephalography. *Int Rev Neurobiol, 68*, 173-195. doi: 10.1016/s0074-7742(05)68007-5

Schoffelen, J.-M., & Gross, J. (2009). Source connectivity analysis with MEG and EEG. *Hum Brain Mapp, 30*(6), 1857-1865. doi: 10.1002/hbm.20745

Schölvinck, M. L., Leopold, D. A., Brookes, M. J., & Khader, P. H. (2013). The contribution of electrophysiology to functional connectivity mapping. *Neuroimage, 80*, 297-306. doi: https://doi.org/10.1016/j.neuroimage.2013.04.010

Schuckit, M. A. (1980). Self-rating of alcohol intoxication by young men with and without family histories of alcoholism. *Journal of studies on alcohol, 41*(3), 242-249.

Sebban, C., Tesolin-Decros, B., Ciprian-Ollivier, J., Perret, L., & Spedding, M. (2002). Effects of phencyclidine (PCP) and MK 801 on the EEGq in the prefrontal cortex of conscious rats; antagonism by clozapine, and antagonists of AMPA-, α1- and 5-HT2A-receptors. *British Journal of Pharmacology, 135*(1), 65-78. doi: 10.1038/sj.bjp.0704451

Sejnowski, T. J., & Paulsen, O. (2006). Network oscillations: emerging computational principles. *J Neurosci, 26*(6), 1673-1676. doi: 10.1523/JNEUROSCI.3737-05d.2006

Shaw, A. D., Saxena, N., Jackson, L., Hall, J. E., Singh, K. D., & Muthukumaraswamy, S. D. (2015). Ketamine amplifies induced gamma frequency oscillations in the Human cerebral cortex. *European Neuropsychopharmacology*(0). doi: http://dx.doi.org/10.1016/j.euroneuro.2015.04.012

Sheth, S. A., Nemoto, M., Guiou, M., Walker, M., Pouratian, N., & Toga, A. W. (2004). Linear and Nonlinear Relationships between Neuronal Activity, Oxygen Metabolism, and Hemodynamic Responses. *Neuron, 42*(2), 347-355. doi: https://doi.org/10.1016/S0896-6273(04)00221-1

Singh, K. D. (2006). Magnetoencephalography. In C. Senior, Russell, T., & Gazzaniga, M. (Ed.), *Methods in Mind* (pp. 291-326). Cambridge, USA: MIT Press.

Singh, K. D., Barnes, G. R., Hillebrand, A., Forde, E. M. E., & Williams, A. L. (2002). Task-Related Changes in Cortical Synchronization Are Spatially Coincident with the Hemodynamic Response. *Neuroimage, 16*(1), 103-114. doi: https://doi.org/10.1006/nimg.2001.1050

Smith, S. M., Fox, P. T., Miller, K. L., Glahn, D. C., Fox, P. M., Mackay, C. E., . . . Beckmann, C. F. (2009). Correspondence of the brain's functional architecture during activation and rest. *Proc Natl Acad Sci U S A, 106*(31), 13040-13045. doi: 10.1073/pnas.0905267106

Smith, S. M., Vidaurre, D., Beckmann, C. F., Glasser, M. F., Jenkinson, M., Miller, K. L., . . . Van Essen, D. C. (2013). Functional connectomics from resting-state fMRI. *Trends in cognitive sciences, 17*(12), 666-682. doi: 10.1016/j.tics.2013.09.016

Sorg, C., Riedl, V., Mühlau, M., Calhoun, V. D., Eichele, T., Läer, L., . . . Wohlschläger, A. M. (2007). Selective changes of resting-state networks in individuals at risk for Alzheimer's disease. *Proceedings of the National Academy of Sciences, 104*(47), 18760-18765. doi: 10.1073/pnas.0708803104

Specchio, N., Boero, G., Michelucci, R., Gambardella, A., Giallonardo, A. T., Fattouch, J., . . . Specchio, L. M. (2008). Effects of levetiracetam on EEG abnormalities in

juvenile myoclonic epilepsy. *Epilepsia, 49*(4), 663-669. doi: 10.1111/j.1528-1167.2007.01523.x

Spencer, Susan S. (2002). Neural Networks in Human Epilepsy: Evidence of and Implications for Treatment. *Epilepsia, 43*(3), 219-227. doi: 10.1046/j.1528-1157.2002.26901.x

Stefan, H., Paulini-Ruf, A., Hopfengärtner, R., & Rampp, S. (2009). Network characteristics of idiopathic generalized epilepsies in combined MEG/EEG. *Epilepsy Res, 85*(2–3), 187-198. doi: https://doi.org/10.1016/j.eplepsyres.2009.03.015

Stone, J. M., Dietrich, C., Edden, R., Mehta, M. A., De Simoni, S., Reed, L. J., . . . Barker, G. J. (2012). Ketamine effects on brain GABA and glutamate levels with 1H-MRS: relationship to ketamine-induced psychopathology. *Molecular psychiatry, 17*(7), 10.1038/mp.2011.1171. doi: 10.1038/mp.2011.171

Strimbu, K., & Tavel, J. A. (2010). What are Biomarkers? *Current opinion in HIV and AIDS, 5*(6), 463-466. doi: 10.1097/COH.0b013e32833ed177

Swettenham, J. B., Muthukumaraswamy, S. D., & Singh, K. D. (2009). Spectral properties of induced and evoked gamma oscillations in human early visual cortex to moving and stationary stimuli. *J Neurophysiol, 102*(2), 1241-1253. doi: 10.1152/jn.91044.2008

Tae, W. S., Hong, S. B., Joo, E. Y., Han, S. J., Cho, J.-W., Seo, D. W., . . . Kim, S. I. (2006). Structural Brain Abnormalities in Juvenile Myoclonic Epilepsy Patients: Volumetry and Voxel-Based Morphometry. *Korean Journal of Radiology, 7*(3), 162-172. doi: 10.3348/kjr.2006.7.3.162

Templeton, D. (2010). *Pharmacokinetics of perampanel, a highly selective AMPA-type glutamate receptor antagonist following once- and multiple- daily dosing.* Paper presented at the 9th European Congress on Epileptology, Rhodes, Greece.

Tewarie, P., Bright, M. G., Hillebrand, A., Robson, S. E., Gascoyne, L. E., Morris, P. G., . . . Brookes, M. J. (2016). Predicting haemodynamic networks using electrophysiology: The role of non-linear and cross-frequency interactions. *Neuroimage, 130*, 273-292. doi: http://dx.doi.org/10.1016/j.neuroimage.2016.01.053

Tewarie, P., Hillebrand, A., van Dellen, E., Schoonheim, M. M., Barkhof, F., Polman, C. H., . . . Stam, C. J. (2014). Structural degree predicts functional network connectivity: A multimodal resting-state fMRI and MEG study. *Neuroimage, 97*, 296-307. doi: http://dx.doi.org/10.1016/j.neuroimage.2014.04.038

Tewarie, P., van Dellen, E., Hillebrand, A., & Stam, C. J. (2015). The minimum spanning tree: An unbiased method for brain network analysis. *Neuroimage, 104*, 177-188. doi: http://doi.org/10.1016/j.neuroimage.2014.10.015

Thomas, R. H., Steer, S., Gilpin, T. R., Glasbey, J. C. D., King, W. H., & Smith, P. E. M. (2012). 056 Variability in adult epilepsy prevalence in the UK. *Journal of Neurology, Neurosurgery & Psychiatry, 83*(3), e1-e1. doi: 10.1136/jnnp-2011-301993.98

Tikka, S. K., Goyal, N., Umesh, S., & Nizamie, S. H. (2013). Juvenile myoclonic epilepsy: Clinical characteristics, standard and quantitative electroencephalography analyses. *Journal of Pediatric Neurosciences, 8*(2), 97-103. doi: 10.4103/1817-1745.117835

Tomasi, D., & Volkow, N. D. (2011). Association between Functional Connectivity Hubs and Brain Networks. *Cerebral Cortex, 21*(9), 2003-2013. doi: 10.1093/cercor/bhq268

Traynelis, S. F., Wollmuth, L. P., McBain, C. J., Menniti, F. S., Vance, K. M., Ogden, K. K., . . . Dingledine, R. (2010). Glutamate Receptor Ion Channels: Structure, Regulation, and Function. *Pharmacological Reviews, 62*(3), 405-496. doi: 10.1124/pr.109.002451

Tyler, M. W., Yourish, H. B., Ionescu, D. F., & Haggarty, S. J. (2017). Classics in Chemical Neuroscience: Ketamine. *ACS Chemical Neuroscience*. doi: 10.1021/acschemneuro.7b00074

Tzourio-Mazoyer, N., Landeau, B., Papathanassiou, D., Crivello, F., Etard, O., Delcroix, N., . . . Joliot, M. (2002). Automated Anatomical Labeling of Activations in SPM Using a Macroscopic Anatomical Parcellation of the MNI MRI Single-Subject Brain. *Neuroimage, 15*(1), 273-289. doi: https://doi.org/10.1006/nimg.2001.0978

Uhlhaas, P. J., & Singer, W. (2006). Neural synchrony in brain disorders: relevance for cognitive dysfunctions and pathophysiology. *Neuron, 52*(1), 155-168. doi: 10.1016/j.neuron.2006.09.020

van den Broek, S. P., Reinders, F., Donderwinkel, M., & Peters, M. J. (1998). Volume conduction effects in EEG and MEG. *Electroencephalography and Clinical Neurophysiology, 106*(6), 522-534. doi: https://doi.org/10.1016/S0013-4694(97)00147-8

van den Heuvel, M. P., & Hulshoff Pol, H. E. (2010). Exploring the brain network: A review on resting-state fMRI functional connectivity. *European Neuropsychopharmacology, 20*(8), 519-534. doi: http://dx.doi.org/10.1016/j.euroneuro.2010.03.008

van den Heuvel, M. P., Scholtens, L. H., Turk, E., Mantini, D., Vanduffel, W., & Feldman Barrett, L. (2016). Multimodal analysis of cortical chemoarchitecture and macroscale fMRI resting-state functional connectivity. *Hum Brain Mapp, 37*(9), 3103-3113. doi: 10.1002/hbm.23229

van den Heuvel, M. P., & Sporns, O. (2011). Rich-Club Organization of the Human Connectome. *The Journal of Neuroscience, 31*(44), 15775-15786. doi: 10.1523/jneurosci.3539-11.2011

Van der Meer, M. L., Tewarie, P., Schoonheim, M. M., Douw, L., Barkhof, F., Polman, C. H., . . . Hillebrand, A. (2013). Cognition in MS correlates with resting-state oscillatory brain activity: An explorative MEG source-space study. *NeuroImage: Clinical, 2*, 727-734. doi: http://doi.org/10.1016/j.nicl.2013.05.003

Vanrumste, B., Jones, R. D., Bones, P. J., & Carroll, G. J. (2005). Slow-wave activity arising from the same area as epileptiform activity in the EEG of paediatric patients with focal epilepsy. *Clinical Neurophysiology, 116*(1), 9-17. doi: https://doi.org/10.1016/j.clinph.2004.07.032

Vaudano, A. E., Laufs, H., Kiebel, S. J., Carmichael, D. W., Hamandi, K., Guye, M., . . . Lemieux, L. (2009). Causal Hierarchy within the Thalamo-Cortical Network in Spike and Wave Discharges. *PLoS ONE, 4*(8), e6475. doi: 10.1371/journal.pone.0006475

Vollmar, C., O'Muircheartaigh, J., Symms, M. R., Barker, G. J., Thompson, P., Kumari, V., . . . Koepp, M. J. (2012). Altered microstructural connectivity in juvenile myoclonic epilepsy: The missing link. *Neurology, 78*(20), 1555-1559. doi: 10.1212/WNL.0b013e3182563b44

Vrba, J. (2002). Magnetoencephalography: the art of finding a needle in a haystack. *Physica C: Superconductivity, 368*(1–4), 1-9. doi: https://doi.org/10.1016/S0921-4534(01)01131-5

Vrba, J., & Robinson, S. E. (2001). Signal processing in magnetoencephalography. *Methods, 25*(2), 249-271. doi: 10.1006/meth.2001.1238

Wang, K., Jiang, T., Yu, C., Tian, L., Li, J., Liu, Y., . . . Li, K. (2008). Spontaneous activity associated with primary visual cortex: a resting-state FMRI study. *Cereb Cortex, 18*(3), 697-704. doi: 10.1093/cercor/bhm105

Wang, Z., Lu, G., Zhang, Z., Zhong, Y., Jiao, Q., Zhang, Z., . . . Liu, Y. (2011). Altered resting state networks in epileptic patients with generalized tonic–clonic seizures. *Brain Research, 1374*, 134-141. doi: https://doi.org/10.1016/j.brainres.2010.12.034

Wens, V., Bourguignon, M., Goldman, S., Marty, B., Op de Beeck, M., Clumeck, C., . . . De Tiege, X. (2014). Inter- and intra-subject variability of neuromagnetic resting state networks. *Brain Topogr, 27*(5), 620-634. doi: 10.1007/s10548-014-0364-8

WHO. (2017). Epilepsy Fact Sheet. Retrieved 6th June, 2017, from http://www.who.int/mediacentre/factsheets/fs999/en/

Wood, C. C. (1982). APPLICATION OF DIPOLE LOCALIZATION METHODS TO SOURCE IDENTIFICATION OF HUMAN EVOKED POTENTIALS*. *Annals of the New York Academy of Sciences, 388*(1), 139-155. doi: 10.1111/j.1749-6632.1982.tb50789.x

Woolrich, M. W., Baker, A., Luckhoo, H., Mohseni, H., Barnes, G., Brookes, M., & Rezek, I. (2013). Dynamic state allocation for MEG source reconstruction. *Neuroimage, 77*, 77-92. doi: 10.1016/j.neuroimage.2013.03.036

Yacoub, E., Harel, N., & Ugurbil, K. (2008). High-field fMRI unveils orientation columns in humans. *Proc Natl Acad Sci U S A, 105*(30), 10607-10612. doi: 10.1073/pnas.0804110105

Yeager, K. A., DiIorio, C., Shafer, P. O., McCarty, F., Letz, R., Henry, T., & Schomer, D. L. (2005). The complexity of treatments for persons with epilepsy. *Epilepsy & Behavior, 7*(4), 679-686. doi: https://doi.org/10.1016/j.yebeh.2005.07.008

Zaccara, G., Giovannelli, F., Cincotta, M., Verrotti, A., & Grillo, E. (2013). The adverse event profile of perampanel: meta-analysis of randomized controlled trials. *Eur J Neurol, 20*(8), 1204-1211. doi: 10.1111/ene.12170

Zhang, Z., Liao, W., Wang, Z., Xu, Q., Yang, F., Mantini, D., . . . Lu, G. (2014). Epileptic discharges specifically affect intrinsic connectivity networks during absence seizures. *Journal of the Neurological Sciences, 336*(1–2), 138-145. doi: https://doi.org/10.1016/j.jns.2013.10.024

Zhang, Z., Lu, G., Zhong, Y., Tan, Q., Chen, H., Liao, W., . . . Liu, Y. (2010). fMRI study of mesial temporal lobe epilepsy using amplitude of low-frequency fluctuation analysis. *Hum Brain Mapp, 31*(12), 1851-1861. doi: 10.1002/hbm.20982

Zhu, Z., Zumer, J. M., Lowenthal, M. E., Padberg, J., Recanzone, G. H., Krubitzer, L. A., . . . Disbrow, E. A. (2009). The relationship between magnetic and electrophysiological responses to complex tactile stimuli. *BMC Neurosci, 10*, 4. doi: 10.1186/1471-2202-10-4

Zumer, J. M., Brookes, M. J., Stevenson, C. M., Francis, S. T., & Morris, P. G. (2010). Relating BOLD fMRI and neural oscillations through convolution and optimal linear weighting. *Neuroimage, 49*(2), 1479-1489. doi: https://doi.org/10.1016/j.neuroimage.2009.09.020

Appendices

A. Correlations between mean band-limited connection strength and head geometry.

	1-4Hz	4-8Hz	8-13Hz	13-30Hz	30-50Hz	50-90Hz
Max. Change/ Pairwise	-0.43	0.03	-0.21	-0.03	-0.2	0.33
PCA/ Pairwise	-0.28	0.01	-0.23	-0.16	0.01	0.43
Max. Change/ Symmetric	-0.16	0.01	-0.12	-0.02	0.19	0.38
PCA/ Symmetric	-0.26	-0.2	-0.14	0.08	0.05	0.21

Appendix A. Correlation values (Pearson's r) between mean connection strength and intracranial volume for each condition and frequency band in the first experimental chapter.

B. Single subject fMRI to band-limited MEG connectivity correlation.

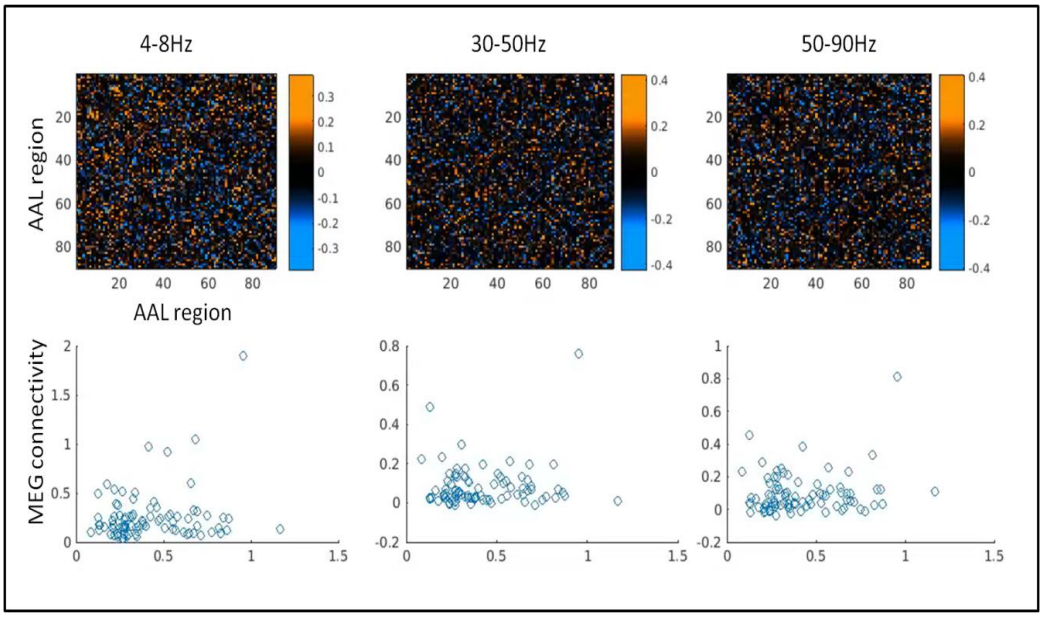

Appendix B. **Top**: Correlation between band-limited MEG connectivity and fMRI across subjects. Each point in this matrix represents the correlation, across subjects, between the z-score of the corresponding connection in (L-R) theta, low-gamma and high-gamma bands with fMRI. There is no clear pattern of correlation between connectivity in any band with fMRI. **Bottom**: There is no statistically significant correlation between global connectivity (i.e. mean of the connectivity matrix) for each participant in fMRI (X) and MEG connectivity (Y) in the theta, low- or high-gamma bands.

C. Descriptive statistics for psychometric questionnaires used during pharmacological intervention.

SHAS		Pre-Dose	Post-Dose
Perampanel	Mean	43.2	195.5
	SD	46.5	159.1
Placebo	Mean	48.5	45.2
	SD	77.9	73.8
BAES - Sedative			
Perampanel	Mean	12.0	25.5

	SD	5.4	11.5
Placebo	Mean	11.3	11.9
	SD	4.9	7.3
BAES - Stimulant			
Perampanel	Mean	30.7	23.8
	SD	14.4	12.1
Placebo	Mean	31.4	27.3
	SD	11.7	14.0
SHS			
Perampanel	Mean	55.3	58.0
	SD	9.2	12.7
Placebo	Mean	54.2	53.4
	SD	9.2	9.5

Appendix C. Descriptive statistics (overall pre- and post-dose mean/SD) for the psychometric questionnaires used to assess perception of drug-related changes in the perampanel experiment.

D. PharmacoMEG - Biphasic Alcohol Effects Scale (BAES) item averages

BAES - Sedative subscale				
	Perampanel		Placebo	
	Pre-dose	Post-dose	Pre-dose	Post-dose
Difficulty in concentrating	1.95	4.05	1.5	1.7
Down	1.6	1.9	1.55	1.45
Heavy head	1.45	3.75	1.6	1.65
Inactive	2.45	3.9	2.1	1.9
Sedated	1.35	4.1	1.4	1.5
Slow thoughts	1.4	3.7	1.45	1.75
Sluggish	1.8	4.1	1.65	1.9

Total	12	25.5	11.25	11.85

BAES - Stimulant subscale

	Perampanel		Placebo	
	Pre-dose	Post-dose	Pre-dose	Post-dose
Elated	3.55	3.5	4.2	3.55
Energized	4.35	2.8	4.75	3.85
Excited	4.55	3.1	3.95	3.65
Stimulated	4.2	3.25	4.6	3.9
Talkative	4.9	4.2	4.65	4.45
Up	5.1	4.25	5.5	4.65
Vigorous	4	2.7	3.7	3.25
Total	30.65	23.8	31.35	27.3

Appendix D. BAES sedative and stimulant subscale item averages.

E. PharmacoMEG - Subjective High Assessment Scale (SHAS) item averages

SHAS

	Perampanel		Placebo	
	Pre-dose	Post-dose	Pre-dose	Post-dose
Uncomfortable	15.7	6.1	8.8	5.5
High	5.1	8.2	7.2	7.3
Clumsy	5.1	21.1	5.8	3.4
Muddled or confused	3.8	12.4	3.1	2.9
Slurred speech	0.7	7.6	1.0	1.6
Dizzy	0.0	18.9	0.9	2.5
Nauseated	0.3	4.5	2.0	1.7
Drunk or intoxicated	0.0	15.8	0.4	0.6
Sleepy	9.7	40.8	14.4	13.5

Distorted sense of time	0.0	7.3	0.9	3.8
Effects of alcohol	0.0	13.7	0.4	0.0
Difficulty concentrating	2.7	27.4	3.1	1.6
Feeling of floating	0.3	12.1	0.9	1.2

Appendix E. SHAS item averages.

F. Clinical characteristic table for JME patients.

				Seizure type (age onset, current frequency, last to scan)			
Patient no.	**Gender**	**Age**	**Status**	**MJ**	**ABS**	**GTCS**	**AEDs (daily dose in mg)**
1	F	18	r-jme	15, 1/m, 1m	15, 1/m, 1m	15, 4/y, 1m	LEV 2250
2	M	26	c-jme	18, 1/y, 1m	n/a	18, 1y, 1m	VPA 500
3	F	21	r-jme	17, 4/y, 2m	17, 4/y, 6m	20, 4/y, 2m	LTG 450
4	F	22	c-jme	12, 6/y, 1 m	n/a	18, <1/y, 3 y	VPA 400
5	F	20	r-jme	20, 1/m, 1 m	n/a	15, 2/w, 1w	LTG 450
6	F	38	c-jme	14, 0, 2y	n/a	24, 1/y, 6m	LEV 3250
7	F	19	r-jme	15, 1/m, 1m	15, 1/m, 1m	15, 1/m, 1m	LEV 2000, ZNM 25
8	F	35	r-jme	15, 8/d, 2 hr	35, <1/y, 2 m	12, <1/y, >1y	LTG 300, CLB 10
9	F	18	r-jme	17, 1/d, 1d	n/a	17, 3/w, 1w	LTG 150, VPA 1500
10	F	18	c-jme	15, 1/d, 9m	n/a	15, 1/y, 9m	LEV 1000
11	M	22	r-jme	18, 2/w, 12 hs	14, 0, 4 y	18, 1/w, 10d	VPA 2500, LEV 500
12	F	33	r-jme	11, 2/m, 3w	n/a	11, 2/m, 3w	LEV 1000
13	F	31	c-jme	10, <1/y, 1y	n/a	8, 4 in life	VPA 1000

14	F	25	r-jme	15, 1/m, 2m	6, none, 1 m	3, 2/y, 4 m	LEV 1500, ZNM 150, LTG 100
15	F	36	r-jme	13, 0, >1y	9, 3/w, 3 d	13, 1/m, 1w	LEV 3000, TPM 500, CLB 40
16	F	38	r-jme	30, 2/y, 5m	10, n, >1y	10, <1/y, 1 m	VPA 800, LTG 300
17	M	22	c-jme	12, 1/y, 1y	13, 1/m, 1 m	13, 2 in life, 7 y	LEV 1000
18	M	44	r-jme	15, 1/d, 1d	n/a	15, 2/y, 5 m	VPA 1500, LEV 2000
19	F	47	r-jme	10, 1/m, 1w	10, 1/w, 1w	10, 1/w, 1w	LTG 600
20	F	26	r-jme	10, 2/w, 4d	n/a	8, 3/y, 1y	ZNM 50, LEV 1500
21	F	20	r-jme	17, 0, >1y	n/a	17, 4/y, 1m	LEV 1000, TPM 250
22	F	20	r-jme	15, 2/w, 2w	8, 3/m, 3m	8, 4/y, 5 m	VPA 2000, TPM 25
23	M	30	r-jme	14, 1/w, 0 d	14, 1/w, 2d	18, 2/y, 3w	VPA 600
24	M	29	r-jme	15, <1/m, 2m	15, 0, >1y	15, 0, 5y	VPA 1500
25	F	31	r-jme	13, 1/m, 1m	n/a	13, <1/y, >1y	TPM 275, LEV 1500

Appendix F. Full clinical characteristics for JME patients included in chapter 5 analysis. Abbreviations as follows. **Seizure type:** MJ - myoclonic jerks, GTCS - generalised tonic clonic seizures, ABS - absence seizures. **Status:** r-jme - treatment refractory, c-jme - treatment controlled. **Anti-epileptic drugs (AEDs):** LEV - levetiracetam, VPA - valproate, LTG - lamotrigine, TPM - topiramate, ZNM - zonisamide, CLB - clobazam

G. Source space kurtosis values for JME patients and controls

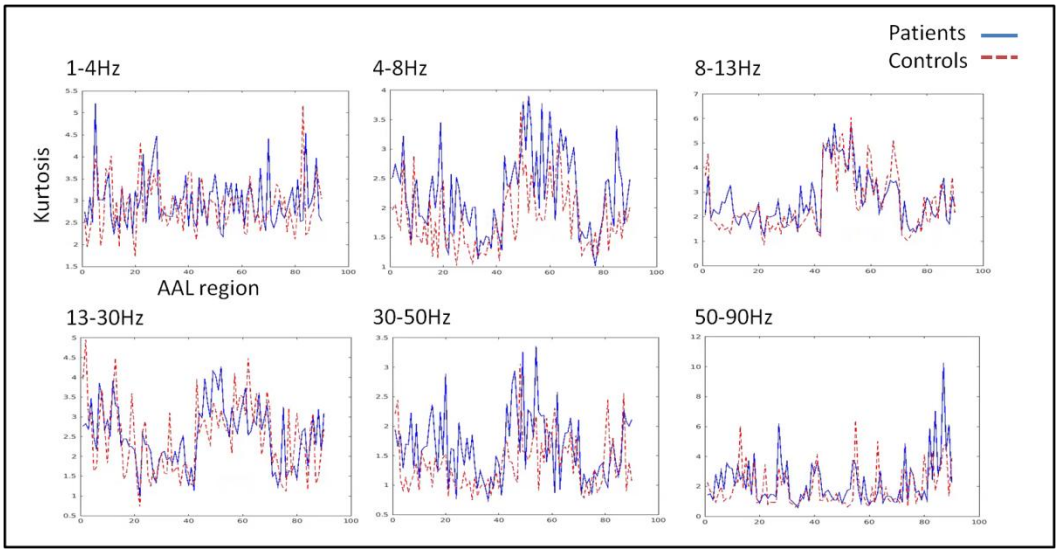

Appendix G. Average kurtosis for each of the 90 AAL regions in JME patients (blue) and healthy controls (red), for each frequency band. Using randomisation testing, no significant group differences were found.